nature portfolio

Peer Review File

Molecular Cobalt Catalysts for Electrocatalytic Acetylene Semi-Hydrogenation

Corresponding Author: Professor Linjie Zhi

This file contains all reviewer reports in order by version, followed by all author rebuttals in order by version.

Version 0:

Reviewer comments:

Reviewer #1

(Remarks to the Author)
The manuscript titled “Molecular Cobalt Catalysts for Highly Selective Electrocatalytic Acetylene Semi-Hydrogenation” investigates the electrocatalytic semi-hydrogenation of acetylene using cobalt phthalocyanine (CoPc) supported on differently functionalized carbon nanotubes (CNTs). The authors compare CoPc with CuPc catalysts, and systematically study the effect of O-, S-, and N-doped CNT supports on catalytic activity. To elucidate the reaction mechanism of CoPc/NCNT, they employ a broad range of techniques, including in situ XANES, FTIR, EPR, DEMS, and DFT calculations. Additional characterization methods such as TEM, Raman spectroscopy, and kinetic isotope effect studies are also used. Finally, they demonstrate the direct electroreduction of acetylene to high concentrations of ethylene in a homemade tandem device, combining a 1 cm2 flow cell with a 25 cm2 flow cell. Overall, the study is interesting and represents a meaningful contribution to the field of electrocatalytic acetylene semi-hydrogenation. However, the manuscript currently suffers from missing experimental details, insufficient depth in some aspects of the data analysis, and a lack of clarity in the presentation of certain results and writing. Before the manuscript can be considered for publication in Nature Communications, the following comments must be thoroughly addressed:
1. On page 4, at the beginning of the Results and Discussion section, additional experimental details are required. For example, the electrolyte conditions should be specified when introducing the LSV data (“Under an Ar atmosphere, the linear sweep voltammetry (LSV) curves of the CoPc/OCNT demonstrated both a more positive onset potential and higher current density across the HER polarization range compared with those of CuPc/OCNT”). The writing should also be more quantitative: rather than stating “a more positive onset potential,” the authors should report the exact numerical difference. Similarly, when presenting selectivity values, the amounts of by-products (e.g. C4 species) should be given. On page 6, the phrase “consistent with the earlier onset potentials observed in LSV measurements” should be clarified by specifying the actual onset potential shift.
2. Throughout the manuscript, the authors tend to draw conclusions too rapidly, and the hypotheses should be formulated more carefully. For example, on page 5 the statement that CoPc/OCNT exhibits “facilitated water dissociation and thus enhanced EASH performance” is not sufficiently supported, as LSV data alone only demonstrate higher or earlier activity and do not provide direct evidence of water dissociation. Similarly, on page 10 the claim that “the variations in polarization curves and selectivity clearly indicated that the ESAH kinetics and reaction pathway on CoPc/XCNT could be effectively tuned by modulating the X heteroatom electronegativity” is overstated, since the correlation with electronegativity remains speculative without additional mechanistic evidence.
3. On page 6, the discussion of water dissociation barriers and Gibbs free energy for *H binding is confusing. The authors state that CoPc/OCNT exhibits stronger H_2O dissociation and a higher barrier for *H coupling, resulting in slower HER kinetics (Figure 1h). However, this appears inconsistent with the earlier LSV and DEMS results, where CoPc/OCNT was described as facilitating the reaction. The authors should reconcile these two observations and clarify how they are connected.
4. Regarding the characterization, for Figure S8, reference pattern should be provided for the XRD data. In addition, there is an inconsistency in Figure S9: the main text refers to FTIR, while the SI shows a Raman spectrum. Also, according to the literature, CoPc can typically be detected in the lower wavenumber region (600–700 cm-1) with Raman, which does not overlap with CNT vibrations (see J. Am. Chem. Soc. 2025, 147, 14, 12298–12307, Fig. S13). The authors should carefully examine this region. For Xanes, reference spectra of bare CoPc in Figure S13 should be provided for comparison.
5. For the AC-STEM images (Figures 2d and S12), the legend for the 3D heat map is missing and should be provided with length-scale if possible.
6. In general, it would be important to include error bars, for example in the ICP-OES data, to highlight the reproducibility of

the synthesis and Co loading. Likewise, Table S2 for the EXAFS Fits should report explicit error values rather than only providing a general description below the table.
7. For the explanation of the XANES-data in Figure 2f the authors should provide a clearer explanation of the significance of the pre-edge shift observed and how this correlates with the different CNTs.
8. The SI should also include the measured electrode potentials. In Figure 3e, it is unclear whether Ecell refers to the working electrode potential or the total cell voltage, this should be specified. In the Methods section, all potentials are described as iR-corrected, yet in the SI no such correction appears to be applied. Please provide the typical ohmic drop values. Additionally, in many current density plots in the SI (e.g. Figure S17), the authors note “The results are presented without iR compensation”, but since no potential values are shown in the graphs, this statement is not meaningful.
9. On page 10, the statement “Impressively, at an industrial-level current density of 500 mA cm-2, the FE for C2H4 remained above 85%, continuing to fall within the profitable region and indicating the excellent economic potential of the CoPc/NCNT catalyst towards EASH (Figure S18)” requires clarification. How is the “profitable region” defined, and what is the energy efficiency of the reaction under these conditions? What metrics are truly required for industrial application? Moreover, Figure S18 shows GC data, which does not support this economic claim. On page 11, the stability discussion is also incomplete. The authors show that at 100 mA cm-2 the catalyst remains stable for 60 h (Figure 3e), but no data are provided at 500 mA cm-2, which would be necessary to support claims of industrial relevance.
10. The authors compare CoPc with supported CoPc on OCNT, SCNT, and NCNT. However, a direct comparison with CoPc on bare CNTs is missing. Including this control is important to clearly demonstrate the necessity and benefit of CNT functionalization.
11. In Figure S22, the data for the lowest loading and lowest current appear significantly different and may represent an outlier. Is this result reproducible? On page 11, the authors state that CoPc/NCNT with 5 wt% CoPc and a loading of 0.4 mg cm-2 was used and gave the best electrocatalytic performance. How does this loading on CNT and catalyst loading compare with other reports on CoPc–CNT systems, for example in CO2RR to CO or methanol? Is the chosen loading consistent with the literature, or does it need to be specifically adjusted for the present reaction? What kind of GDE is used?
12. Regarding the change in Co oxidation state observed by in situ XANES: can the authors provide clearer insights into the specific oxidation state transition (e.g., from which to which state)? The statement “This valence reduction was correlated with electron transfer from Co to adsorbed C2H2 species, facilitating rapid acetylene reduction and clearly confirming Co as the primary active site” is difficult to follow. Is this conclusion directly supported by the presented data, or is it primarily drawn from the literature?
13. The peak assignments of the in situ FTIR data in Figure 4b do not align with the cited reference. The authors assign the bands at 1650 and 1559 cm-1 to the *C≡C bond of C2H2 and the generated *C=C bond adsorbed on CoPc/NCNT, respectively. However, according to the reference, adsorbed *C2H2 species can be detected at 1641 cm-1 over ED–Cu NPs, while the band at 1577 cm-1 corresponds to *C2H3, the key intermediate of C2H2 hydrogenation. Therefore, a more consistent assignment according to that reference would be 1650 cm-1 to *C2H2 and 1559 cm-1 to *C2H3. This interpretation would also better match the observed peak evolution, where the 1650 cm-1 band increases at higher overpotentials. Are these overpotential-dependent changes correlated with product selectivity? Furthermore, do the relative intensity changes of these two peaks align with the expected reaction pathway? The authors should also examine whether additional informative spectral regions around 2000 cm-1 are present in the FTIR spectra.
14. On page 13, the discussion of pH variation and radical scavenger experiments is too brief and the conclusions are drawn too quickly. The pH was only varied slightly (from ~13.7 to ~14.3), which corresponds to a relatively small change in OH- concentration. The authors should also specify which concentrations of KOH corresponds to which pH. In addition, when introducing t-BuOH as a radical scavenger, the exact concentration used (50 mM) should be reported in the main text. This is a relatively high concentration, and it should be clarified whether the observed effect can be attributed specifically to radical scavenging or to other interactions with the system.
15. The reported EASH reaction kinetics follow the trend K+ > Na+ > TMA+, with C2H2 conversion decreasing from K+ to 10.4% TMA+. How does this trend compare with previous literature? Have larger or smaller cations such as Cs+ or Li+ been tested? It is worth noting that molecular catalysts often exhibit very different cation-dependent effects compared to metallic catalysts (see Yu, S., Yamauchi, H., Wang, S. et al. Nat. Catal. 7, 1000–1009 (2024)).
16. More details about the gas feed are required. Was the acetylene introduced in ethylene or in argon? More details about the gas feed mixing is required. Additional clarification is also needed on the 1 cm2 and 25 cm2 flow cell setups, how exactly are they configured and operated? In the text, the authors state: “To satisfy the requirements for the industrial production of polymer-grade ethylene, the EASH performance was subsequently assessed under realistic conditions with 0.5% acetylene impurities (5000 ppm) in crude ethylene (Figure S33).” However, Figure S33 shows LSV curves of different gas concentrations.
17. The Methods section requires substantial revision, as both the main text and the Supporting Information currently provide too few details to ensure reproducibility. The experimental procedures should be described comprehensively, including complete information on catalyst synthesis and functionalization (precursors, solvents, conditions, purification), electrode preparation and loading (mass loading, electrode area, binder composition, deposition procedure), and electrochemical testing protocols (cell configuration, electrolyte composition and preparation, gas feed composition and flow rates, reference and counter electrode details, iR compensation). In addition, the in situ and operando experiments (XANES, FTIR, EPR, DEMS) must be described in sufficient detail, including setups, acquisition parameters, and data analysis methods. Calibration and quantification procedures (e.g., GC, ICP-OES) should also be reported, together with error analysis and reproducibility tests. Without this level of detail, the results cannot be reliably reproduced, and the section must therefore be carefully revised and expanded to meet the standards of Nature Communications.
Minor comments:
-Page 5, ESAE should be ESAH.
-The authors should write the minus sign for the current densities (I assume negative currents were applied).
-Hard to distinguish the colors (such as blue and green) in many of the plots.

(Remarks on code availability)

Reviewer #2

(Remarks to the Author)
In this work, the authors report a molecular cobalt phthalocyanine (CoPc) catalyst platform that promotes electrocatalytic acetylene semi-hydrogenation (EASH) reaction activity through electronic regulation. They also investigate the performance modulation strategies and reaction mechanisms of the corresponding molecular catalysts. The utilization of analogous molecular catalysts (CoPc and CuPc) for EASH catalysis have been previously reported [10.1016/j.cej.2021.134129]. Moreover, the authors' research and conclusions on the performance enhancement mechanism of CoPc/XCNT are not sufficiently clear. Therefore, I do not recommend publishing this work in Nature Communications.
1.Apart from the already reported feasibility of metal phthalocyanines in the EASH process, the employed CoPc/OCNT and CuPc/OCNT are also widely used in various electrocatalytic reactions including CO2RR, ORR, HER, and etc. (Angew. Chem. Int. Ed. 2024, 63, e202310623; Chem. Soc. Rev. 2021, 50, 12985; Nature, 2019, 575, 639). By simply combining the two points together, the present work is lack of innovation to be published in Nature Communications.
2.Except for the novelty issue, the data and analysis is not adequately to support their hypothesis and conclusions. For example, to exclude the CPET pathway, the author claimed that “the pH was varied from ~13.7 to ~14.3, negligible changes were observed in the polarization curves and FE for C2H4 on CoPc/NCNT”, which is contradictory to the data shown in Figure S27.
3.In Page 13, the authors claimed that a hydrogen transfer mechanism could bypass the HER competitive, which is groundless. It has been widely reported that H2 could also obtained by the combination of two water-derived *H, called Tafel step (J. Phys. Chem. C, 2018, 122, 23943.). Thus, the real reason for the improved C2H4 selectivity is not the claimed mechanism, which needs further discussion.
4.The observed performance disparities between CoPC/NCTN and other samples are predominantly attributable to the difference in water dissociation ability. However, this seems inconsistent with the kinetic isotope experiment results for catalysts. The LSV or kinetic isotope experiment results for catalysts under argon gas should be provided for further comparison.
5.The as-reported TOF value is too high to convince the reviewer. According to the data in the previous literature (Chem. Eng. J. 2022, 431, 134129), the bare CoPc only exhibited a TOF value of 0.29 min-1 at a current of 100 mA. How can the TOF of the as-reported CoPc/NCNT reach 9700 min-1 at a current of 500 mA? More details are needed for the TOF calculation. Besides, the claimed 24 h continuous operation under ethylene-rich simulated gas flow could not be regarded as an advancement compared to the recent progress (Nat. Catal.2021, 4, 557; 10.31635/ccschem.024.202404849; 10.1002/anie.202509501; 10.31635/ccschem.022.202101750;)
6.In Figure 1g, comparing the d-band centers of different metals is quite uncommon and meaningless. Meanwhile, in Figures 1h, I and 4k, the author employed unusual plotting methods to present the reaction diagrams, which resulted in poorer data readability and a higher likelihood of misinterpretation. For example, in the conventional *H generation process, it is necessary to calculate the steady-state *H2O and *H+*OH as the initial and final states of the water dissociation process, as well as the corresponding transition states, while considering the *OH desorption process. It is very incomplete for the author to only calculate the energy barrier from *H2O to *H+*OH. The generation processes of H2 and C4 also face similar issues.
7.The manuscript does not present any calculation methods, and lacks the display of relevant and representative adsorption models. For single-atom catalysts, the selection of adsorption sites is crucial and needs to be demonstrated. In the processes of water dissociation and hydrogenation, it is necessary to clarify whether C and O species occupy the metal sites, and where *H is adsorbed.

(Remarks on code availability)

Reviewer #3

(Remarks to the Author)
In this work, the authors report a CoPc-OCNT catalyst towards EASH, achieving FE of 86.7% under 500 mA cm-2. The manuscript attributes the enhanced activity to the excellent hydrogenation ability of CoPc, but similar arguments were already reported in prior studies (Chem. Eng. J. 2022, 431: 134129). Therefore, the reviewer considers the current form of this work lacks of novelty and not suitable for publication in Nature Communications.

1. The authors choose the CoPc/OCNT as the model catalyst due to its better ability of water dissociation. How about NiPc/OCNT and FePc/OCNT, which has been proved the great activity on water dissociation. Besides, the FE of C2H4 decreased and FE of H2 increased sharply under high current densities, suggesting the inferior ability of CoPC/OCNT to tune the *H. The authors propose the CoPc/OCNT can inhibit C-C coupling to generate C4 byproducts, while the key Co sites may have no activity on C-C coupling.

2. The authors use the different carbon substrate (N-CNT, S-CNT, O-CNT) to tune coordination of Co center and optimize its catalytic performance. How about the performance of CoPc/CNT without doping? The CoPc/NCNT achieves the better performance. The authors should prove the increased performance is not originate the change of physical properties (conductivity, hydrophilicity, adsorption capacity).

3. The most electrochemical results presented in this study lack error bars, which may raise concerns about the reproducibility and reliability of the reported data.

4. The in-situ FT-IR data presented in this study are underexplored. The analysis of water peaks range from 3000-4000 cm-1 may be benefit of revealing the tune of water dissociation.

5. The selectivity performance using t-BuOH in electrolyte should be provide to the demonstrate the role of *H, while the LSV curves are not enough.

6. The authors design a tandem system to generate high-purity C2H4. However, the reviewer wants know if such a design has practical significance. Whether the added big-area reactor is better than other methods for removing low concentrations of C2H2. The technical economic analysis may be better to demonstrate the necessity of the design.

7. Some typographical typos exist in the manuscript and the authors should carefully check it (e.g., affinity—strong, Y-axis title of Figure 5d, the calculation of FE in Performance assessment).

(Remarks on code availability)

Reviewer #4

(Remarks to the Author)
This manuscript reports the synthesis of carbon nanotube-supported cobalt phtalocyanine (CoPc) complexes through silanoxyl links, and their electrocatalytic activity during the selective semi-hydrogenation reaction of acetylene to ethylene, mainly in pure form but also in ethylene-rich streams (actual commercial process). The characterization of the materials is comprehensive, the electrocatalytic results are well executed and the mechanistic part is sound. The results demonstrate that the axially NH2-complexed CoPc material is much more selective than the others (O- or SH-) due to the electronics of the coordination sphere, which allows a faster H2O dissociation and slower undesired C-C coupling. The fact that such a subtle change in the coordination of the supported Co cation enables a significant increase of the selectivity without compromising the catalytic activity is remarkable, moreover in a solid-supported catalyst, and will guide the design of future solid catalysts for this reaction. Therefore, publication in Nat. Commun. is suitable and recommended. However, it must be said that many electrocatalysts for this reaction has been recently published (many of them cited in the text but not compared in Table S3, which is clearly uncomplete), thus some work must be done to really contextualize the new catalyst. Some comments follow:
- The key finding here is the action of the N-axial ligand on the metal Pc. This is the point to highlight. I would prepare the N-axial ligand/Cu-Pc material and confirm that the catalytic activity improves in the same way (no need for a deep characterization, the ligation should be similar to the Co complex).
- The catalyst must be characterized after reaction. Is the complex stable? Evolves to an active species?
- With the better numbers obtained here, could the process substitute the current thermocatalytic process in any way?
- The conversion and selectivity numbers given in the introduction for the industrial semi-hydrogenation reaction of acetylene in ethylene streams are clearly underestimated, since a >99.99% selectivity for acetylene conversion is required (<10 ppm in the final stream). See and cite if appropriate: Nat. Catal., 2024, 7, 452–463. Indeed, the reaction conditions are also exaggerated, the industrial process operates at <100 ºC.
- The necessity or not of carbon nanotubes to support the complexes must be justified. If a carbon support with dangling hydroxyls could also do the job, this should be commented in the text, since that would give a much more affordable catalyst (perhaps worth of study in a different study). Other hydroxyl-containing supports could also be suitable, please read and cite if appropriate the following examples on semi-hydrogenation reaction of acetylene in ethylene streams under industrial conditions: ACS Catal. 2017, 7, 3721–3729; J. Am. Chem. Soc. 2018, 140, 8827–8832.
- Table S3 must be properly completed, or removed. The comparison between electro and thermocatalysts is perhaps unnecessary, otherwise the Table can be huge (see SI in the above-suggested references).

(Remarks on code availability)

Version 1:

Reviewer comments:

Reviewer #1

(Remarks to the Author)
In the revised manuscript, many of the comments have been addressed. However, several key concerns remain:
1. Figure captions throughout the manuscript still frequently lack essential details. For example, in Fig. R2, the inclusion of a higher CoPc loading should be explicitly explained in the caption. Similarly, in Fig. R3, it would be helpful to specify that the data correspond to the Co K-edge. This issue occurs repeatedly across the manuscript, and more detailed figure captions would greatly improve clarity and readability.
2. In Fig. R5, the newly added colour scale is still not visible.
3. For Tables R1 and R2, the authors should clearly state how the error bars were obtained. In addition, the magnitude of the error bars should be consistent with the reported values. In Table R2, some errors are larger than the corresponding values, which suggests that there may be an issue with the data analysis or error estimation.
4. I am concerned that iR compensation has not been applied. Without proper iR correction, it is difficult to meaningfully

compare the LSV behavior at higher current densities across different catalysts.
5. The Methods section still lacks important experimental details. For example, if a sputtered gold film was required for the FIT measurements, the sputtering procedure should be described. In addition, it is unclear whether the XANES measurements were performed using a laboratory setup or at a synchrotron facility. The use of “RapidXAFS 2M” is mentioned, but this technique/setup is not sufficiently explained and is unfamiliar without further clarification

(Remarks on code availability)

Reviewer #2

(Remarks to the Author)
The authors have made substantial improvements to the work in response to the previous round of review. The revised version is significantly more polished and addresses many of the concerns raised in the initial evaluation. Based on the current quality and scientific merit of the study, I, in principle, recommend that this work be considered for publication in Nature Communications.
However, while the overall structure, methodology, and presentation of results are now much stronger, there are still several details that require careful revision and clarification before the manuscript can be accepted for publication. These include, but are not limited to, the following points:
1. Physical quantities such as E, G, T, S, etc., should be in italic format.
2. The abbreviation for "generalized gradient approximation" should be checked. It is usually GGA, not GCA.
3. The chemical reaction equations should be checked for correctness. For example:
*C2H2 + H+ e– → C2H3 (10)
2*C2H3 + *C2H3 → *C4H6 (14)
4. Transition states, such as *H–OH, are generally not considered stable states and should be clearly indicated.
5. Software tools mentioned in the manuscript, such as VTST, should be properly cited.

(Remarks on code availability)

Reviewer #3

(Remarks to the Author)
The reviewer appreciates the authors’ efforts to revise the manuscript and respond to the comments. However, I regret that the manuscript is still not suitable for publication in this journal. A major concern regarding the novelty of this work is that the CoPc catalytic system has already been reported (Chem. Eng. J. 2022, 431: 134129). A critical issue is that the CoPc catalyst itself does not reach the performance level previously reported in the literature. Consequently, the apparent benefit of introducing NCNT cannot be reliably attributed to a true support effect, and the work fails to demonstrate that NCNT provides a meaningful or generalizable advantage for CoPc-based catalysts. Regarding the tandem system, feeding the exhaust from a small electrolyzer into a larger-area reactor does not convincingly demonstrate practical relevance. Achieving higher conversion in a single appropriately scaled reactor would be more rational and informative. Overall, despite the authors’ considerable experimental effort, the manuscript does not demonstrate sufficient novelty or advancement for publication in Nature Communications.

(Remarks on code availability)

Reviewer #4

(Remarks to the Author)
The revision has fulfilled this Reviewer´s requirements. The manuscript seems ready for publication.

(Remarks on code availability)

Version 2:

Reviewer comments:

Reviewer #1

(Remarks to the Author)
The authors have adequately addressed the concerns raised in the previous review. I recommend acceptance of the manuscript for publication in Nature Communications.

(Remarks on code availability)

Response to *Reviewers*' Comments

Dear Editors and Reviewers:

We would like to greatly appreciate you giving us the opportunity to revise our manuscript.

We carefully studied the reviewer's comments and tried our best to revise the manuscript according to the comments. The manuscript has been revised following the comments and suggestions of the reviewers, and point by point replies are given below. Thanks again to the editors and reviewers for their hard work.

Molecular Cobalt Catalysts for Highly Selective Electrocatalytic Acetylene Semi-Hydrogenation

Research Article, No. NCOMMS-25-62672A, Nature Communications

Response to Reviewer #1:

General Comments:

The manuscript titled "Molecular Cobalt Catalysts for Highly Selective Electrocatalytic Acetylene Semi-Hydrogenation" investigates the electrocatalytic semi-hydrogenation of acetylene using cobalt phthalocyanine (CoPc) supported on differently functionalized carbon nanotubes (CNTs). The authors compare CoPc with CuPc catalysts, and systematically study the effect of O-, S-, and N-doped CNT supports on catalytic activity. To elucidate the reaction mechanism of CoPc/NCNT, they employ a broad range of techniques, including in situ XANES, FTIR, EPR, DEMS, and DFT calculations. Additional characterization methods such as TEM, Raman spectroscopy, and kinetic isotope effect studies are also used. Finally, they demonstrate the direct electroreduction of acetylene to high concentrations of ethylene in a homemade tandem device, combining a 1 cm^2 flow cell with a 25 cm^2 flow cell. Overall, the study is interesting and represents a meaningful contribution to the field of electrocatalytic acetylene semi-hydrogenation. However, the manuscript currently suffers from missing experimental details, insufficient depth in some aspects of the data analysis, and a lack of clarity in the presentation of certain results and writing. Before the manuscript can be considered for publication in Nature Communications, the following comments must be thoroughly addressed:

Response: We appreciate the reviewer's thoughtful summary and constructive suggestions. These opinions help to improve the academic rigor of our article. In response, we have carefully revised the manuscript and Supplementary Information, incorporating new experimental data, figures, references, and discussion to address each of the reviewer's comments point by point. Detailed descriptions of these amendments are provided below. We believe that these revisions have substantially improved the overall quality of this work.

Specific Comments:

Comment 1: On page 4, at the beginning of the Results and Discussion section, additional experimental details are required. For example, the electrolyte conditions should be specified when introducing the LSV data ("Under an Ar atmosphere, the linear sweep voltammetry (LSV) curves of the CoPc/OCNT demonstrated both a more positive onset potential and higher current density across the HER polarization range compared with those of CuPc/OCNT"). The writing should also be more quantitative: rather than stating "a more positive onset potential," the authors should report the exact numerical difference. Similarly, when presenting selectivity values, the amounts of by-products (e.g. C_4 species) should be given. On page 6, the phrase "consistent with the earlier onset potentials observed in LSV measurements" should be clarified by specifying the actual onset potential shift.

Response: We acknowledge the reviewer's helpful comments and suggestions. We have revised the manuscript accordingly to provide more comprehensive experimental details and quantitative comparisons. The main revisions are summarized as follows:

Page 5-6: "The EASH performance of metal phthalocyanines was evaluated in a normal flow cell device with an electrode surface area of 1 cm^2 under a 100% C_2H_2 feed, in which Hg/HgO and Pt foil served as the reference and counter electrodes, respectively, and an anion exchange membrane separated two chambers filled with 1.0 M KOH aqueous solution (Supplementary Fig. S1)."

Page 6: "Under an Ar atmosphere in 1.0 M KOH electrolyte, the linear sweep voltammetry (LSV) curves…"

We appreciate the suggestion to increase the quantitative rigor of the manuscript. Accordingly, we have revised the manuscript throughout to provide explicit numerical values wherever comparative statements were previously qualitative. Specifically:

Page 6: "…the CoPc/OCNT catalyst exhibited an onset potential of −0.26 V *vs.* reversible hydrogen electrode (V_{RHE}), approximately 30 mV more positive than the −0.29 V of CuPc/OCNT, and also delivered a higher current density across the HER polarization range (e.g., −83.8 mA cm^{-2} *vs.* −33.9 mA cm^{-2} at −0.8 V_{RHE})…"

Page 6: "…with C_4 byproduct formation persisting at ~1.5%"

Page 6: "This trend is consistent with the ~30 and ~100 mV positive shifts in the HER and EASH onset potentials, respectively, from CoPc/OCNT to CuPc/OCNT observed in the LSV

measurements."

Comment 2: Throughout the manuscript, the authors tend to draw conclusions too rapidly, and the hypotheses should be formulated more carefully. For example, on page 5 the statement that CoPc/OCNT exhibits "facilitated water dissociation and thus enhanced EASH performance" is not sufficiently supported, as LSV data alone only demonstrate higher or earlier activity and do not provide direct evidence of water dissociation. Similarly, on page 10 the claim that "the variations in polarization curves and selectivity clearly indicated that the EASH kinetics and reaction pathway on CoPc/XCNT could be effectively tuned by modulating the X heteroatom electronegativity" is overstated, since the correlation with electronegativity remains speculative without additional mechanistic evidence.

Response to comment 2: We thank the reviewer for this thoughtful suggestion.

We agree that, in the original version, the discussion on water dissociation and heteroatom effects could have been presented more cautiously. In the revised manuscript, we have carefully refined the wording and improved the logical continuity between the hypotheses and the subsequent mechanistic evidence.

(1) Clarification of the water dissociation part on Page 5:

On page 5, the wording that CoPc/OCNT exhibits "facilitated water dissociation and thus enhanced EASH performance" based solely on LSV data was indeed premature. As the review noted, LSVs reflect only apparent activity and onset behaviour, not the elementary water-dissociation step directly. In the revised version, we have relocated this statement to Page 6, following direct evidence from isotope-labeling experiments and DFT calculations, which confirm that CoPc/OCNT significantly lowers the energy barrier for the $^{*}H_2O \rightarrow {}^{*}OH + {}^{*}H$ step compared with CuPc/OCNT.

Page 6: "The H_2 (m/z = 2) was detected at –0.28 V_{RHE} on CoPc/OCNT, appearing 40 mV earlier than on CuPc/OCNT, while the C_2H_4 (m/z=28) signal for CoPc/OCNT emerged at –0.2 V_{RHE}, 120 mV more positive than that of CuPc/OCNT."

(2) Clarification of the heteroatom effect description on Page 10:

We recognize that our conclusion was drawn somewhat early. Since a more detailed mechanistic discussion is provided later in the manuscript, we have rephrased the statement to enhance logical coherence and scientific rigor. The revised text now reads: "Overall, the above

characterizations reveal the CoPc-like Co-(pyrrolic N)$_4$ structure with X-atom modification in CoPc/XCNT, which significantly regulates the electronic distribution at the Co center."

Comment 3: On page 6, the discussion of water dissociation barriers and Gibbs free energy for *H binding is confusing. The authors state that CoPc/OCNT exhibits stronger H_2O dissociation and a higher barrier for *H coupling, resulting in slower HER kinetics (Figure 1h). However, this appears inconsistent with the earlier LSV and DEMS results, where CoPc/OCNT was described as facilitating the reaction. The authors should reconcile these two observations and clarify how they are connected.

Response to comment 3: We sincerely thank the reviewer for this insightful comment and for pointing out this important issue, which is indeed crucial for understanding the catalytic mechanism.

Inspired by this suggestion, we have re-examined the HER mechanisms to gain a deeper understanding. In alkaline media, HER typically proceeds via Volmer-Heyrovsky and/or Volmer-Tafel steps, in which Volmer step, Heyrovsky step, and Tafel step refers to water dissociation (Volmer: $H_2O + e^- + {}^* \rightarrow H^* + OH^-$), electrochemical desorption (Heyrovsky: $H^* + H_2O + e^- \rightarrow H_2 + OH^-$), and chemical recombination (Tafel: $H^* + H^* \rightarrow H_2$), respectively. As shown in Figure R1, the calculated Tafel slopes are 153 and 282 mV dec^{-1} for CoPc/OCNT and CuPc/OCNT, respectively, both higher than 120 mV dec^{-1}, indicating that the Volmer step is the rate-determining step (Sci. Rep., **5**, 13801 (2015); Angew. Chem. Int. Ed. **64**, e202504667 (2025)). Therefore, we have calculated the energy barrier for the water dissociation associated Volmer step. As shown in Figure 1h, CoPc/OCNT exhibits a substantially lower energy barrier for H_2O dissociation than CuPc/OCNT, suggesting that the Volmer step is much more favorable on CoPc/OCNT. Therefore, CoPc/OCNT displays higher HER activity than CuPc/OCNT, consistent with the LSV and DEMS results.

In addition, we would like to note that the high HER performance of CoPc/OCNT does not imply a higher H_2 generation rate during EASH. In contrast, under EASH conditions, the H_2 generation on CoPc/OCNT is in fact lower than that on CuPc/OCNT. A similar phenomenon was also observed in previous work on EASH systems (Nat. Commun. **14**, 8384 (2023)). This phenomenon can be attributed to the competition between EASH and HER on the catalyst surface. Namely, the *H produced through the H_2O dissociation is quickly captured by adsorbed C_2H_2 to form C_2H_4, which reduces the surface *H level and thus slows down HER. In most cases, the

byproduct H_2 is generated via chemical recombination between $^*H$ rather than electrochemical desorption ($H^* + H_2O + e^- \rightarrow H_2 + OH^-$). Therefore, to explain this phenomenon, calculations of $^*H$ coupling were also performed. One can see that CoPc/OCNT gives a slightly higher energy barrier for $^*H$ coupling, thereby suppressing the byproduct H_2 formation under EASH. We acknowledge that our original phrasing might have been misleading, and we have now revised the text to clarify the relationship between the theoretical and experimental results.

To avoid misunderstanding, we have revised the text on page 6 as follows:

Page 6-7: "Subsequent analysis of water dissociation barriers shows that CoPc/OCNT had a markedly lower barrier for H_2O dissociation than CuPc/OCNT (Fig. 1h and Supplementary Fig. S3). Therefore, the facilitated H_2O dissociation not only leads to higher HER activity under Ar, as the H_2O dissociation-associated Volmer step is rate-determining, consistent with earlier LSV and DEMS results, but also, under C_2H_2, the rapidly generated $^*H$ is preferentially consumed by hydrogenation of adsorbed C_2H_2, which, together with the elevated C–C coupling barrier and $^*H$–$^*H$ coupling barrier (Fig. 1i, Supplementary Figs. S3 and S4), accounts for the high C_2H_4 selectivity and the absence of detectable C_4 products on CoPc/OCNT."

Comment 4: Regarding the characterization, for Figure S8, reference pattern should be provided for the XRD data. In addition, there is an inconsistency in Figure S9: the main text refers to FTIR, while the SI shows a Raman spectrum. Also, according to the literature, CoPc can typically be detected in the lower wavenumber region (600–700 cm^{-1}) with Raman, which does not overlap with CNT vibrations (see J. Am. Chem. Soc. 2025, 147, 14, 12298–12307, Fig. S13). The authors should carefully examine this region. For Xanes, reference spectra of bare CoPc in Figure S13 should be provided for comparison.

Response to comment 4: We thank the reviewer for these valuable comments.

Following this suggestion, the reference diffraction patterns of CoPc and CNT have been added in Fig. S8 for comparison (Fig. R1). No characteristic diffraction peaks of CoPc were observed in CoPc/XCNT, indicating that CoPc is well-dispersed on the functionalized CNT surface.

The inconsistency in Figure S9 has been corrected (the spectrum is indeed Raman rather than FTIR). Following the reviewer's suggestion, we carefully re-examined the 600–700 cm^{-1} region of the Raman spectra (Fig. R2). For the optimized CoPc/XCNT catalyst, no CoPc-related Raman peaks

are detected in this region, which is consistent with the XRD results and further supports the high dispersion of CoPc. To further certify this, we also measured a sample with higher CoPc loading (CoPcNCNT-10, CoPc/NCNT=1:10, m/m). In this case, clear CoPc characteristic peaks appear in the 600–700 cm^{-1} and 1500-1600 cm^{-1} regions of the Raman spectrum, further confirming that their absence in CoPc/XCNT arises from the high dispersion of CoPc. The reference (J. Am. Chem. Soc. 2025, 147, 12298–12307) has also been included in the revised manuscript for comparison and discussion.

Regarding the XANES data, the soft XANES spectra (O, N, and S K-edge) in Fig. S13 were used to probe the electronic interaction between the functionalised CNT supports and the Co atom in CoPc. To assess the influence on CoPc, hard Co K-edge XANES of bare CoPc has already been provided as a reference in the main text (Fig. R3), where a detailed comparison of the Co electronic structure in CoPc and CoPc/XCNT is presented.

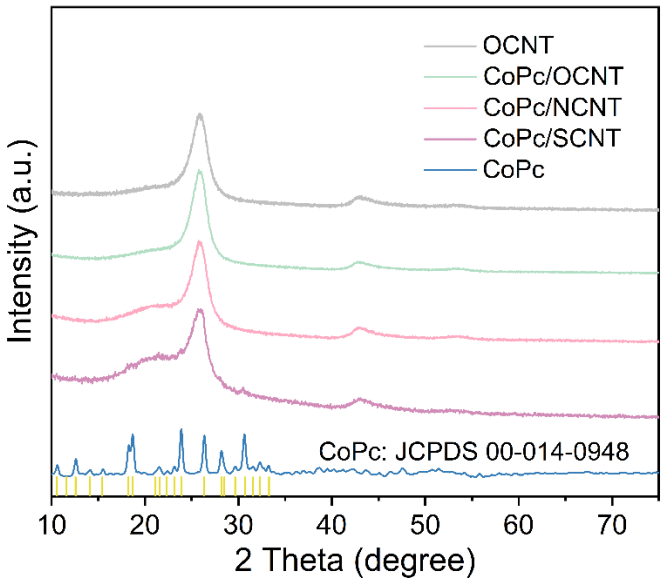

Fig. R1 | XRD patterns of OCNT, CoPc, CoPc/OCNT, CoPc/NCNT, and CoPc/SCNT.

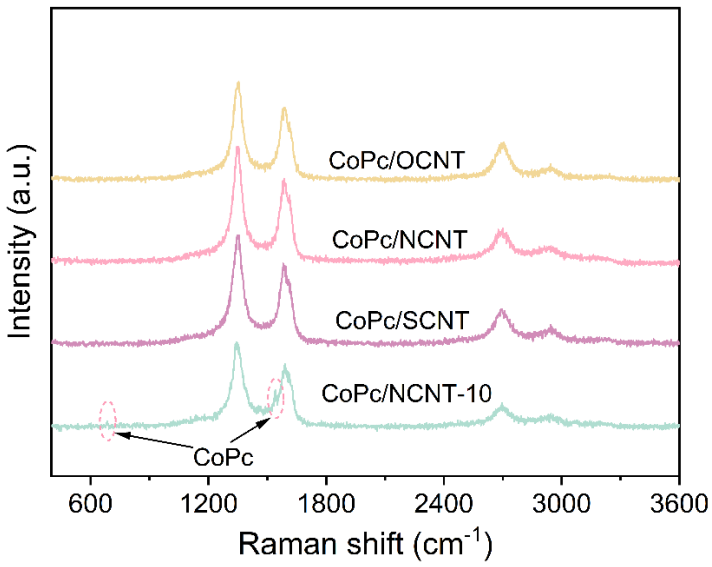

Fig. R2 | Raman spectra of CoPc/OCNT, CoPc/NCNT, and CoPc/SCNT.

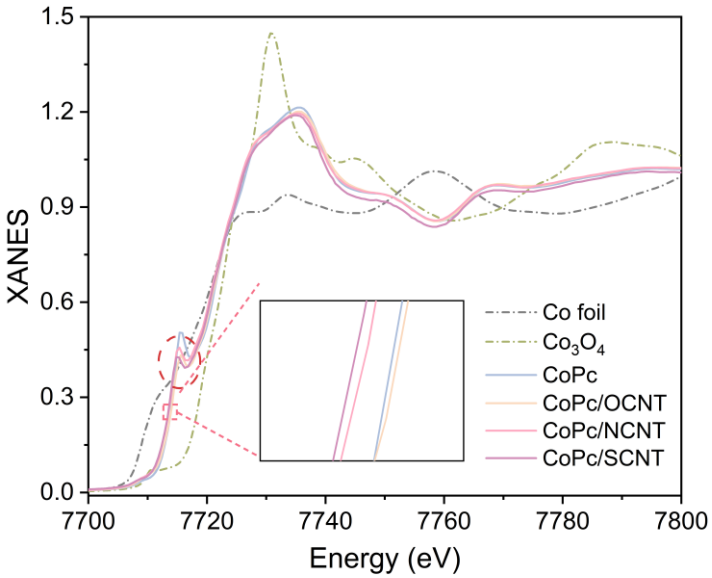

Fig. R3 | XANES spectra of the Co foil, Co_3O_4, CoPc, CoPc/OCNT, CoPc/NCNT, and CoPc/SCNT.

Comment 5: For the AC-STEM images (Figures 2d and S12), the legend for the 3D heat map is missing and should be provided with length-scale if possible.

Response to comment 5: We appreciate the reviewer for pointing this out.

The missing legend for the 3D intensity heat map has now been added to Fig. R4 (Revised Manuscript Fig. 2d) and R5 (Revised Supplementary Fig. S14), together with the corresponding color scale and length-scale bar, as shown below.

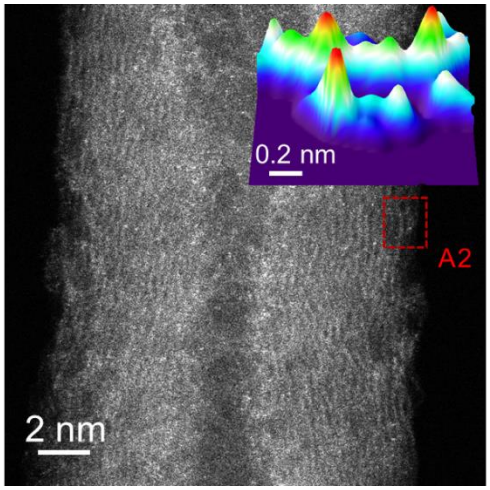

Fig. R4 | AC-STEM images and 3D atom-overlapping Gaussian-function map for CoPc/NCNT.

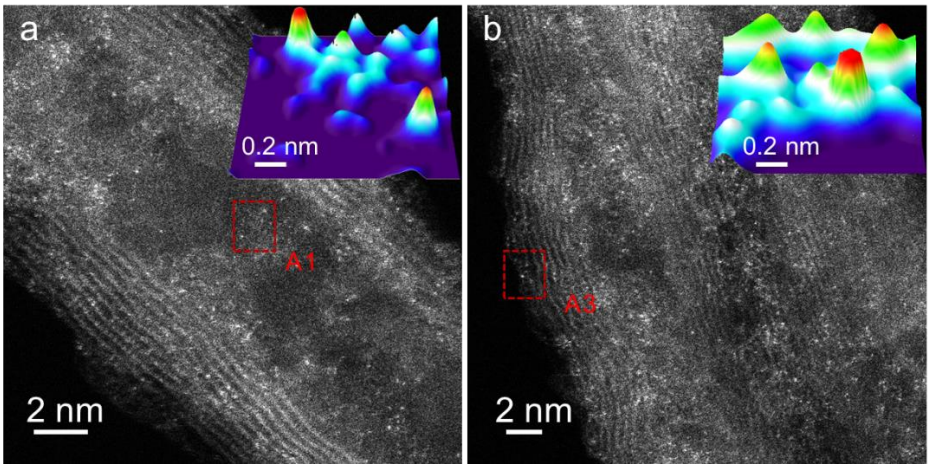

Fig. R5 | AC-STEM images and 3D atom-overlapping Gaussian-function map for (a) CoPc/OCNT and (b) CoPc/SCNT.

Comment 6: In general, it would be important to include error bars, for example in the ICP-OES data, to highlight the reproducibility of the synthesis and Co loading. Likewise, Table S2 for the EXAFS Fits should report explicit error values rather than only providing a general description below the table.

Response to comment 6: We appreciate the reviewer for this valuable comment.

The ICP-OES data have been updated based on three independent synthesis batches, and the corresponding standard deviations are now included in Table R1, as shown below. These results confirm the good reproducibility of the synthesis and Co loading.

Table R2 has been revised to explicitly list the fitting uncertainties for bond length and Debye–

Waller factor, rather than providing only a general note.

We have added these results to the revised Supplementary Information (Page S28)

Table R1 | Co mass loading of CoPc/OCNT, CoPc/NCNT, and CoPc/SCNT.

Catalysts	Loading (wt. %)	Standard Deviation (%)
CoPc/OCNT	0.55	±0.01
CoPc/NCNT	0.47	±0.055
CoPc/SCNT	0.57	±0.026

Table R2 | Co K-edge EXAFS curve-fitting parameters of CoPc/XCNT and reference samples.

Sample	Path	CN	R (Å)	σ^2 ($\times10^{-3}$Å^2)	ΔE_0 (eV)	R factor
Co foil	Co-Co	**12**	2.49±0.003	6±0.3	0.7±0.03	0.001
CoPc/OCNT	Co-N	4.1	1.91±0.007	3.3±1.2	5.0±2.58	0.017
	Co-O	1.1	1.96±0.03	2.3±4.8		
CoPc/NCNT	Co-N1	4.0	1.92±0.02	3.4±1.1	-0.47±3.25	0.014
	Co-N2	1.1	2.13±0.04	1.0±0.5		
CoPc/SCNT	Co-N	4.3	1.90±0.05	5.7±4.4	·0.02±7.29	0.015
	Co-S	0.8	2.18±0.03	1.6±5.8		

CN: coordination numbers; R: bond distance; σ^2: Debye-Waller factors; ΔE_0: the inner potential correction. R factor: goodness of fit. S_0^2 (0.8) was obtained from the experimental EXAFS fit of Co foil reference by fixing CN as the known crystallographic value and was fixed to all the samples.

Comment 7: For the explanation of the XANES-data in Figure 2f the authors should provide a clearer explanation of the significance of the pre-edge shift observed and how this correlates with the different CNTs.

Response to comment 7: We thank the reviewer for this helpful comment.

In the revised manuscript, we have clarified the overall characterization sequence and the

specific significance of the Co K-edge pre-edge feature in Figure 2f, as well as its correlation with the different CNT supports.

First, soft X-ray absorption spectroscopy (O, N, and S K-edge XANES) was carried out at a synchrotron beamline to probe the electronic interaction between CoPc and the heteroatom-doped CNT supports. These spectra identify the formation of axial Co–O, Co–N, and Co–S bonds in CoPc/OCNT, CoPc/NCNT, and CoPc/SCNT, respectively, confirming strong d–p orbital coupling between CoPc and the XCNT supports. Next, Co 2p XPS was used to evaluate the Co valence state. The Co $2p_{3/2}$ binding energy follows the order CoPc/SCNT < CoPc < CoPc/NCNT < CoPc/OCNT, indicating that the Co valence increases from S- to N- to O-coordinated CoPc, in line with the increasing electronegativity (and decreasing electron-donating ability) of the axial ligands. Finally, Co K-edge XANES and EXAFS were employed to resolve the fine local coordination structure of Co in CoPc/XCNT. In Fig. 2f, all CoPc/XCNT samples display a distinct pre-edge peak at ~7715 eV, which originates from the 1s → 3d transition of the square-planar Co–N_4 center and thus confirms that the in-plane Co–N_4 configuration of CoPc is preserved on the CNT supports. Moreover, the pre-edge (and edge) position shows a systematic shift that correlates with the heteroatom in the CNT: compared with bare CoPc, CoPc/OCNT shifts to higher energy, whereas CoPc/NCNT and CoPc/SCNT shift to lower energy. This energy sequence (CoPc/OCNT > CoPc > CoPc/NCNT > CoPc/SCNT) reflects the stronger electron-withdrawing character of axial O compared with N and S, leading to the highest Co valence in CoPc/OCNT and progressively lower Co valence in CoPc/NCNT and CoPc/SCNT. This trend is fully consistent with the Co 2p XPS results and demonstrates that the heteroatom-doped CNTs can regulate the Co 3d electronic structure via axial coordination.

We have added the above results and discussions to the revised manuscript (Page 10).

Page 10: "In particular, the Co $2p_{3/2}$ binding energies followed the order CoPc/SCNT (779.1 eV) < CoPc (779.8 eV) < CoPc/NCNT (780.8 eV) < CoPc/OCNT (780.9 eV), indicating a gradual increase in Co valence from S- to N- to O-coordinated CoPc. This trend was consistent with the increasing electronegativity and decreasing electron-donating ability of the axial ligands from S to N to O, confirming that the Co electronic structure can be precisely tuned by the heteroatom-doped CNT support. To further elucidate the local coordination environment of Co in CoPc/XCNT, Co K-edge

XANES and extended X-ray absorption fine structure (EXAFS) analyses were performed. As shown in Fig. 2f, the near-edge absorption intensity of the Co K-edge for CoPc-XCNT was between those of Co foil and Co_3O_4, confirming that Co was in a positively charged state. All CoPc/XCNT catalysts exhibited a distinct pre-edge feature at ~7715 eV, which was characteristic of the 1s→3d transition of the square-planar Co–N_4 center, demonstrating that the in-plane Co–N_4 configuration of CoPc was retained on the CNT supports. Notably, the pre-edge (and edge) position exhibited a systematic shift that correlates with the heteroatom in the CNT: compared with bare CoPc, CoPc/OCNT showed a shift to higher energy, while CoPc/NCNT and CoPc/SCNT shift to lower energy. This energy sequence (CoPc/OCNT > CoPc > CoPc/NCNT > CoPc/SCNT) reflected the stronger electron-withdrawing character of axial O relative to N and S, leading to a higher Co valence in CoPc/OCNT and a progressively lower valence in CoPc/NCNT and CoPc/SCNT, fully consistent with the XPS results."

Comment 8: The SI should also include the measured electrode potentials. In Figure 3e, it is unclear whether E_{cell} refers to the working electrode potential or the total cell voltage, this should be specified. In the Methods section, all potentials are described as iR-corrected, yet in the SI no such correction appears to be applied. Please provide the typical ohmic drop values. Additionally, in many current density plots in the SI (e.g. Figure S17), the authors note "The results are presented without iR compensation", but since no potential values are shown in the graphs, this statement is not meaningful.

Response to comment 8: We thank the reviewer for these careful comments on the electrochemical data presentation and fully agree that the potential definitions and iR treatment should be clearly and consistently stated.

First, we apologize for the inaccurate wording regarding iR correction in the original Methods section. After carefully re-checking all datasets, we confirm that all electrochemical data in this work are presented without iR compensation. This has now been explicitly stated in the Methods and corrected consistently throughout the main text and Supplementary Information.

Second, in Figure 3e, E_{cell} refers to the total cell voltage (i.e., the full cell voltage between cathode and anode measured by the potentiostat), not the single working-electrode potential. We have revised the Figure 3e caption to clearly specify that E_{cell} is the overall cell voltage and that it is

shown without iR correction. Following the reviewer's suggestion, we have also added the measured cell voltages at different current densities to the revised Supplementary Information (Fig. R6), so that the operating potentials of the electrodes are explicitly documented.

Regarding the ohmic drop, because of the specific flow-cell design used in this work, we were not able to obtain reliable solution resistances from conventional EIS measurements. Instead, we determined (i) the intrinsic resistance of the catalyst by a four-point probe setup and (ii) the overall resistance of the electrocatalytic system using the potentiostat. As summarised in Table R3, the resistances of the three CoPc/XCNT electrodes vary only slightly, indicating that the ohmic losses are very similar across these samples and do not account for the observed differences in activity and selectivity. In line with this, we have simplified and corrected the captions of the relevant SI figures (e.g., the original Figure S17) by removing redundant statements such as "without iR compensation" and we now state once in the SI that all potentials in this work are reported without iR correction unless otherwise noted.

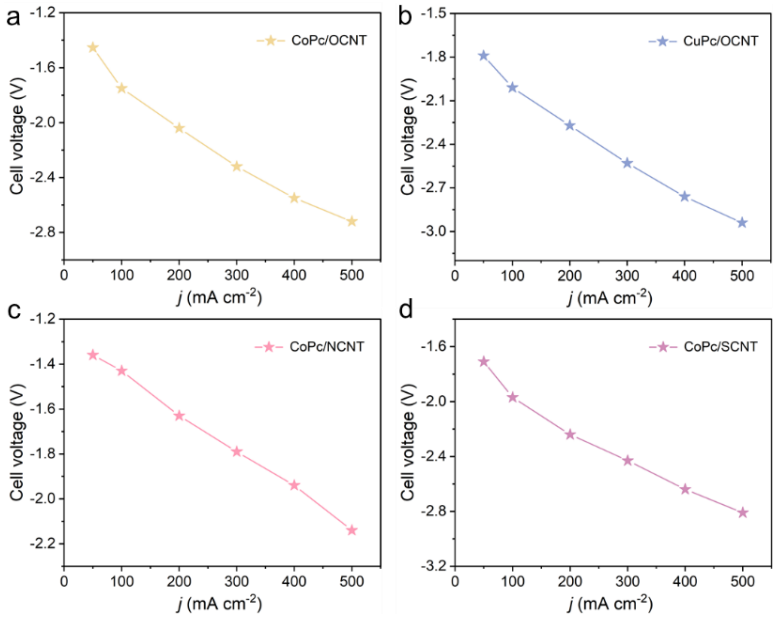

Fig. R6 | The obtained cell voltage in C_2H_2 flow over CoPc/OCNT, CuPc/OCNT, CoPc/NCNT, and CoPc/SCNT under different current densities.

Table R3 | The catalyst resistances and system resistances of measured at working conditions.

Sample	Catalyst resistances (Ω)	System resistances (Ω)

CoPc/OCNT	0.018±0.003	1.9±0.1
CoPc/NCNT	0.029±0.011	2.0±0.2
CoPc/SCNT	0.086±0.009	2.2±0.2

Comment 9: On page 10, the statement "Impressively, at an industrial-level current density of 500 mA cm^{-2}, the FE for C_2H_4 remained above 85%, continuing to fall within the profitable region and indicating the excellent economic potential of the CoPc/NCNT catalyst towards EASH (Figure S18)" requires clarification. How is the "profitable region" defined, and what is the energy efficiency of the reaction under these conditions? What metrics are truly required for industrial application? Moreover, Figure S18 shows GC data, which does not support this economic claim. On page 11, the stability discussion is also incomplete. The authors show that at 100 mA cm^{-2} the catalyst remains stable for 60 h (Figure 3e), but no data are provided at 500 mA cm^{-2}, which would be necessary to support claims of industrial relevance.

Response to comment 9: We thank the reviewer for this visionary comment.

In the revised manuscript, we clarify that the term "profitable region" is adopted from the techno-economic analysis reported in Nat. Sustain. **6**, 827–837 (2023), where the cost of electrocatalytic acetylene semi-hydrogenation was evaluated under defined boundary conditions, including capital, operating, and materials costs. In that work, operation at about 0.4 A cm^{-2} with FE(C_2H_4) ≥ 70% was identified as a regime in which the process can be economically viable (Fig. R7). In our system, CoPc/NCNT reaches FE(C_2H_4) >85% at 0.5 A cm^{-2} in 1 M KOH, which lies within and in fact exceeds the current-density/Faraday-efficiency window identified in that work. Furthermore, we have conducted a full process-level techno-economic assessment based on the same framework (Nat. Sustain. **6**, 827–837 (2023)). The results demonstrate that C_2H_4 production using CoPc/NCNT can attain a gross margin of approximately 19.7%, underscoring its strong potential for industrial implementation (Revised Supplementary Note 2, Page 32). Following the discussion in Nat. Sustain. **6**, 827–837 (2023), we think that relevant industrial metrics include high FE(C_2H_4) at different current densities, low cell voltage, and high energy efficiency, long-term stability at the target current density, high single-pass acetylene conversion, and polymer-grade ethylene purity, as well as favourable system-level costs.

Regarding stability, we agree that data at 500 mA cm^{-2} are important to support any statement about industrial relevance. In addition to the 60 h test at 100 mA cm^{-2} shown in Fig. 3e, we have now carried out a stability test at 500 mA cm^{-2} in 1 M KOH. As shown in Fig. R8, CoPc/NCNT maintains FE(C_2H_4) above 80% with almost no decay in performance over 10 h of continuous operation at 500 mA cm^{-2}.

The related contents have been included in the revised manuscript and supplementary information (Page 12, Supplementary Fig. S26 and Note 2 in Page S13 and S32, respectively).

Page 12: "Under a more demanding current density of −500 mA cm^{-2} in 1 M KOH, CoPc/NCNT still sustains an FE(C_2H_4) above 80% over 10 h of continuous operation (Supplementary Fig. S25)."

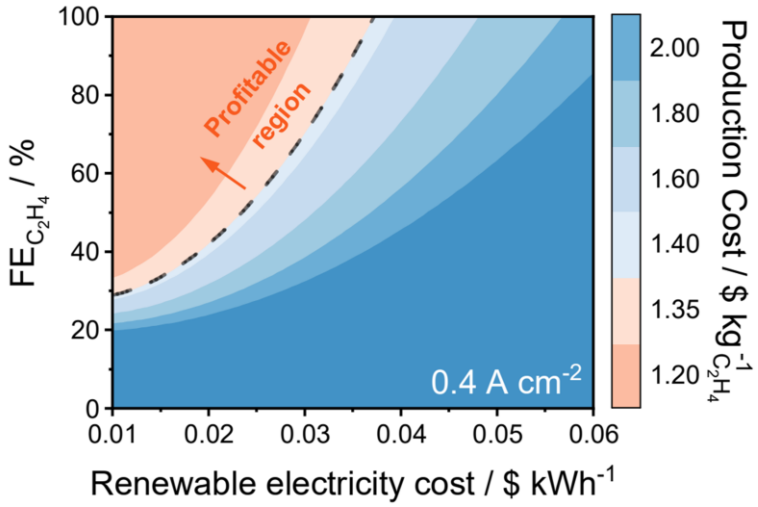

Fig. R7 | Techno-economic analysis results under different current densities from 0.4 A cm^{-2}.

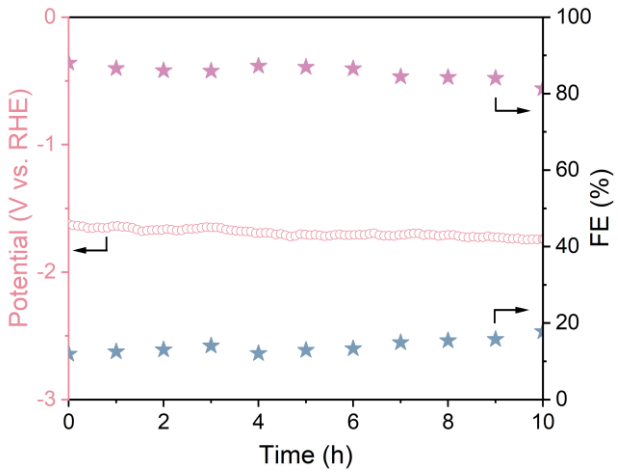

Fig. R8 | Long-term stability using CoPc/NCNT at a constant current density of −500 mA cm^{-2}.

Comment 10: The authors compare CoPc with supported CoPc on OCNT, SCNT, and NCNT. However, a direct comparison with CoPc on bare CNTs is missing. Including this control is important to clearly demonstrate the necessity and benefit of CNT functionalization.

Response to comment 10: We appreciate the reviewer for this valuable comment.

In the revised manuscript, we have now included CoPc supported on bare commercial CNTs (CoPc/CNT) as an additional control to directly assess the effect of CNT functionalization. As shown in the revised Fig. R9a, the presence of oxygen functionalities still leads to a higher polarization current density in the LSV of CoPc/OCNT compared with CoPc/CNT. The product distribution at 100 mA cm^{-2} (Fig. R9b,c) further highlights the benefit of functionalization. CoPc/CNT exhibits notable parasitic reactions, with Faradaic efficiencies of 11.7% for H_2, 0.47% for over-hydrogenation to C_2H_6, and 0.44% for C–C coupling products. In contrast, CoPc/OCNT shows Faradaic efficiencies of 8.1% for H_2, 0% for C_2H_6 and C_4 products, indicating strongly suppressed side reactions and improved selectivity. These new results further demonstrate that CNT functionalisation is essential for optimising the intrinsic performance of molecular CoPc in EASH.

The related contents have been included in the revised manuscript and supplementary information (Page 11, Supplementary Fig. S23, Page S12).

Page 11: "Compared with the CoPc supported on bare commercial carbon nanotubes (CoPc/CNT), most CoPc/XCNT catalysts significantly suppress side reactions and enhance selectivity, indicating the effectiveness of molecular regulation in enhancing EASH performance (Supplementary Fig. S23)."

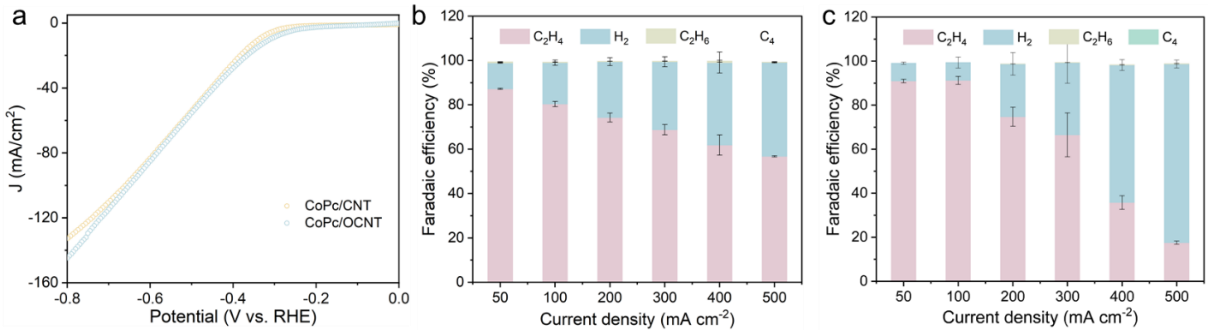

Fig. R9 | (a) LSV curves and Faraday efficiency of the obtained products using CoPc/CNT (b) and CoPc/OCNT (c) at various current densities.

Comment 11: In Figure S22, the data for the lowest loading and lowest current appear significantly different and may represent an outlier. Is this result reproducible? On page 11, the authors state that CoPc/NCNT with 5 wt% CoPc and a loading of 0.4 mg cm^{-2} was used and gave the best electrocatalytic performance. How does this loading on CNT and catalyst loading compare with other reports on CoPc–CNT systems, for example in CO_2RR to CO or methanol? Is the chosen loading consistent with the literature, or does it need to be specifically adjusted for the present reaction? What kind of GDE is used?

Response to comment 11: We appreciate the reviewer for this insightful comment.

1. Reproducibility of the lowest-loading data in Figure S22

Thank you for pointing this out. We have now repeated the measurements of the varied loading experiments at least three times in independent experiments under identical conditions (CoPc/NCNT with 5 wt% CoPc in 1 M KOH). The new results are reproducible and exhibit the same trend in the loading effects as observed previously, in which the CoPc/NCNT with the loading of 0.4 mg cm^{-2} exhibits the best EASH performance (Fig. R10). Error bars have been included in Fig. S29 in the revised Supplementary Information.

2. Comparison of CoPc/NCNT loading with literature and rationale for our choice

As stated on page 11, we finally used CoPc/NCNT with 5 wt% CoPc and a total catalyst loading of 0.4 mg cm^{-2} on the gas diffusion electrode, which corresponds to an effective CoPc loading of ~0.02 mg cm^{-2}. In this work, these values were chosen following the systematic investigation in the corresponding parameter experiments: we systematically varied both the CoPc content and the total loading and identified 5 wt% and 0.4 mg cm^{-2} as the best compromise between high FE for C_2H_4 and high (partial) current density for EASH in 1 M KOH (Fig. R10).

To directly address the reviewer's concern, we also compared our loading with four representative reports on CoPc–CNT systems used in gas-diffusion configurations for CO_2RR to CO or methanol electrocatalysis (Nat. Nanotech. **20**, 515-522 (2025); Nat. Comm. **16**, 7359 (2025); Nat. Comm. **8**, 14675 (2017); Nat. Comm. **7**, 987-999 (2024)). In those studies, the total catalyst loading is typically on the order of 0.4–1.2 mg cm^{-2}, with CoPc contents from a few to several tens of wt%. Our electrode (5 wt% CoPc, 0.4 mg cm^{-2}) lies well within the range used in the literature and, in terms of CoPc amount per geometric area, is in many cases slightly lower (Table R4). Meanwhile,

we have to note that the optimal loading window is unavoidably reaction- and setup-dependent. For the present acetylene hydrogenation in 1 M KOH, the screening shown in Figure S22 indicates that the chosen loading is specifically suited to balance intrinsic activity and mass transport in our GDE flow cell.

3. Type of GDE

The gas diffusion electrode used in this study is a commercial carbon-paper GDE, Sigracet 28BC (SGL Carbon), with a microporous layer, purchased from Fuel Cell Store. This information has been added to the Experimental section in the revised manuscript (Page 21).

Page 21: "The GDL (SGL, 28BC), Pt foil (0.4-mm thickness), anion exchange membrane (fumasep FAB-PK-130) was purchased from Fuel Cell Store."

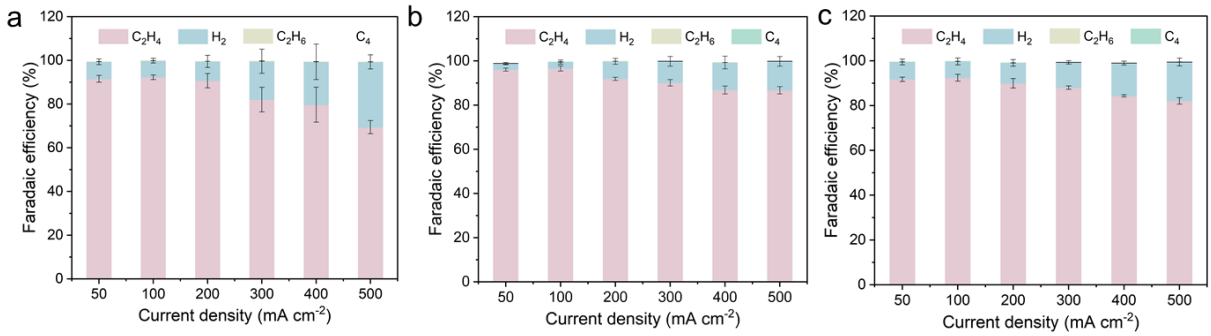

Fig. R10 | Faraday efficiency of the obtained products over (a) CoPc/NCNT-1, (b) CoPc/NCNT-5, and (c) CoPc/NCNT-10 at various current densities.

Table R4 | Benchmarking of CoPc loading and total catalyst loading against literature.

Catalyst	CoPc loading (wt%)	Catalyst loading (mg cm^{-2})	Reference
CoPc/NCNT	5	0.4	This work
CoPc-NH_2/CNT	6.5	1.2	Nat. Nanotech. **20**, 515-522 (2025).
CoPc/CNT(III)	6.67	0.4	Nat. Comm. **16**, 7359 (2025).
CoPc-CN	6	0.4	Nat. Comm. **8**, 14675 (2017).
CoPc/CNT	5	0.4	Nat. Comm. **7**, 987-999 (2024).

Comment 12: Regarding the change in Co oxidation state observed by in situ XANES: can the authors provide clearer insights into the specific oxidation state transition (e.g., from which to which

state)? The statement "This valence reduction was correlated with electron transfer from Co to adsorbed C_2H_2 species, facilitating rapid acetylene reduction and clearly confirming Co as the primary active site" is difficult to follow. Is this conclusion directly supported by the presented data, or is it primarily drawn from the literature?

Response to comment 12: We thank the reviewer for the valuable suggestion.

In the Co K-edge XANES of CoPc/NCNT, the spectrum at open-circuit potential lies between Co foil and CoO, indicating a $Co^{\delta+}$ state between metallic Co and Co(II). Under EASH-relevant cathodic potentials, the absorption edge shifts to lower energy and the white-line intensity decreases, showing that the Co centres become partially reduced during operation. The original sentence stating that "this valence reduction was correlated with electron transfer from Co to adsorbed C_2H_2 species, facilitating rapid acetylene reduction and clearly confirming Co as the primary active site" was a bit strong and has been revised. In the updated text, the in situ XANES data are presented as evidence that the Co centres in CoPc/NCNT are electronically responsive under EASH conditions and directly participate in the electrochemical process. The idea of charge redistribution between metal sites and adsorbed C_2H_2 is guided by the Cu-based EASH study in Nat. Commun. **12**, 7072 (2021), where C_2H_2 adsorption was shown to change the apparent oxidation state of Cu owing to electron transfer between Cu and the antibonding π orbital of $^*C_2H_2$. In our case, the conclusion that Co provides the main active sites is based on the negligible EASH activity of the bare NCNT supports, the pronounced increase in activity after introducing CoPc, and the potential-dependent changes observed at the Co K-edge under working conditions, interpreted together with this literature precedent, rather than on the XANES data alone.

We added the above discussions to the revised manuscript (Page 15).

Page 15: "The spectrum at open-circuit potential resembles that of molecular CoPc and lies between Co foil and CoO, indicating a $Co^{\delta+}$ state between metallic Co and Co(II). As the applied potential becomes more negative, the absorption edge shifts progressively to lower energy and the white-line intensity decreases (Fig. 4a), showing that the Co centres become partially reduced during operation. Together with the negligible EASH activity of bare NCNT and the pronounced activity enhancement after introducing CoPc, it is safe to conclude that CoPc-derived Co centres serve as the primary active sites in CoPc/NCNT[8]."

Comment 13: The peak assignments of the in situ FTIR data in Figure 4b do not align with the cited reference. The authors assign the bands at 1650 and 1559 cm^{-1} to the $^{*}C{\equiv}C$ bond of C_2H_2 and the generated $^{*}C{=}C$ bond adsorbed on CoPc/NCNT, respectively. However, according to the reference, adsorbed $^{*}C_2H_2$ species can be detected at 1641 cm^{-1} over ED–Cu NPs, while the band at 1577 cm^{-1} corresponds to $^{*}C_2H_3$, the key intermediate of C_2H_2 hydrogenation. Therefore, a more consistent assignment according to that reference would be 1650 cm^{-1} to $^{*}C_2H_2$ and 1559 cm^{-1} to $^{*}C_2H_3$. This interpretation would also better match the observed peak evolution, where the 1650 cm^{-1} band increases at higher overpotentials. Are these overpotential-dependent changes correlated with product selectivity? Furthermore, do the relative intensity changes of these two peaks align with the expected reaction pathway? The authors should also examine whether additional informative spectral regions around 2000 cm^{-1} are present in the FTIR spectra.

Response to comment 13: We appreciate the reviewer for this valuable comment.

In light of the cited reference and the reviewer's comment, the bands at 1650 and 1559 cm^{-1} in Figure 4b have been reassigned to adsorbed $^{*}C_2H_2$ and $^{*}C_2H_3$, respectively (Fig. R11). This assignment is consistent with the reported values for $^{*}C_2H_2$ (~1640 cm^{-1}) and $^{*}C_2H_3$ (~1570–1580 cm^{-1}) in the referenced work (Nat. Sustain. **6**, 827-837 (2023)), and with recent in situ FTIR data for EASH reported in Angew. Chem. Int. Ed. **64**, e202423381 (2025).

Regarding the potential-dependent evolution of these bands, we note that the in situ FTIR measurements were performed in an H-type cell, where C_2H_2 reaches the catalyst surface mainly via dissolution and diffusion in the liquid phase. Under these conditions, increasing cathodic overpotential enhances the accumulation and adsorption of C_2H_2 at the electrode–electrolyte interface, resulting in the growth of the 1650 cm^{-1} ($^{*}C_2H_2$) band at more negative potentials. The 1559 cm^{-1} band, assigned to $^{*}C_2H_2$, appears at intermediate potentials and then gradually increases, which is consistent with $^{*}C_2H_2 \rightarrow {}^{*}C_2H_3 \rightarrow C_2H_4$ as the main hydrogenation sequence. In the flow cell used for performance testing, gas-phase feed and mass transport conditions are different, and the dependence of product selectivity on potential is less pronounced.

The relative intensity changes of the two bands are in line with the expected reaction pathway. At low overpotentials, the $^{*}C_2H_2$ band is weak, and the $^{*}C_2H_3$ band is barely detectable, indicating limited activation of C_2H_2. With increasing overpotential, the $^{*}C_2H_2$ band at 1650 cm^{-1} increases,

and the $^{*}C_2H_3$ band at 1559 cm^{-1} grows and then tends towards saturation, which is consistent with $^{*}C_2H_2$ acting as a transient intermediate that is continuously converted to C_2H_4. This behaviour agrees with the intermediate evolution reported in Angew. Chem. Int. Ed. **64**, e202423381 (2025), and supports our proposed EASH mechanism as well.

Finally, the FTIR spectra were re-examined in the region around 2000 cm^{-1}. No additional well-resolved bands attributable to C≡C stretching or metal–hydride species were observed in this range; the signal is essentially featureless apart from background contributions. For this reason, this region is not shown in the main figure, and it does not alter the assignments or mechanistic interpretation based on the 1650 and 1559 cm^{-1} bands.

The related contents have been included in the revised manuscript (Page 15).

Page 15: "Subsequently, the EASH pathway on CoPc/NCNT and the associated interfacial water structure were investigated using potential-dependent in situ attenuated total reflectance Fourier transform infrared (ATR-FTIR) spectroscopy. In the O–H stretching region, the broad band between 2900 and 3700 cm^{-1} can be deconvoluted into contributions from 4-coordinated hydrogen-bonded water (4-HB·H_2O), 2-coordinated hydrogen-bonded water (2-HB·H_2O), and K^{+}-hydrated water (K·H_2O). With increasingly negative potentials, the intensity of the 4-HB·H_2O component decreases, while that of 2-HB·H_2O increases, suggesting that the interfacial hydrogen-bond network becomes more weakly bound and that water dissociation is facilitated[45], thereby increasing the availability of $^{*}H$ for the semi-hydrogenation of acetylene. In the lower-wavenumber region, positive bands at 1650 and 1559 cm^{-1} can be assigned to adsorbed $^{*}C_2H_2$ and the generated $^{*}C_2H_3$ intermediate on CoPc/NCNT, respectively. The intensity of the band corresponding to $^{*}C_2H_4$ grows continuously with potential, consistent with the high ethylene selectivity observed on CoPc/NCNT."

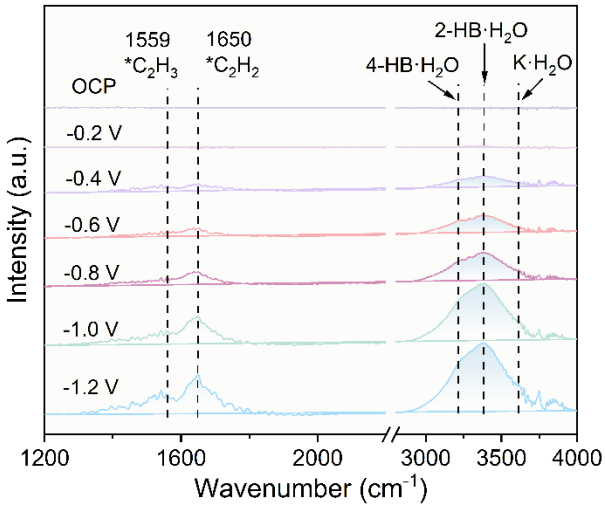

Fig. R11 | In situ electrochemical FT-IR spectra of CoPc/NCNT electrode for acetylene semi-hydrogenation in acetylene-saturated 1 M KOH solution.

Comment 14: On page 13, the discussion of pH variation and radical scavenger experiments is too brief and the conclusions are drawn too quickly. The pH was only varied slightly (from ~13.7 to ~14.3), which corresponds to a relatively small change in OH^- concentration. The authors should also specify which concentrations of KOH corresponds to which pH. In addition, when introducing *t*-BuOH as a radical scavenger, the exact concentration used (50 mM) should be reported in the main text. This is a relatively high concentration, and it should be clarified whether the observed effect can be attributed specifically to radical scavenging or to other interactions with the system.

Response to comment 14: We acknowledge the reviewer's constructive comments and suggestions.

In the revised manuscript, we specify the KOH concentrations and corresponding pH values and extend the pH window. The measurements were carried out in 0.5, 1.0, 2.0, and 5.0 M KOH (pH ≈ 13.7, 14.0, 14.3, and 14.7, respectively; see Fig. R12). Across this wider range of OH^- concentration, the polarization curves and FE for C_2H_4 on CoPc/NCNT change only marginally, even though the OH^- concentration varies by almost two orders of magnitude. This behaviour is difficult to reconcile with a dominant electron–proton coupled pathway of the form $^*C_xH_y + H_2O + e^- \rightarrow {}^*C_xH_{y+1} + OH^-$, for which a pronounced pH dependence would be expected. In the text, we now avoid the wording "effectively ruling out" and state more cautiously that an electron–proton coupled mechanism is unlikely to be the main pathway under our conditions.

For the radical scavenger experiment, we now explicitly report in the main text that *t*-BuOH

was added at a concentration of 50 mM. Although this is a noticeable amount, it is still below the 0.1–1.0 M range commonly used for alcohol-based *H scavengers in related electrochemical studies (Adv. Mater. e15346 (2025); Adv. Energy Mater. **15**, e03613 (2025); ACS Nano **19**, 8189−8199 (2025); Angew. Chem. Int. Ed. e202518122 (2025)). To further address the reviewer's concern, we performed additional measurements at a lower *t*-BuOH concentration of 20 mM (Fig. R13). After adding 20 mM or 50 mM *t*-BuOH, both the current density and the C_2H_2 conversion decrease markedly. This consistent suppression, together with the established role of *t*-BuOH as a *H scavenger, supports our assignment that the observed effect mainly arises from quenching of *H intermediates rather than from unspecific interactions of *t*-BuOH with the system.

We added the above results and discussions to the revised manuscript and supplementary information (Pages 15, Page S20, Supplementary Fig. S37-S39).

Page 15: "If the rate-determining step followed a proton-coupled electron transfer pathway of the form $^*C_xH_y + H_2O + e^- \rightarrow {}^*C_xH_{y+1} + OH^-$, the EASH activity would display a pronounced sensitivity to pH or OH^- concentration. The polarization curves and the C_2H_4 FE of CoPc/NCNT were then recorded in KOH solutions ranging from 0.5 to 5.0 M (pH≈13.7 to 14.7). With increasing pH, the polarization current density increases gradually, which can be mainly attributed to improved electrolyte conductivity and mass transport (Supplementary Fig. S37). In contrast, the onset potentials and the FE for C_2H_4 show no significant changes across this one-order-of-magnitude variation in OH^- concentration (Supplementary Fig. S38). Such behaviour is not typical of a step controlled by proton-coupled electron transfer, and suggests that the key hydrogenation step does not directly depend on the bulk proton or hydroxide activity under the present conditions. The role of *H intermediates was further probed by adding tert-butanol (*t*-BuOH), a radical scavenger that deactivates *H via 2-methyl-2-propanol formation. Upon addition of *t*-BuOH, the polarization current density and C_2H_2 conversion decrease markedly (Supplementary Fig. S39). The combination of a weak pH dependence and a strong sensitivity to *H scavenging indicates that surface-bound *H, rather than a direct proton-coupled electron-transfer step, serves as the key reactive intermediate in the electrocatalytic hydrogenation of C_2H_2 on CoPc/NCNT[46]."

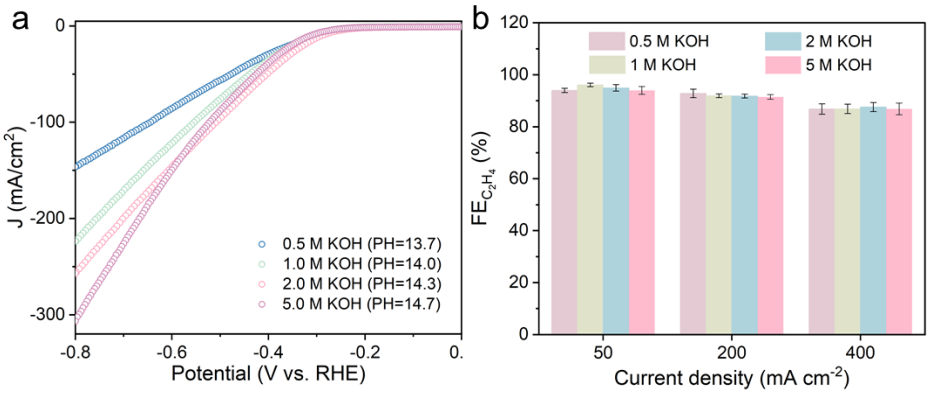

Fig. R12 | The effect of the KOH concentration on the (a) LSV curves and (b) Faraday efficiency of the obtained C_2H_4 over CoPc/NCNT.

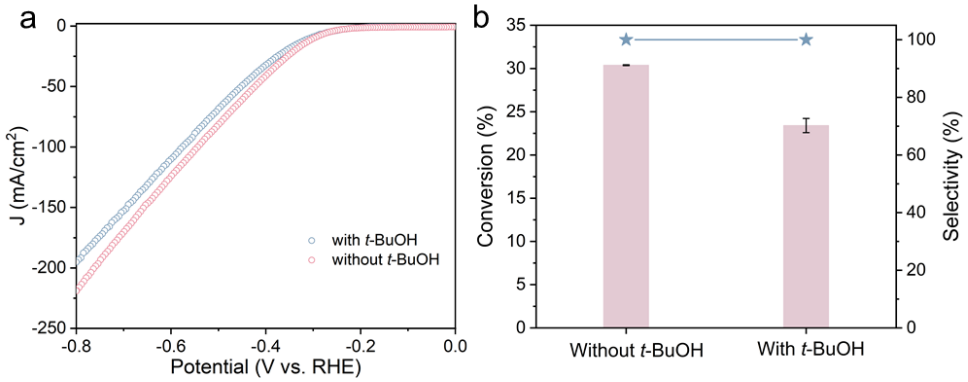

Fig. R13 | (a) LSV curves and (b) C_2H_2 conversion over CoPc/NCNT in 1.0 M KOH solution with and without 20 mM *t*-BuOH.

Comment 15: The reported EASH reaction kinetics follow the trend $K^+ > Na^+ > TMA^+$, with C_2H_2 conversion decreasing from K^+ to 10.4% TMA^+. How does this trend compare with previous literature? Have larger or smaller cations such as Cs^+ or Li^+ been tested? It is worth noting that molecular catalysts often exhibit very different cation-dependent effects compared to metallic catalysts (see Yu, S., Yamauchi, H., Wang, S. et al. Nat. Catal. 7, 1000–1009 (2024)).

Response to comment 15: We appreciate the reviewer's valuable comment.

In the original submission, we reported a cation dependence of $K^+ > Na^+ > TMA^+$, with C_2H_2 conversion dropping to 10.4% in the presence of TMA^+. In the revised version, we have added measurements in LiOH; the overall trend now becomes $K^+ > Na^+ > Li^+ > TMA^+$ in both current density and C_2H_2 conversion. This sequence is consistent with the cation effect reported for

electrocatalytic acetylene semi-hydrogenation in Nat. Commun. **14**, 8384 (2023), where K^+ is also the most promoting alkali cation, and large organic cations strongly suppress the reaction. The sub-series $K^+ > Na^+ > Li^+$ further agrees with the trend $Cs^+ > K^+ > Na^+ > Li^+$ observed by Yu et al for molecular CO_2-to-CO electrocatalysts (Nat. Catal. **7**, 1000–1009 (2024)), which we now explicitly cite in the revised manuscript. These trends can be understood in terms of ionic radius, hydration, and interfacial accumulation: moderately hydrated K^+ can approach the inner Helmholtz plane and more effectively modulate the local electric field and water structure, whereas the more strongly hydrated Na^+ and Li^+ remain further from the interface, and the bulky TMA^+ cation perturbs the interfacial region and severely suppresses EASH activity.

We added the above results and discussions to the revised manuscript (Page 16) and Supplementary Information (Page S21).

Page 16: "Large hydration numbers and effective ionic radii are expected to weaken specific interactions between cations and Co active sites. This effect was examined by substituting compact $K^+(H_2O)_7$ (n=7, r=3.3 Å) and $Na^+(H_2O)_{13}$ (n=13, r=3.6 Å) with more strongly hydrated $Li^+(H_2O)_n$ (larger hydration shell, r=3.8 Å) and bulky TMA^+ (n=18, r=4.5 Å) in 1 M KOH electrolytes (Supplementary Fig. S40). Under these conditions, the EASH kinetics follow the sequence $K^+ > Na^+ > Li^+ > TMA^+$, with C_2H_2 conversion decreasing from 30.3% (K^+) to 10.4% (TMA^+). This trend can be attributed to the ability of the cations to perturb and disrupt the interfacial hydration shell. Namely, the relatively compact $K^+(H_2O)_7$ cluster likely polarises interfacial H_2O networks more effectively than more strongly hydrated or bulkier cations, thereby facilitating water dissociation and the formation of reactive $^*H$ species on CoPc/NCNT."

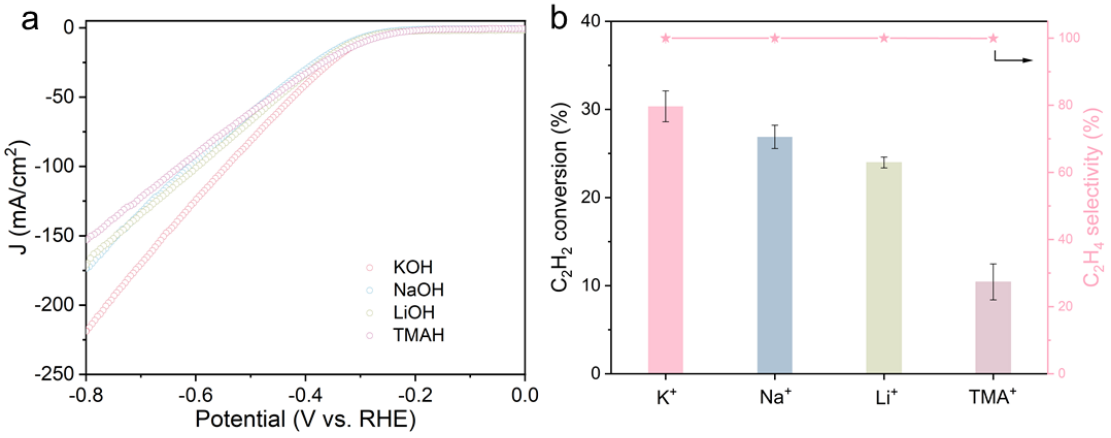

Fig. R14 | (a) LSV curves and (b) C_2H_2 conversion in 100% C_2H_2 flow over CoPc/NCNT with 1 M

KOH, NaOH, LiOH, and TMAH electrolyte.

Comment 16: More details about the gas feed are required. Was the acetylene introduced in ethylene or in argon? More details about the gas feed mixing is required. Additional clarification is also needed on the 1 cm^2 and 25 cm^2 flow cell setups, how exactly are they configured and operated? In the text, the authors state: "To satisfy the requirements for the industrial production of polymer-grade ethylene, the EASH performance was subsequently assessed under realistic conditions with 0.5% acetylene impurities (5000 ppm) in crude ethylene (Figure S33)." However, Figure S33 shows LSV curves of different gas concentrations.

Response to comment 16: We thank the reviewer for this important question and for the opportunity to clarify the experimental details.

In the 1 cm^2 flow cell, the inlet gas was 100% acetylene, used to evaluate the intrinsic catalytic activity toward acetylene semi-hydrogenation. Since the industrial scenario typically involves removing trace acetylene impurities from ethylene feed gas, we further examined the performance under different acetylene concentrations (original Fig. S33). These various concentrations were generated using a custom-built gas-mixing system, in which high-purity argon was used to dilute pure acetylene to the desired ratios.

Because acetylene is only sparingly soluble in the electrolyte, the semi-hydrogenation activity decreases significantly at lower acetylene concentrations, as shown in Fig. S33. To better simulate industrial conditions and validate the scalability, we designed a 25 cm^2 large-area flow cell, which was tested using a commercially purchased mixed gas (0.5% C_2H_2, 20% C_2H_4, balanced with Ar) representing a realistic crude ethylene stream. Under these conditions, the CoPc/NCNT catalyst exhibited excellent stability over 110 hours of continuous operation, demonstrating strong potential for industrial application.

Furthermore, we constructed a two-stage reactor system by coupling the 1 cm^2 and 25 cm^2 flow cells in series. The small cell was used to pre-convert pure acetylene to a low-acetylene mixture, which was then fed into the large-area cell to produce high-purity ethylene directly. This configuration highlights the practical relevance and scalability of our catalyst system.

All corresponding descriptions have been added to the revised manuscript for clarity (Methods, Page 22).

Comment 17: The Methods section requires substantial revision, as both the main text and the Supporting Information currently provide too few details to ensure reproducibility. The experimental procedures should be described comprehensively, including complete information on catalyst synthesis and functionalization (precursors, solvents, conditions, purification), electrode preparation and loading (mass loading, electrode area, binder composition, deposition procedure), and electrochemical testing protocols (cell configuration, electrolyte composition and preparation, gas feed composition and flow rates, reference and counter electrode details, iR compensation). In addition, the in situ and operando experiments (XANES, FTIR, EPR, DEMS) must be described in sufficient detail, including setups, acquisition parameters, and data analysis methods. Calibration and quantification procedures (e.g., GC, ICP-OES) should also be reported, together with error analysis and reproducibility tests. Without this level of detail, the results cannot be reliably reproduced, and the section must therefore be carefully revised and expanded to meet the standards of Nature Communications.

Response to comment 17: We sincerely thank the reviewer for emphasizing the importance of methodological transparency and reproducibility. We have thoroughly revised and expanded the Methods section in the revised manuscript to provide comprehensive experimental details that fully meet Nature Communications standards. The revisions are briefly summarized as follows.

Catalyst synthesis and functionalization: We have added full descriptions of precursor identities, solvent types, reaction concentrations, temperatures, times, and purification steps. The procedures for CNT functionalization and CoPc immobilization are now described step-by-step to ensure reproducibility.

Electrode preparation: We have included detailed information on ink formulation (binder type and ratio, solvent, concentration), catalyst mass loading, electrode area, and drop-casting procedure, along with the drying conditions.

Electrochemical testing: We have provided complete descriptions of the cell configuration (three-electrode setup, electrode arrangement, gas-diffusion electrode use), electrolyte composition and pretreatment, gas flow rate and composition, reference and counter electrode specifications, and clarified that all potentials are reported without iR compensation.

In situ and operando characterizations (XANES, FTIR, EPR, DEMS): We have expanded

the corresponding subsections with detailed information on the experimental setups, detection modes, data acquisition parameters, and data processing procedures.

Quantification and calibration: We have added descriptions of GC calibration using standard gases, ICP-OES calibration curves, and error ranges, and reproducibility tests based on three independent synthesis batches.

All newly added details have been highlighted in the revised manuscript (Methods, Pages 21-25). We appreciate the reviewer's comment, which has significantly improved the completeness, rigor, and reproducibility of our experimental section.

Comment 18: Minor comments:

-Page 5, ESAE should be EASH.

-The authors should write the minus sign for the current densities (I assume negative currents were applied).

-Hard to distinguish the colors (such as blue and green) in many of the plots.

Response to comment 18: We thank the reviewer for these careful observations. The typo on page 5 has been corrected from ESAE to EASH. The minus signs for current densities have been added throughout the manuscript and the Supporting Information to accurately indicate the applied cathodic currents. In addition, the color schemes of all relevant plots have been adjusted to improve contrast and readability, particularly for the blue and green traces.

Response to Reviewer #2:

General Comments:

In this work, the authors report a molecular cobalt phthalocyanine (CoPc) catalyst platform that promotes electrocatalytic acetylene semi-hydrogenation (EASH) reaction activity through electronic regulation. They also investigate the performance modulation strategies and reaction mechanisms of the corresponding molecular catalysts. The utilization of analogous molecular catalysts (CoPc and CuPc) for EASH catalysis have been previously reported [10.1016/j.cej.2021.134129]. Moreover, the authors' research and conclusions on the performance enhancement mechanism of CoPc/XCNT are not sufficiently clear. Therefore, I do not recommend publishing this work in Nature Communications.

Response: We thank the reviewer for the overall assessment and for carefully reading our manuscript.

We fully acknowledge that CoPc- and CuPc-based molecular catalysts for EASH have been reported previously (Chem. Eng. J. **431**, 134129 (2022)), and we agree that the original version did not clearly enough articulate how our work goes beyond these studies in both concept and performance. In the revised version, we emphasise that our contribution is not the use of CoPc or CuPc per se, but the establishment of a comparative MPc/XCNT platform and a coordination-engineering strategy that together link water dissociation, *H management, and C–C coupling:

1. **MPc/OCNT platform and water-dissociation–C–C coupling relationship**

Instead of focusing on one CoPc system, we construct a comparative MPc/OCNT platform (M = Cu, Co, Ni, Fe) under identical conditions. Within this platform, CoPc/OCNT is identified as the composition that combines faster water dissociation with a more suitable adsorption environment for key intermediates, leading to strongly suppressed C–C coupling compared with CuPc/OCNT. The same “water-dissociation-assisted suppression” of C–C coupling is also observed on NiPc/OCNT and FePc/OCNT, for which the C_4H_6 Faradaic efficiency remains below 0.15%. However, the side reactions differ: NiPc/OCNT suffers from severe HER, while FePc/OCNT is limited by pronounced over-hydrogenation to C_2H_6. These comparisons indicate that accelerating water dissociation is a general lever to mitigate C–C coupling within the MPc/OCNT family, but the

metal centre determines whether the generated *H is channelled into selective semi-hydrogenation, HER, or over-hydrogenation.

2. Axial coordination engineering on CoPc and CuPc for high-current EASH

While CoPc/OCNT already suppresses C_4 formation, it suffers from increasing HER at current densities above ~200 mA cm^{-2}. Guided by the mechanistic insight from the MPc/OCNT series, we introduce axial coordination control by immobilising CoPc on nitrogen- and sulfur-functionalised CNTs to obtain CoPc/NCNT and CoPc/SCNT. This allows us to tune water-dissociation kinetics and *H utilisation at the Co centre. Among these catalysts, CoPc/NCNT exhibits the fastest water dissociation and the most favourable *H utilisation, which alleviates HER at high current densities and completely suppresses detectable C–C coupling, with no C_4 products observed over the entire tested current range. To test whether this concept is general, we also synthesised CuPc/NCNT. CuPc/NCNT shows enhanced water-activation behaviour compared with CuPc/OCNT, and at 100 mA cm^{-2} the C_4H_6 Faradaic efficiency decreases from 1.40% on CuPc/OCNT to 0.80% on CuPc/NCNT. This marked reduction in C_4 formation confirms that axial N-coordination can also mitigate C–C coupling on CuPc, indicating that the coordination strategy is transferable within the MPc framework rather than being specific to CoPc.

3. Quantitative performance benchmark against the prior CoPc system

Using the TOF definition from Nat. Sustain. **6**, 827–837 (2023) and updated ICP-OES and gas-flow data, CoPc/NCNT reaches a TOF of 7019 min^{-1} at 500 mA cm^{-2}, far exceeding the performance of the homogeneous CoPc electrode (TOF = 0.29 min^{-1} at 100 mA cm^{-2}) reported in *Chem. Eng. J.*, even though ~11 times less CoPc is used in the current work. Under crude-ethylene-like feeds, CoPc/NCNT maintains >98% acetylene conversion and >95% C_2H_4 selectivity for 110 h. We now present these numbers explicitly as a direct comparison, and we have softened overly strong wording, positioning our data as a substantial step toward industrially relevant EASH rather than as an absolute record.

We appreciate the reviewer's concerns and, in response to the detailed comments, have added Ni/Fe/Cu controls, extended stability data, and refined mechanistic analysis. We hope that the revised manuscript makes it clearer that our work uses the MPc/XCNT platform and axial coordination engineering to establish and exploit a general link between water dissociation, C–C coupling, and EASH performance, rather than simply combining known CoPc/OCNT and

CuPc/OCNT motifs.

Specific Comments:

Comment 1: Apart from the already reported feasibility of metal phthalocyanines in the EASH process, the employed CoPc/OCNT and CuPc/OCNT are also widely used in various electrocatalytic reactions including CO_2RR, ORR, HER, and etc. (Angew. Chem. Int. Ed. 2024, 63, e202310623; Chem. Soc. Rev. 2021, 50, 12985; Nature, 2019, 575, 639). By simply combining the two points together, the present work is lack of innovation to be published in Nature Communications.

Response to comment 1: We thank the reviewer for this important comment.

We fully agree that metal phthalocyanines, including CoPc and CuPc, are now a well-established molecular platform in electrocatalysis, with extensive work in EASH, CO_2RR, ORR, HER, and related reactions. In the revised manuscript, we explicitly acknowledge this background and have re-positioned our contribution accordingly.

Our intention is not to claim novelty in using CoPc or CuPc per se, but rather in how we use a family of MPc/OCNT catalysts as a mechanistic platform and then translate the insight into a targeted coordination-engineering strategy. In particular:

1. **From a single CoPc catalyst to a comparative MPc/OCNT study of water dissociation and C–C coupling**

The previous EASH work demonstrated that CoPc and CuPc are feasible molecular catalysts. Building on this, we intentionally construct a broader MPc/OCNT series (M = Cu, Co, Ni, Fe) and use it as a controlled platform to dissect how different metal centres regulate water dissociation, *H coverage, and C–C coupling under the same support and morphology. Within this series, we find that CoPc/OCNT balances fast water activation with moderated *H binding, thereby suppressing C_4 formation relative to CuPc/OCNT. We then show that the same water-dissociation-assisted suppression of C_4 formation appears on NiPc/OCNT and FePc/OCNT, where the C_4H_6 FE remains below 0.15%. However, NiPc/OCNT is dominated by HER, and FePc/OCNT suffers from strong over-hydrogenation to C_2H_6. These comparisons reveal that enhancing water dissociation is a general way to mitigate C–C coupling and improve EASH activity within the MPc/OCNT family, while the specific metal centre determines how the generated *H is distributed among EASH, HER, and over-hydrogenation. We regard this "water dissociation–C–C coupling" relationship, established

across a controlled MPc/OCNT platform, as going beyond simply showing that CoPc/OCNT or CuPc/OCNT can catalyse EASH.

2. Axial coordination engineering on CoPc and CuPc for highly selective EASH

Guided by the above findings, we deliberately modify the molecular environment via axial coordination on amino- and thiol-functionalised CNTs, generating CoPc/NCNT and CoPc/SCNT. This tuning adjusts the Co electronic structure, water-dissociation kinetics, and *H binding, and leads to CoPc/NCNT as an optimised composition that combines rapid water dissociation with controlled *H coverage, thereby easing HER at high current densities and completely suppressing detectable C–C coupling (no C_4 products observed under our conditions). The optimised CoPc/NCNT delivers 86.7% C_2H_4 FE and 99.99% C_2H_4 selectivity at 500 mA cm^{-2}, complete suppression of C_4 products, a TOF of 7019 min^{-1} with ~11-fold lower CoPc usage than the Chem. Eng. J. system, and 110 h stability under crude-ethylene-like feed. To test generality on Cu, we additionally synthesised CuPc/NCNT. Compared with CuPc/OCNT, CuPc/NCNT shows enhanced water-activation behaviour, and at 100 mA cm^{-2} the C_4H_6 FE decreases from 1.40% on CuPc/OCNT to 0.80% on CuPc/NCNT. This clear drop in C_4H_6 formation demonstrates that axial N-coordination on CuPc also suppresses C–C coupling, indicating that the coordination strategy derived from the Co platform is transferable to other metal–phthalocyanine catalysts.

In light of the broader MPc literature, we have revised the Introduction and Discussion to clearly state that the main contribution of this work lies in (i) using a comparative MPc/OCNT platform to connect metal-centre identity, interfacial water activation, and C–C coupling in EASH, and (ii) translating this mechanistic understanding into an axial coordination strategy (with both N- and S-functionalised CNTs, and applied to both CoPc and CuPc) that delivers highly selective EASH at high current densities. We hope this makes it clearer that our study goes beyond a simple recombination of previously reported CoPc/OCNT and CuPc/OCNT motifs. And the work on MPc/OCNT has been cited in the introduction of our revised manuscript to highlight our contributions.

Comment 2: Except for the novelty issue, the data and analysis is not adequately to support their hypothesis and conclusions. For example, to exclude the CPET pathway, the author claimed that "the pH was varied from ~13.7 to ~14.3, negligible changes were observed in the polarization curves

and FE for C_2H_4 on CoPc/NCNT", which is contradictory to the data shown in Figure S27.

Response to comment 2: We acknowledge the reviewer's kind comments and suggestions.

For CPET-type EASH, Nat. Commun. **12**, 7072 (2021) has shown that lowering pH (increasing proton availability) typically leads to a clear increase in C_2H_4 Faradaic efficiency (Fig. R15), while the overall current density decreases due to lower KOH concentration (reduced conductivity and slower mass transport). This behaviour (monotonic enhancement of C_2H_4 selectivity with decreasing pH, accompanied by a drop in limiting current) is a characteristic signature of a proton-coupled electron transfer process. In contrast, non-CPET behaviour has been systematically discussed in Nat. Commun. **14**, 8384 (2023), where the C_2H_4 selectivity shows no systematic dependence on pH, while the LSV limiting current density still decreases at lower KOH concentration because of increased resistance and mass-transport limitations (Fig. R16). In other words, in a non-CPET regime, the pH mainly affects the solution environment (conductivity, diffusion) rather than the intrinsic surface kinetics of the rate-determining step.

Our updated pH-dependent measurements on CoPc/NCNT are consistent with this second scenario. As shown in the revised Fig. R17, decreasing KOH concentration (pH from 14.3 to 13.7) leads to a gradual decrease in the limiting current density in the LSV curves, which we now explicitly attribute to increased ohmic and mass-transfer limitations. However, the C_2H_4 Faradaic efficiency in this pH window does not exhibit a clear monotonic trend and fluctuates within the experimental uncertainty, rather than increasing systematically at lower pH as would be expected for a CPET-controlled process. We have extended the pH range to 13.7–14.7 and still do not observe a clear correlation between pH and C_2H_4 selectivity. Together with the literature benchmarks, these revised data and analyses support our conclusion that the rate-determining step on CoPc/NCNT does not follow a classical CPET pathway in the studied pH window.

All updated pH-dependent data and detailed discussion have been included in the revised manuscript (Page 15) and Supplementary Information (Page S20, Supplementary Fig. S37-S38).

Page 15: "If the rate-determining step followed a proton-coupled electron transfer pathway of the form $^*C_xH_y + H_2O + e^- \rightarrow {}^*C_xH_{y+1} + OH^-$, the EASH activity would display a pronounced sensitivity to pH or OH^- concentration. The polarization curves and the C_2H_4 FE of CoPc/NCNT were then recorded in KOH solutions ranging from 0.5 to 5.0 M (pH≈13.7 to 14.7). With increasing

pH, the polarization current density increases gradually, which can be mainly attributed to improved electrolyte conductivity and mass transport (Supplementary Fig. S37)[8]. In contrast, the onset potentials and the FE for C_2H_4 show no significant changes across this one-order-of-magnitude variation in OH^- concentration (Supplementary Fig. S38). Such behaviour is not typical of a step controlled by proton-coupled electron transfer, and suggests that the key hydrogenation step does not directly depend on the bulk proton or hydroxide activity under the present conditions."

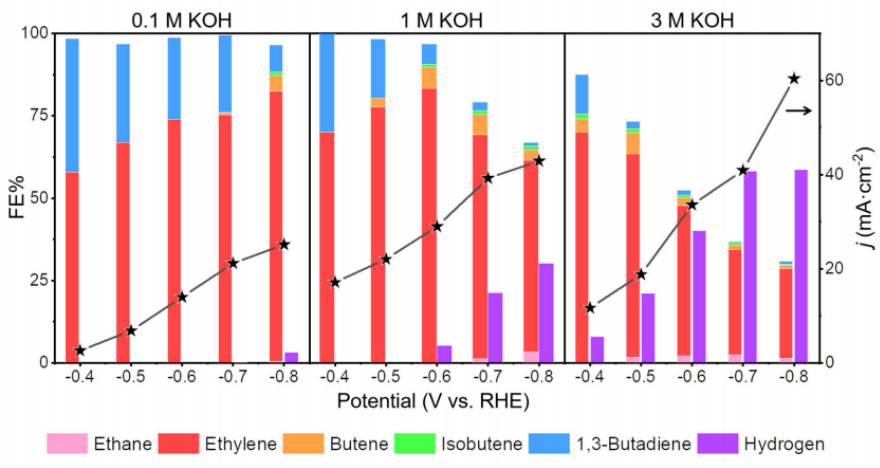

Fig. R15 | The EASH performance of the Cu/GDL-CP under different KOH concentrations.

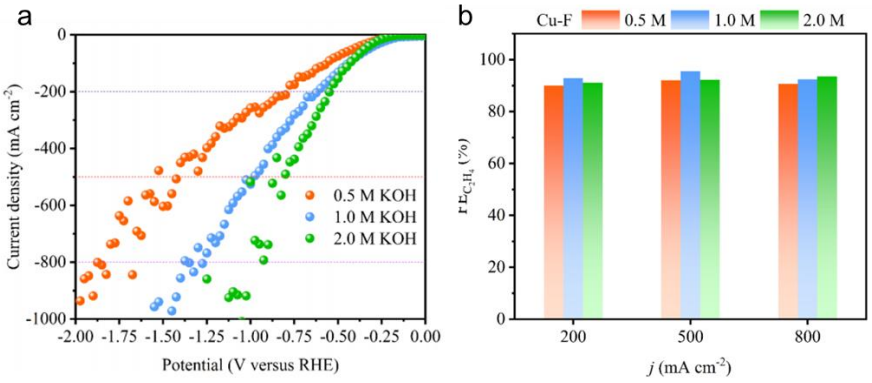

Fig. R16 | The effect of the KOH concentration on the (a) LSV curves and (b) FE over Cu-F.

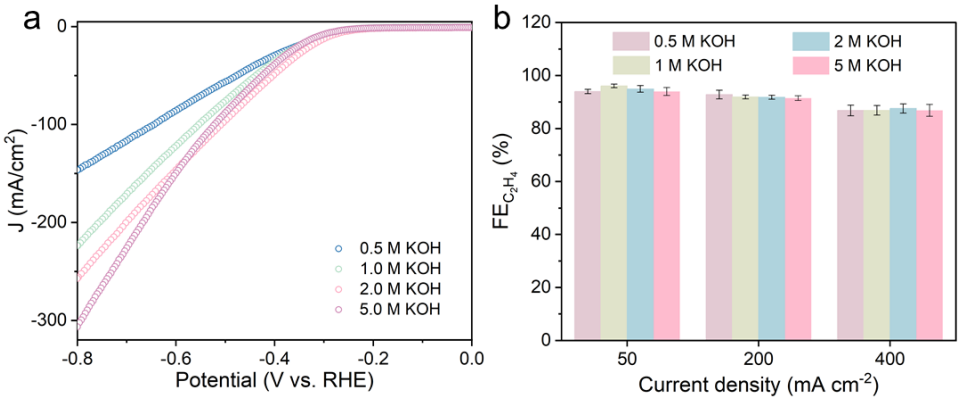

Fig. R17 | The effect of the KOH concentration on the (a) LSV curves and (b) Faraday efficiency of the obtained products over CoPc/NCNT.

Comment 3: In Page 13, the authors claimed that a hydrogen transfer mechanism could bypass the HER competitive, which is groundless. It has been widely reported that H_2 could also obtained by the combination of two water-derived $^*H$, called Tafel step (J. Phys. Chem. C, 2018, 122, 23943.). Thus, the real reason for the improved C_2H_4 selectivity is not the claimed mechanism, which needs further discussion.

Response to comment 3: We thank the reviewer for this important comment and fully agree that our original wording was misleading.

As correctly pointed out, in alkaline media H_2 can be formed not only via a Heyrovsky-type electrochemical step, but also via the Tafel recombination of two water-derived $^*H$ species, as widely reported in the literature (e.g., J. Phys. Chem. C **122**, 23943 (2018)). Our intention was not to claim that HER is completely bypassed, but rather that under low to intermediate current densities the water-derived $^*H$ is preferentially channelled into the hydrogenation of $^*C_2H_2$, thereby mitigating the competitive Heyrovsky-type HER pathway. Indeed, as shown in Fig. R18, the Faradaic efficiency of H_2 remains below 5% at low current densities, while at 500 mA cm^{-2} it increases to 13.3%. This rise in H_2 FE at high current density is consistent with accelerated water dissociation and a high surface coverage of $^*H$, which favours H–H recombination via the Tafel step. Thus, even though the Heyrovsky route can be effectively suppressed in the presence of abundant $^*C_2H_2$, the Tafel-type pathway remains operative when $^*H$ accumulates at very high current densities.

To avoid overstatement, we have revised the text on Page 16 as follows:

"Specifically, water-derived $^*H$ intermediates are preferentially consumed via sequential hydrogen

transfer to adsorbed C_2H_2, which mitigates competitive HER pathways (in particular the Heyrovsky-type route) and enables selective semi-hydrogenation in the low-to-intermediate current-density regime."

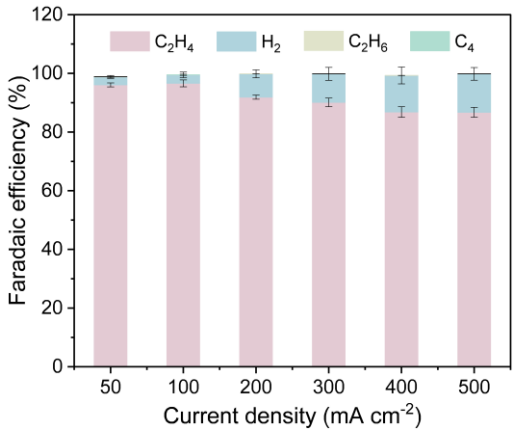

Fig. R18 | Faraday efficiency of the obtained products at various current densities over CoPc/NCNT.

Comment 4: The observed performance disparities between CoPC/NCNT and other samples are predominantly attributable to the difference in water dissociation ability. However, this seems inconsistent with the kinetic isotope experiment results for catalysts. The LSV or kinetic isotope experiment results for catalysts under argon gas should be provided for further comparison.

Response to comment 4: We thank the reviewer for this helpful comment.

In the original manuscript, the kinetic isotope effect was evaluated under C_2H_2 by replacing H_2O with D_2O, and we found that the KIE (H/D) value of CoPc/NCNT is smaller than that of CoPc/OCNT and CoPc/SCNT, which is consistent with a lower barrier for water dissociation and hence faster water-activation kinetics on CoPc/NCNT. To further support this conclusion, we have performed LSV measurements under Ar. As shown in the revised Fig. R19, CoPc/NCNT exhibits a Tafel slope of 121 mV dec^{-1}, notably smaller than those of CoPc/OCNT (156 mV dec^{-1}) and CoPc/SCNT (206 mV dec^{-1}). In alkaline media, such a decrease in Tafel slope is commonly associated with facilitated water dissociation in the Volmer step. The Ar-saturated LSV/Tafel data therefore agree well with the KIE results and together confirm that CoPc/NCNT possesses the fastest water-dissociation kinetics among the three catalysts.

These additional data and the corresponding discussion have been included in the revised manuscript (Page 17) and Supplementary Information (Page S22, Supplementary Fig. S42).

Page 17: "LSV and Tafel analysis in Ar saturated electrolyte (Fig. 4e) yields a Tafel slope of 121 mV dec^{-1} for CoPc/NCNT, lower than those of CoPc/OCNT (156 mV dec^{-1}) and CoPc/SCNT (206 mV dec^{-1}), a trend typically associated with more facile water activation in alkaline media (Supplementary Fig. S42)."

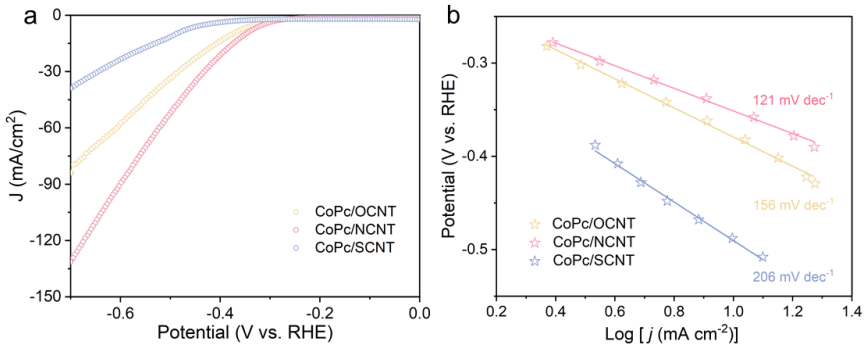

Fig. R19 | (a) LSV curves and (b) Tafel plots under an Ar feed in 1 cm^2 flow cell.

Comment 5: The as-reported TOF value is too high to convince the reviewer. According to the data in the previous literature (Chem. Eng. J. 2022, 431, 134129), the bare CoPc only exhibited a TOF value of 0.29 min^{-1} at a current of 100 mA. How can the TOF of the as-reported CoPc/NCNT reach 9700 min^{-1} at a current of 500 mA? More details are needed for the TOF calculation. Besides, the claimed 24 h continuous operation under ethylene-rich simulated gas flow could not be regarded as an advancement compared to the recent progress (Nat. Catal. 2021, 4, 557; 10.31635/ccschem.024.202404849; 10.1002/anie.202509501; 10.31635/ccschem.022.202101750;)

Response to comment 5: We thank the reviewer for carefully checking our TOF analysis and stability data. We agree that the very high TOF value initially reported requires clear justification, and we have revisited both the calculation and the long-term operation experiments in the revised manuscript.

For the TOF calculation, we follow the definition used in Nat. Sustain. 6, 827–837 (2023):

$$\text{TOF } (min^{-1}) = \frac{\text{amount of } C_2H_4 \text{ molecules produced per min}}{\text{amount of Co sites}}$$

In Chem. Eng. J. 2022, 431, 134129, bare CoPc was used at a loading of 0.2 mg cm^{-2} and a current density of 100 mA cm^{-2}. In our work, the CoPc/NCNT loading is 0.4 mg cm^{-2} at 500 mA cm^{-2} under otherwise comparable conditions. However, according to ICP–OES, the Co content in

our CoPc/NCNT electrode (0.4 mg × 0.47 wt% = 0.00188 mg Co per geometric electrode) is about 11 times lower than the CoPc amount in the Chem. Eng. J. study, while the current density is five times higher. At 500 mA cm^{-2}, the acetylene conversion and C_2H_4 selectivity are 30.4% and 99.99%, respectively. Using an inlet gas flow of 20 mL min^{-1} and the measured outlet flow of 16.5 mL min^{-1} (corrected in the revised manuscript), and a molar gas volume of 22.4 L mol^{-1}, the TOF is calculated as:

$$\text{TOF (min}^{-1}) = \frac{16.5\times0.304\times0.9999/22.4}{0.00188/58.93} = 7019\ \text{min}^{-1}$$

This updated value (7019 min^{-1}) is lower than the original 9700 min^{-1} due to the corrected gas-flow treatment and Co content, but it still reflects the combination of a much lower Co loading and a higher geometric current density compared with the homogeneous CoPc system in Chem. Eng. J. All assumptions, parameters, and intermediate steps used in this calculation have now been added to the Supplementary Information for transparency. Regarding stability, we agree that the 24 h continuous operation originally shown under ethylene-rich simulated gas flow is not sufficient to claim an advance over the recent state-of-the-art. In response to the reviewer's comment, we have extended the durability tests of CoPc/NCNT under a crude acetylene stream. The revised data show that CoPc/NCNT can operate continuously for 110 h while maintaining an acetylene conversion above 98% and a C_2H_4 selectivity above 94% (Fig. R20). These conversion, selectivity, and stability data metrics rank among the most competitive values reported in the recent literature (Table R5).

We added these figures and discussions to the revised manuscript (Page 12 and 20, Fig. 5b) and Supplementary Information (Page S29 and S31, Supplementary Table S3 and Supplementary Note 2).

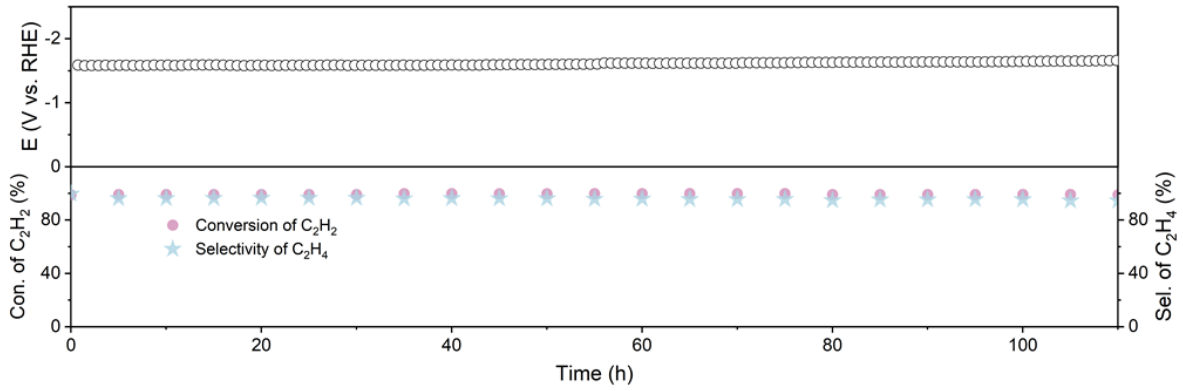

Fig. R20 | Long-term operation of ESAE over CoPc/NCNT under ethylene-rich environment,

measured using a three-electrode flow cell (25 cm^2) in 1 M KOH at room temperature under ethylene-rich simulated gas (0.5% C_2H_2, 20%C_2H_4 balanced with Ar) flow (20 mL min^{-1}).

Table R5 | Performance summary of recently reported acetylene semi-hydrogenation electrocatalysts.

Entry	Material	Flow composition	SV (mL g_{cat}^{-1} h^{-1})	TOF (min^{-1})	Selectivity (%)	Stability (h)	Ref.
1	CoPc/NCNT	C_2H_2=100	3×10^5	**9.7×10^3**	100	60	This work
2	CoPc/NCNT	C_2H_2/C_2H_4/Ar=0.5/20/79.5	1.5×10^5	**4.6**	99.5	110	This work
3	ED-Cu NPs	C_2H_2=100	9×10^5	**5.3×10^2**	100	56	Nat. Sustain. **6**, 827-837 (2023)
4	Cu-F	C_2H_2/Ar=70/30	1.6×10^3	**17.6**	94	43	Nat. Commun. **14**, 8384 (2023)
5	Cu MPs	Saturated by C_2H_2	1.4×10^3	**5.1**	80	100	Nat. Commun. **12**, 7072 (2021)
6	NHC-Cu	C_2H_2/C_2H_4=1/99	9.6×10^5	**1.26**	99	100	Nat. Commun. **12**, 6574 (2021)
7	Cu dendrites	C_2H_2=100	6.6×10^4	/	98	120	Nat. Catal. **4**, 557-564 (2021)
8	LD-Cu	C_2H_2/Ar=5/95	/	/	92	5	Nat. Catal. **4**, 565-574 (2021)
9	Ag NWs	C_2H_2/C_2H_4=1/99	/	/	99	60	CCS Chem. **5**, 200-208 (2023)
10	Cu NDs	C_2H_2/C_2H_4/Ar=0.5/20/79.5	1.4×10^5	/	94	130	Nat. Commun. **14**, 2137 (2023)
11	Cu-PCC	C_2H_2/C_2H_4=15/85	/	/	97	12	Nat. Commun. **14**, 2137 (2023)
12	CuO_{1-x} NRs	C_2H_2/C_2H_4=2.2/97.8	/	/	95.1	20	Adv. Mater. **36**, 2408681 (2024)
13	Cu SA/NC	C_2H_2/C_2H_4=1/99	/	/	97	8	Angew. Chem. Int. Ed. e202307848 (2023)
14	CuBcpi–BuOK	C_2H_2/Ar=15/85	9×10^5	/	93	200 (MEA electrolyzer)	Angew. Chem. Int. Ed. **64**, e202509501 (2025)
15	v-Cu NCs	C_2H_2/C_2H_4=1/99	/	/	97.4	50	CCS Chem. **7**, 2844–2853 (2025)

Comment 6: In Figure 1g, comparing the d-band centers of different metals is quite uncommon and meaningless. Meanwhile, in Figures 1h, i and 4k, the author employed unusual plotting methods to

present the reaction diagrams, which resulted in poorer data readability and a higher likelihood of misinterpretation. For example, in the conventional $^*H$ generation process, it is necessary to calculate the steady-state $^*H_2O$ and $^*H+^*OH$ as the initial and final states of the water dissociation process, as well as the corresponding transition states, while considering the $^*OH$ desorption process. It is very incomplete for the author to only calculate the energy barrier from $^*H_2O$ to $^*H+^*OH$. The generation processes of H_2 and C_4 also face similar issues.

Response to comment 6: We thank the reviewer for these constructive suggestions. We agree that the original electronic descriptors and reaction profiles may not be reader-friendly, and we have substantially revised the relevant figures and text accordingly.

First, regarding Figure 1g, our intention was not to compare d-band centres in an abstract way, but to highlight how the electronic structure of different metal centres governs their interaction with acetylene and hydrogen-derived intermediates in EASH. Since the semi-hydrogenation reaction predominantly occurs at the metal sites, the position of the metal d-band relative to the adsorbate p/s orbitals is a key factor in determining adsorption strength and activation behaviour. In particular, Zhang et al. (Small **19**, 2205845 (2023)) reported that the energy gap ($\Delta\varepsilon$) between the metal d-band centre and the π orbital of acetylene can serve as an effective descriptor for acetylene electrocatalytic activity. Inspired by this, we use the d-band centre as a compact descriptor to rationalise the trends across the MPc/OCNT series.

Second, we acknowledge that the reaction diagrams in Figures 1h, 1i, and 4k were not presented in a sufficiently standard format and could lead to misinterpretation. Following the reviewer's advice, we have reprocessed all DFT data and redrawn the energy profiles in a more conventional way (Fig. R21). For water dissociation, we now explicitly show $^*H_2O$ and $^*H + ^*OH$ as the initial and final states on the reaction coordinate, include the corresponding transition state, and add the subsequent $^*OH$ desorption step, so that the full elementary sequence $^*H_2O \rightarrow {}^*H + {}^*OH \rightarrow {}^* + OH^-$ is represented. For H_2 evolution, we now provide the complete pathway from $^*H$ formation to H–H coupling and H_2 desorption, including all relevant intermediates and transition states. For C_4 formation, we have similarly expanded the energy profile to cover the key C–C coupling and subsequent hydrogenation steps, rather than only showing a single barrier.

The full computational methods, adsorption-site selection, and representative adsorption

configurations for all intermediates are now described in detail in the revised Methods section, and Supplementary Information, and the updated reaction diagrams follow the conventions used in recent literature. We note that, after this more complete treatment, the overall trends and mechanistic conclusions remain consistent with those in the original manuscript. We are grateful to the reviewer for pointing out these issues, which have helped us to improve both the rigour and the clarity of our theoretical analysis and data presentation.

Page 25: "The C_2H_2 hydrogenation process to C_2H_4 can be delineated by equations (9)-(11):

$$^* + C_2H_2 \rightarrow {}^*C_2H_2 \quad (9)$$

$$^*C_2H_2 + H+ e^- \rightarrow {}^*C_2H_3 \quad (10)$$

$$^*C_2H_3 + H+ e^- \rightarrow {}^*C_2H_4 \quad (11)$$

The hydrogen combination proceeded through equations (12)-(13):

$$^* + 2H \rightarrow 2{}^*H \quad (12)$$

$$^*H + {}^*H \rightarrow {}^*H_2 \quad (13)$$

The C-C coupling proceeded through this equation (14):

$$2{}^*C_2H_3 + {}^*C_2H_3 \rightarrow {}^*C_4H_6 \quad (14)$$

While the water dissociation proceeded through equations (15)-(18):

$$^* + H_2O \rightarrow {}^*H_2O \quad (15)$$

$$^*H_2O \rightarrow {}^*H\text{–}OH \quad (16)$$

$$^*H\text{–}OH \rightarrow {}^*H + {}^*OH \quad (17)$$

$$^*H + {}^*OH \rightarrow {}^*H + OH \quad (18)$$"

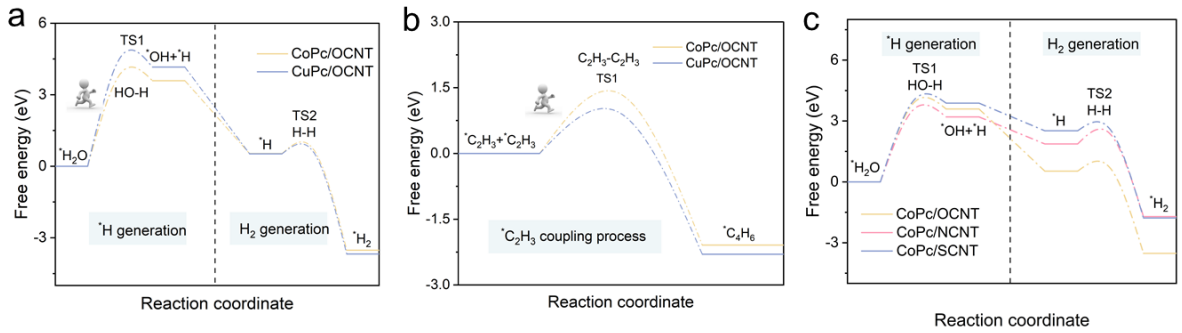

Fig. R21 | (a) Free energy diagram for the $^*H$ generation and H_2 generation process of CoPc/OCNT and CuPc/OCNT. (b) Corresponding free energy diagram of $^*C_2H_3$ to C_4H_6. (c) Free energy diagram for $^*H$ generation and H_2 formation over CoPc/OCNT, CoPc/NCNT, and CoPc/SCNT.

Comment 7: The manuscript does not present any calculation methods, and lacks the display of relevant and representative adsorption models. For single-atom catalysts, the selection of adsorption sites is crucial and needs to be demonstrated. In the processes of water dissociation and hydrogenation, it is necessary to clarify whether C and O species occupy the metal sites, and where $^*H$ is adsorbed.

Response to comment 7: We thank the reviewer for this important comment.

In the revised manuscript, we now provide a detailed description of our DFT methods (including model construction, exchange–correlation functional, k-point sampling, and convergence criteria) and explicitly display representative adsorption configurations relevant to water dissociation and EASH. The structural models of the CoPc/XCNT catalysts are built on reported in recent work (Nat. Catal. **7**, 987–999 (2024); Angew. Chem. Int. Ed. **64**, e202517033 (2025)), and are further constrained by our own XAFS, XPS, and AC-STEM analyses, which point to isolated Co centres with a well-defined coordination environment. The selected adsorption geometries for reactants and intermediates are guided by both these experimental results and previous computational studies on related metal sites (e.g. Angew. Chem. Int. Ed. **62**, e202307848 (2023); Adv. Mater. **35**, 2303818 (2023)).

We have also clarified how adsorption sites are chosen and how the key species are distributed during water dissociation and hydrogenation. Our in situ ATR-FTIR, in situ XAFS, and control experiments on the bare XCNT supports show that the carbon framework alone is essentially inactive and that Co is the dominant active centre, with no clear evidence for a second, highly active site. Consistent with this, our DFT screening indicates that both H_2O and C_2H_2 preferentially interact with the Co site (Fig. R22-R24). Along the water dissociation pathway, H_2O adsorbs at Co and splits to yield $^*OH$ and $^*H$, with Co-bound configurations being energetically favoured over adsorption on adjacent C or N sites. During the subsequent hydrogenation steps, $^*H$ is mainly stabilised on Co and reacts with Co-bound $^*C_2H_2$ (and $^*C_2H_3$) to form $^*C_2H_4$, rather than involving $^*H$ adsorbed on the carbon support. These findings support the picture that the isolated Co centres act as the primary sites for both water activation and hydrocarbon hydrogenation, while O-containing species do not permanently block the Co sites under the relevant potentials.

The expanded computational methodology and representative adsorption models are now

included in the revised manuscript (Page 25) and supplementary information (Supplementary Figs. S3, S4, and S44).

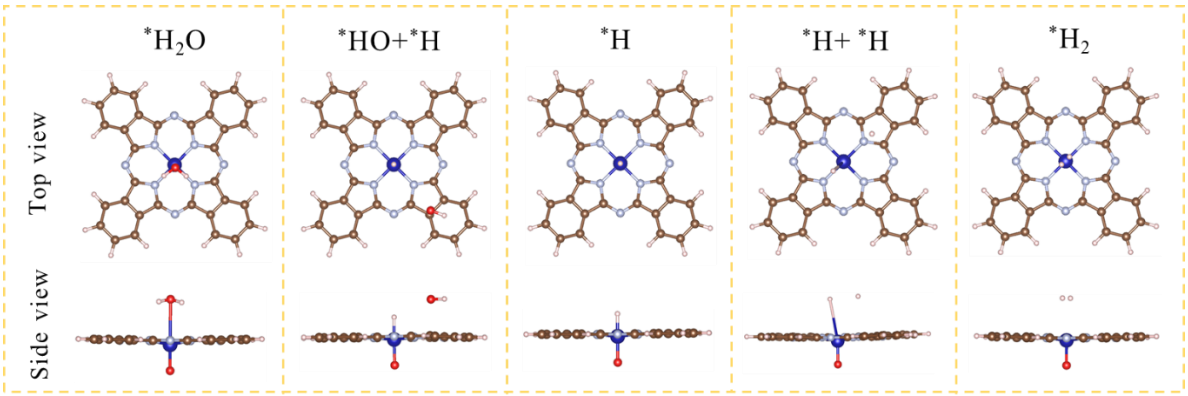

Fig. R22 | Theoretical adsorption models H_2O dissociation and H_2 generation over the surface of CoPc/OCNT.

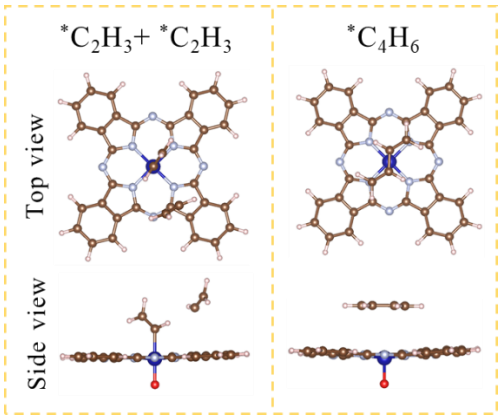

Fig. R23 | Theoretical adsorption models of $^*C_2H_3$ to C_4H_6 over the surface of CoPc/OCNT.

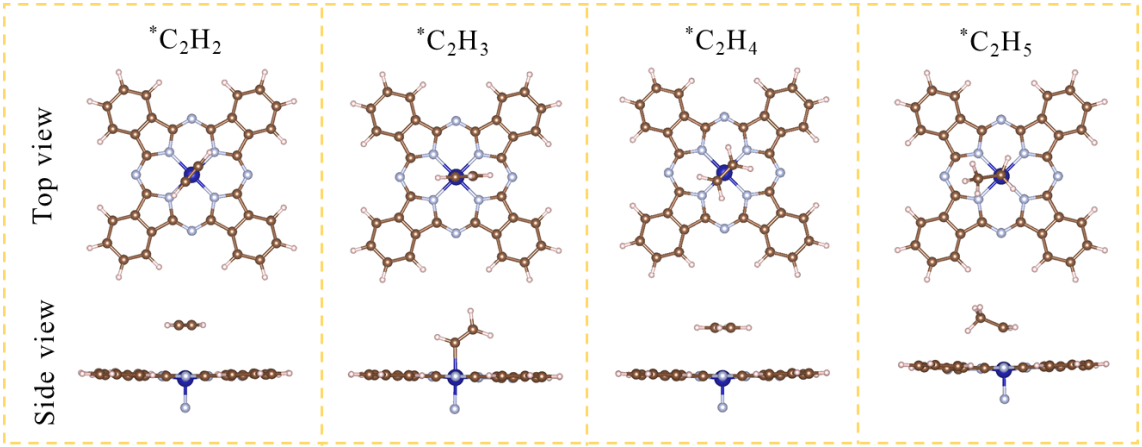

Fig. R24 | Theoretical adsorption models of the hydrogenation process of C_2H_2 over the surface of CoPc/NCNT.

Response to Reviewer #3:

General Comments:

In this work, the authors report a CoPc-OCNT catalyst towards EASH, achieving FE of 86.7% under 500 mA cm^{-2}. The manuscript attributes the enhanced activity to the excellent hydrogenation ability of CoPc, but similar arguments were already reported in prior studies (Chem. Eng. J. 2022, 431: 134129). Therefore, the reviewer considers the current form of this work lacks of novelty and not suitable for publication in Nature Communications.

Response: Thank the reviewer for these comments and valuable suggestions, which are helpful for us to improve the manuscript quality.

We fully agree that the work of Liu et al. (Chem. Eng. J. 2022, 431, 134129) represents an important milestone, as it first identified CoPc as an efficient EASH catalyst and attributed its performance to favourable acetylene adsorption/hydrogenation behaviour. At the same time, several key challenges remain: CoPc was used as a homogeneous molecular catalyst at relatively high loading, which increases catalyst cost; the activity and durability were limited (TOF of 0.29 min^{-1} at −100 mA cm^{-2} and stability of ~40 h); and the performance was demonstrated only at comparatively low current densities. These factors constrain the practical applicability of that system for industrial ethylene purification and motivate the search for catalysts that deliver substantive improvements under more realistic operating conditions. CoPc itself, however, offers the advantage of a well-defined coordination environment, which is highly attractive for precise structural design and mechanistic analysis.

In the revised manuscript, we clarify that our study is designed to address these open issues and to go beyond the Chem. Eng. J. work along three main lines:

1. Comparative MPc/OCNT platform and Co vs Cu mechanistic insight

During our preliminary exploration of EASH catalysts, we found that Co-based systems can match or even surpass the performance of Cu-based analogues, which contrasts with the current literature where roughly 60–70% of reported EASH studies focus on Cu. This discrepancy motivated us to construct a CNT-supported metal phthalocyanine platform, MPc/OCNT (M = Fe, Ni, Cu, Co), to compare their behaviour under strictly identical conditions. Within this series, CoPc/OCNT exhibits faster water dissociation and a more favourable adsorption environment for key

intermediates, which correlates with a markedly lower tendency towards C–C coupling. This model platform allows us to disentangle how different metal centres regulate water dissociation, $^{*}H$ management and C–C coupling, rather than attributing the performance difference simply to the intrinsic hydrogenation ability of CoPc.

2. Water dissociation and C–C coupling across different metals

To examine whether enhanced water dissociation can generally mitigate C–C coupling, we synthesised NiPc/OCNT and FePc/OCNT with the same structural motif. At 100 mA cm^{-2}, the C_4H_6 Faradaic efficiencies of NiPc/OCNT and FePc/OCNT are both below 0.15%, showing that strong promotion of water dissociation indeed suppresses C_4 formation within this molecular platform. This extends the CoPc concept to other metal centres and provides a mechanistic link between interfacial water activation and C–C coupling behaviour, which was not explored in the Chem. Eng. J. study.

3. Axial coordination engineering of CoPc for industrially relevant performance

While CoPc/OCNT already suppresses C–C coupling, it still suffers from pronounced HER at current densities above 200 mA cm^{-2}, which is unfavourable for industrial operation. Guided by the mechanistic insights from the MPc/OCNT series, we introduced axial coordination control by immobilising CoPc on amino- and thiol-functionalised CNTs (NCNT and SCNT). This strategy allows us to tune water dissociation kinetics and $^{*}H$ utilisation more precisely. Among these catalysts, CoPc/NCNT exhibits faster water dissociation and more efficient $^{*}H$ use, strongly suppressing HER at high current densities. As a result, CoPc/NCNT achieves a C_2H_4 Faradaic efficiency of 86.7% at −500 mA cm^{-2} with 99.99% C_2H_4 selectivity, complete suppression of C_4 products, a turnover frequency of 7019 min^{-1} (about five orders of magnitude higher than the 0.29 min^{-1} at −100 mA cm^{-2} reported in Chem. Eng. J.), an eleven-fold lower CoPc usage, and an extended stability from 40 h to 110 h. To test generality on Cu, we additionally synthesised CuPc/NCNT. Compared with CuPc/OCNT, CuPc/NCNT shows enhanced water-activation behaviour, and at −100 mA cm^{-2} the C_4H_6 FE decreases from 1.40% on CuPc/OCNT to 0.80% on CuPc/NCNT. This clear drop in C_4H_6 formation demonstrates that axial N-coordination on CuPc also suppresses C–C coupling, indicating that the coordination strategy derived from the Co platform is transferable to other metal–phthalocyanine catalysts.

We have revised the manuscript to present these points more clearly and to position our contribution as (i) establishing a comparative MPc/OCNT platform that links water dissociation, $^{*}H$

regulation, and C–C coupling for different metal centres, and (ii) translating these mechanistic insights into axial coordination engineering of CoPc/NCNT to move EASH performance closer to industrial requirements, in clear contrast to the earlier CoPc system.

Specific Comments:

Comment 1: The authors choose the CoPc/OCNT as the model catalyst due to its better ability of water dissociation. How about NiPc/OCNT and FePc/OCNT, which has been proved the great activity on water dissociation. Besides, the FE of C_2H_4 decreased and FE of H_2 increased sharply under high current densities, suggesting the inferior ability of CoPC/OCNT to tune the $^*H$. The authors propose the CoPc/OCNT can inhibit C-C coupling to generate C_4 byproducts, while the key Co sites may have no activity on C-C coupling.

Response to comment 1: We thank the reviewer for this thoughtful comment.

At the outset of our work, we have observed that Co-based catalysts can deliver higher EASH activity than Cu-based analogues. This is intriguing given that the majority (≈60–70%) of reported EASH studies still focus on Cu-based systems, and it motivated us to probe whether Co and Cu follow distinct reaction pathways. To do so in a controlled manner, we selected CNT-supported metal phthalocyanines (MPc/OCNT, M = Cu, Co) as a model platform. Within this series, CoPc/OCNT emerged as a promising model because it combines relatively fast water dissociation with a favourable adsorption environment for key intermediates, which correlates with a reduced tendency toward C–C coupling.

Motivated by the reviewer's comment, we have extended the study of CoPc/OCNT and CuPc/OCNT to a broader comparative MPc/OCNT platform (M = Cu, Co, Ni, Fe). This expansion allows us to systematically investigate the effect of the metal center, thereby further strengthening the novelty of our work. We have synthesised NiPc/OCNT and FePc/OCNT and evaluated them under identical conditions. As shown in Fig. R25, LSV curves and Tafel slopes under Ar indicate that both NiPc/OCNT and FePc/OCNT promote water dissociation more efficiently than CuPc/OCNT. Quantitative product analysis at −100 mA cm^{-2} shows that the FEs of C_4H_6 on FePc/OCNT and NiPc/OCNT are both below 0.15%, much lower than that of CuPc/OCNT (1.40%), consistent with the idea that accelerated water dissociation helps to alleviate C–C coupling and C_4

formation (Fig. R26). However, FePc/OCNT suffers from pronounced overhydrogenation, and NiPc/OCNT exhibits a strong HER contribution. Therefore, CoPc/OCNT exhibits the most effective suppression of C_4 formation while maintaining high C_2H_4 selectivity, which is why it was chosen as the model system in this study.

Regarding the behaviour of CoPc/OCNT at different current densities, we agree that its ability to manage $^*H$ becomes limited at high currents. At low current densities (50–100 mA cm^{-2}), CoPc/OCNT delivers excellent EASH performance, with C_2H_4 FE above 90% and low H_2 FE, indicating efficient utilisation of water-derived $^*H$ for semi-hydrogenation. When the current density is increased to higher values (e.g. 300–500 mA cm^{-2}), the C_2H_4 FE decreases while the H_2 FE rises sharply. This trend is consistent with accelerated water dissociation at high overpotential, leading to a high surface coverage of $^*H$; a substantial fraction of this $^*H$ then recombines to H_2 via HER rather than being fully consumed by C_2H_2 hydrogenation. Our DFT results support this proposal: although CoPc/OCNT has a higher H_2O dissociation barrier than CoPc/NCNT, it exhibits a lower H–H coupling barrier than CoPc/NCNT, indicating that at high $^*H$ coverage, CoPc/OCNT more readily channels $^*H$ into H_2 formation. In contrast, CoPc/NCNT maintains a higher barrier for H–H coupling while still facilitating water dissociation, which improves $^*H$ utilisation for EASH and alleviates HER at high current densities.

Regarding the possibility that Co sites might be intrinsically inactive for C–C coupling, our product analysis shows that primitive CoPc still generates a measurable amount of C_4H_6 (FE = 0.12% at −100 mA cm^{-2}, Fig. R27). This suggests that Co centres can mediate C–C coupling. But the water-dissociation kinetics and intermediate binding energetics in CoPc/OCNT favour the semi-hydrogenation pathway to C_2H_4 over further C–C coupling. We also note that cobalt complexes have been reported to form C_2 products in CO_2 electroreduction, including Co corrole catalysts that yield ethanol as a major product and Co-phthalocyanine-based conjugated polymers that selectively reduce CO_2 to ethanol (Nat. Commun. **10**, 3864 (2019); Mater. Rep. Energy **3**, 100176 (2023)). These precedents are consistent with Co sites being capable of C–C bond formation, while in our EASH system the reaction environment created by CoPc/OCNT steers the reaction toward selective C_2H_4 production with strongly suppressed C_4 by-products.

We added these figures and discussions to the revised Manuscript (Page 7) and Supplementary Information (Supplementary Fig. S6 and S7).

Page 7: “To assess the generality of this water-dissociation-governed suppression of C–C coupling, we also synthesised NiPc/OCNT and FePc/OCNT and evaluated them under identical conditions. LSV curves and Tafel slopes under Ar indicate that both NiPc/OCNT and FePc/OCNT promote water dissociation more efficiently than CuPc/OCNT (Supplementary Fig. S6). Quantitative product analysis at −100 mA cm^{-2} shows that the Faradaic efficiencies of C_4H_6 on FePc/OCNT and NiPc/OCNT are both below 0.15%, much lower than that of CuPc/OCNT (1.40%), which is consistent with the view that accelerated water dissociation helps to alleviate C–C coupling and C_4 formation (Supplementary Fig. S7). Therefore, within this MPc/OCNT series, CoPc/OCNT exhibited the most effective suppression of C_4 formation while maintaining high C_2H_4 selectivity.”

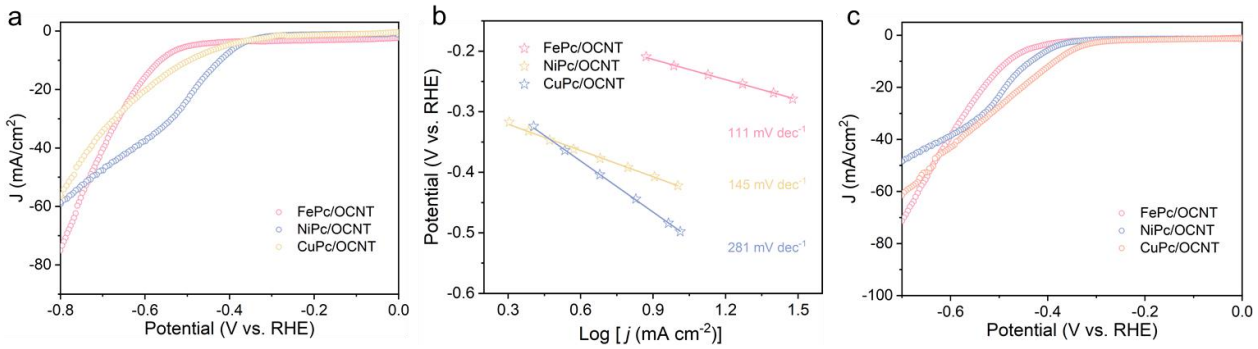

Fig. R25 | (a) LSV curves and (b) Tafel plots in Ar. (c) LSV curves under C_2H_2 flow.

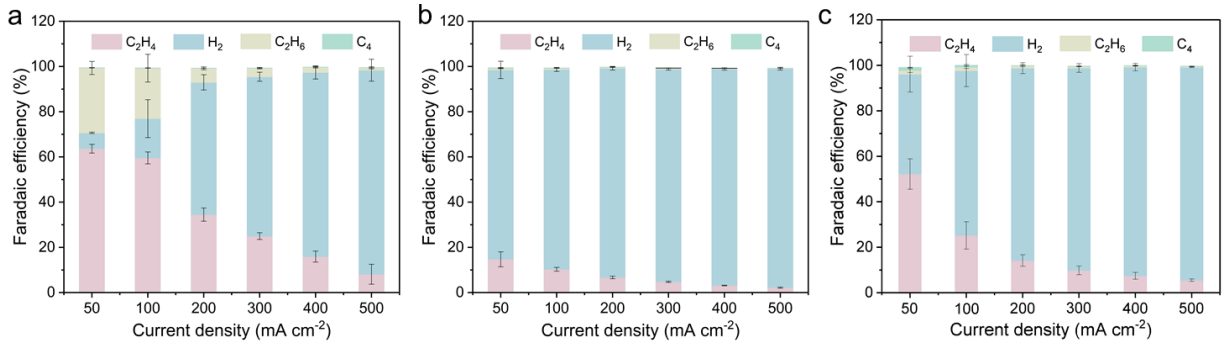

Fig. R26 | Faraday efficiency of the obtained products over (a) FePc/OCNT, (b) NiPc/OCNT, and (c) CuPc/OCNT.

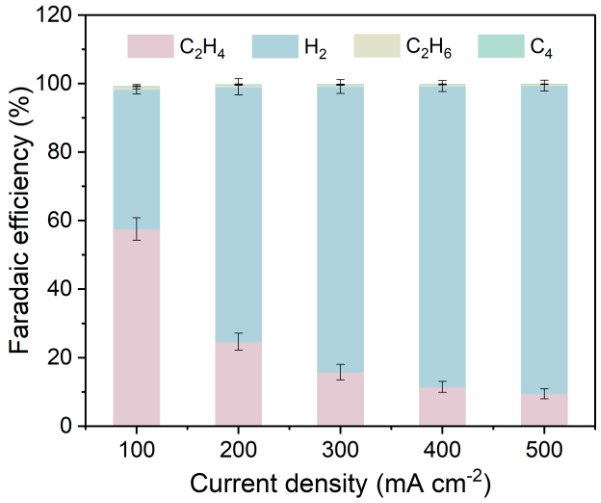

Fig. R27 | Faraday efficiency of the obtained products over CoPc at various current density.

Comment 2: The authors use the different carbon substrate (N-CNT, S-CNT, O-CNT) to tune coordination of Co center and optimize its catalytic performance. How about the performance of CoPc/CNT without doping? The CoPc/NCNT achieves the better performance. The authors should prove the increased performance is not originate the change of physical properties (conductivity, hydrophilicity, adsorption capacity).

Response to comment 2: We appreciate the reviewer's insightful comment.

In the revised manuscript, we have now included CoPc supported on bare commercial CNTs (CoPc/CNT) as an additional control to directly assess the effect of CNT functionalization. The electrochemical performance of CoPc/CNT is compared with that of CoPc/OCNT in Fig. R28. As shown by LSV curves (Fig. R28a), the presence of oxygen functionalities leads to a higher limiting current density in the CoPc/OCNT compared with CoPc/CNT. The product distribution at 100 mA cm^{-2} (Fig. R28b, c) further highlights the benefit of functionalisation: CoPc/CNT exhibits notable parasitic reactions, with Faradaic efficiencies of 11.7% for H_2, 0.47% for over-hydrogenation to C_2H_6, and 0.44% for C–C coupling products (C_4H_6). In contrast, CoPc/OCNT at the same current density shows FE values of 8.1% for H_2, and 0% for C_2H_6 and C_4 products, indicating strongly suppressed side reactions and improved selectivity. These new data, now highlighted in the main text, demonstrate that CNT functionalisation is necessary to be beneficial for optimising the intrinsic performance of molecular CoPc in EASH.

As the reviewer correctly points out, functionalising CNTs with different heteroatom-

containing groups inevitably affects their physical properties. In our work, we first oxidised commercial CNTs to obtain OCNT and then grafted amino and thiol groups via silane coupling to prepare NCNT and SCNT, respectively. These O, N and S functionalities were introduced with the explicit aim of electronically interacting with CoPc and tuning the coordination environment of the Co centre, but they may also lead to changes in conductivity, wettability, and gas adsorption. To disentangle these effects, we kept the CoPc loading essentially identical across CoPc/OCNT, CoPc/NCNT, and CoPc/SCNT (CoPc/NCNT is even slightly lower, Table R6) and systematically characterised the physical properties of both the catalysts and the corresponding bare supports. Four-probe measurements show that the resistance increases from CoPc/OCNT to CoPc/NCNT and further to CoPc/SCNT (Table R7), and contact-angle measurements reveal that the surface becomes more hydrophobic along the same series (CoPc/OCNT < CoPc/NCNT < CoPc/SCNT, Fig. R29). C_2H_2-temperature programmed desorption results indicates a gradual increase in C_2H_2 uptake from CoPc/OCNT to CoPc/NCNT to CoPc/NCNT (Fig. R30). If the activity gain were dominated by such physical factors, one would expect CoPc/SCNT, with the highest resistance, largest contact angle, and highest C_2H_2 uptake, to show the best performance. In contrast, the observed catalytic trend is CoPc/NCNT > CoPc/OCNT > CoPc/SCNT, which does not follow the simple order of conductivity, hydrophilicity, or adsorption capacity. To further separate the role of the carbon substrates from that of the molecular CoPc sites, we also evaluated the EASH activity of the bare OCNT, NCNT, and SCNT supports under identical conditions (Fig. R31). All three substrates exhibit very low activity, and NCNT and SCNT even perform worse than OCNT, despite their more pronounced changes in resistance, wettability and C_2H_2 adsorption. This again suggests that the improved performance of CoPc/NCNT cannot be ascribed to the physical properties of the functionalised carbons alone.

Taken together, these results indicate that the enhanced EASH activity of CoPc/NCNT is not simply a consequence of favourable conductivity, hydrophilicity, or adsorption of the carbon support. Instead, they support our conclusion that the dominant effect arises from the modified coordination environment and electronic structure of the Co centres induced by the N-containing surface groups, as corroborated by the spectroscopic and DFT analysis in the revised manuscript.

We added these figures and discussions to the revised Manuscript (Pages 11 and 13) and Supplementary Information (Supplementary Figs. S23, S34, and S35).

Page 11: “Compared with the CoPc supported on bare commercial carbon nanotubes (CoPc/CNT),

most CoPc/XCNT catalysts significantly suppress side reactions and enhance selectivity, indicating the effectiveness of molecular regulation in enhancing EASH performance (Supplementary Fig. S23)."

Page 13: "Before discussing the mechanistic role of molecular regulation, we first examined whether the enhanced activity of CoPc/NCNT could simply originate from changes in the physical properties of the carbon support. Four probe tests show that the resistance increases from 0.018 Ω·cm for CoPc/OCNT to 0.029 Ω·cm for CoPc/NCNT and 0.086 Ω·cm for CoPc/SCNT (Supplementary Table S4), indicating a slight increase in overall resistance. Contact angle measurements reveal that the surface becomes more hydrophobic, with the contact angle increasing from 65.5° (CoPc/OCNT) to 92.1° (CoPc/NCNT) and 96.4° (CoPc/SCNT) (Supplementary Fig. S34). C_2H_2-temperature programmed desorption results indicates a gradual increase in C_2H_2 uptake from CoPc/OCNT to CoPc/NCNT to CoPc/NCNT (Supplementary Fig. S35). Besides, the EASH activity of the bare OCNT, NCNT, and SCNT supports remains low and in some cases even decreases after functionalisation (Supplementary Fig. S32). These results indicate that the superior performance of CoPc/NCNT cannot be rationalised solely by favourable conductivity, hydrophilicity, substrates, or C_2H_2 adsorption, and instead mainly arises from the modified coordination environment and electronic structure of the Co centres induced by heteroatom doping."

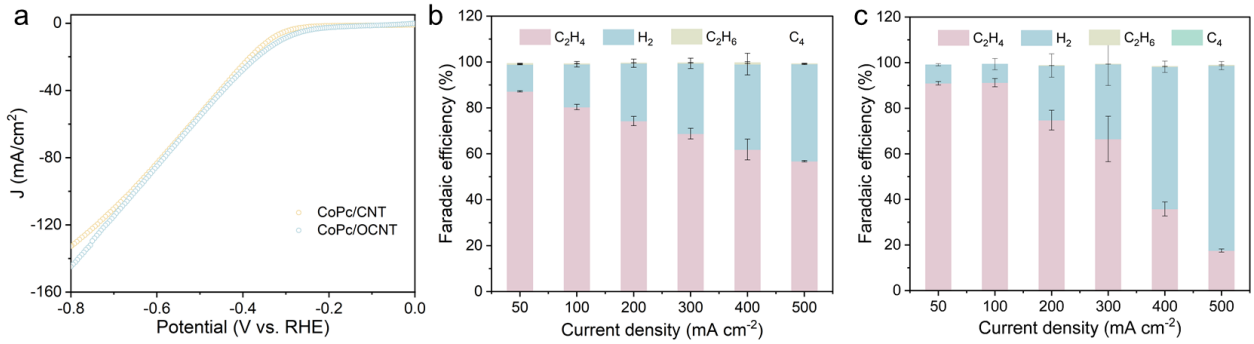

Fig. R28 | (a) LSV curves and Faraday efficiency of the obtained products using (b) CoPc/CNT and (c) CoPc/OCNT at various current densities.

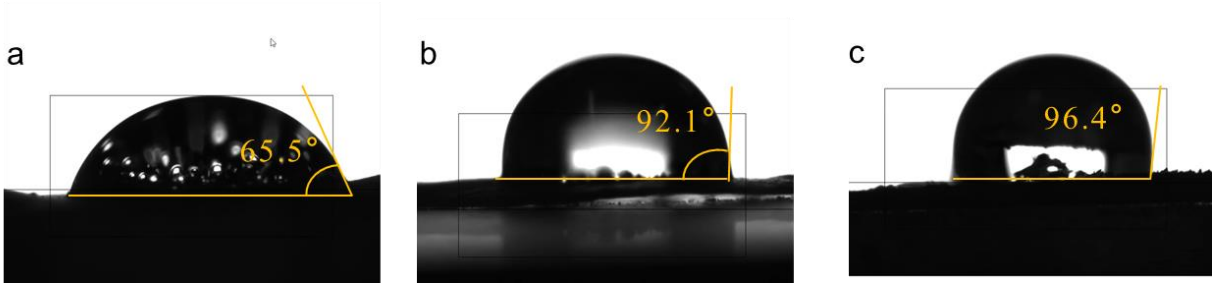

Fig. R29 | Water droplet contact angle measurements of (a) CoPc/OCNT, (b) CoPc/NCNT, and (c) CoPc/SCNT.

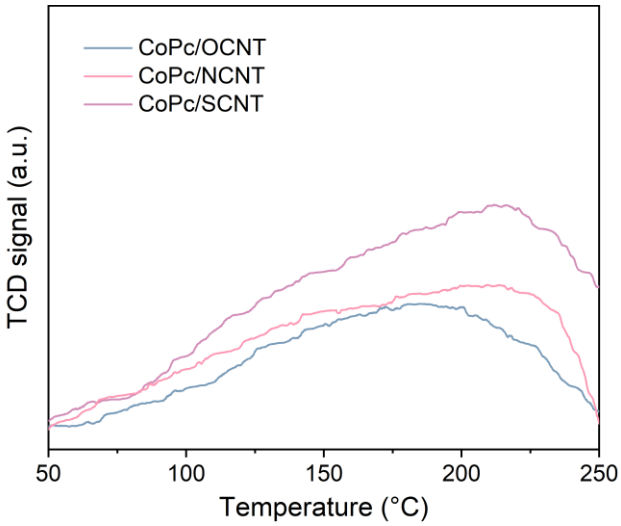

Fig. R30 | TPD curves of C_2H_2 on CoPc/OCNT, CoPc/NCNT, and CoPc/SCNT.

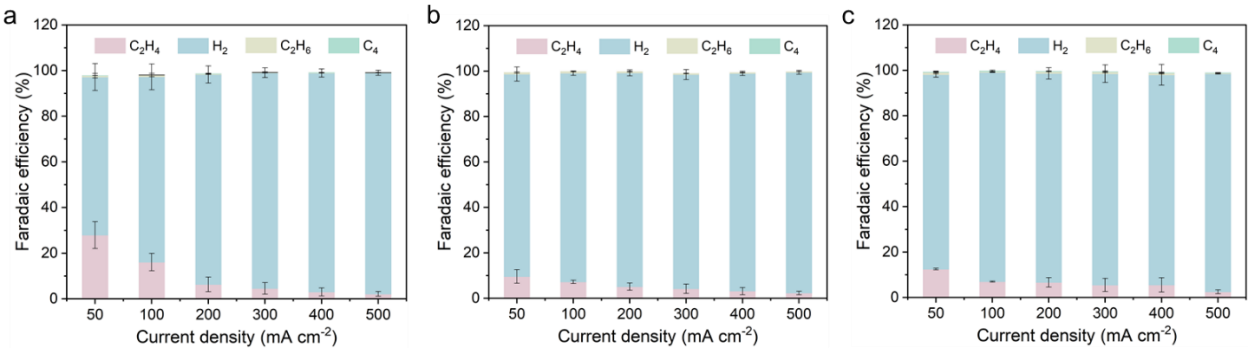

Fig R31 | Faraday efficiency of the obtained products over OCNT (a), NCNT (b), and SCNT (c) at various current densities.

Table R6 | Co mass loading of CoPc/OCNT, CoPc/NCNT, and CoPc/SCNT.

Catalysts	Loading (wt. %)	Standard Deviation (%)

CoPc/OCNT	0.55	±0.01
CoPc/NCNT	0.47	±0.055
CoPc/SCNT	0.57	±0.026

Table R7 | The catalyst resistances and system resistances of measured at working conditions.

Sample	Catalyst resistances (Ω cm)	System resistances (Ω)
CoPc/OCNT	0.018±0.003	1.9±0.1
CoPc/NCNT	0.029±0.011	2.0±0.1
CoPc/SCNT	0.086±0.009	2.1±0.1

Comment 3: The most electrochemical results presented in this study lack error bars, which may raise concerns about the reproducibility and reliability of the reported data.

Response to comment 3: We thank the reviewer for raising this important point.

In the revised manuscript, we have systematically reassessed all electrochemical data and added error bars to the key quantitative results, including Faradaic efficiencies, conversion, and selectivity values. These data now represent the mean ± standard deviation of at least three independent measurements using separately prepared electrodes. We believe these additions more clearly demonstrate the reproducibility and reliability of the reported electrochemical performance.

Comment 4: The in-situ FT-IR data presented in this study are underexplored. The analysis of water peaks range from 3000-4000 cm^{-1} may be benefit of revealing the tune of water dissociation.

Response to comment 4: We thank the reviewer for this valuable suggestion.

In the revised manuscript, we have further analysed the in situ ATR-FTIR spectra in the O–H stretching region to better elucidate the role of water dissociation. Specifically, the broad O–H stretching band of interfacial H_2O between 2900 and 3700 cm^{-1} was deconvoluted into three components, which can be assigned to 4-coordinated hydrogen-bonded water (4-HB·H_2O, low-wavenumber component), 2-coordinated hydrogen-bonded water (2-HB·H_2O, main component) and K^+-hydrated water (K·H_2O, high-wavenumber component), in line with previous reports [Angew.

Chem. Int. Ed. 2025, e17221]. As the potential shifts negatively, the *in situ* ATR-FTIR spectra of CoPc/NCNT display a gradual decrease in the 4-HB·H_2O component accompanied by an increase in the 2-HB·H_2O contribution, which becomes the dominant interfacial water species (Fig. R32). Because 2-HB·H_2O is more weakly hydrogen-bonded than 4-HB·H_2O and can be more readily dissociated to release protons, this evolution of the interfacial water structure indicates that CoPc/NCNT promotes H_2O dissociation and enhances the supply of $^*H$ for EASH.

We added these figures and discussions to the revised Manuscript (Page 15).

Page 15: "In the O–H stretching region, the broad band between 2900 and 3700 cm^{-1} can be deconvoluted into contributions from 4-coordinated hydrogen-bonded water (4-HB·H_2O), 2-coordinated hydrogen-bonded water (2-HB·H_2O), and K^+-hydrated water (K·H_2O). With increasingly negative potentials, the intensity of the 4-HB·H_2O component decreases, while that of 2-HB·H_2O increases, suggesting that the interfacial hydrogen-bond network becomes more weakly bound and that water dissociation is facilitated, thereby increasing the availability of $^*H$ for the semi-hydrogenation of acetylene."

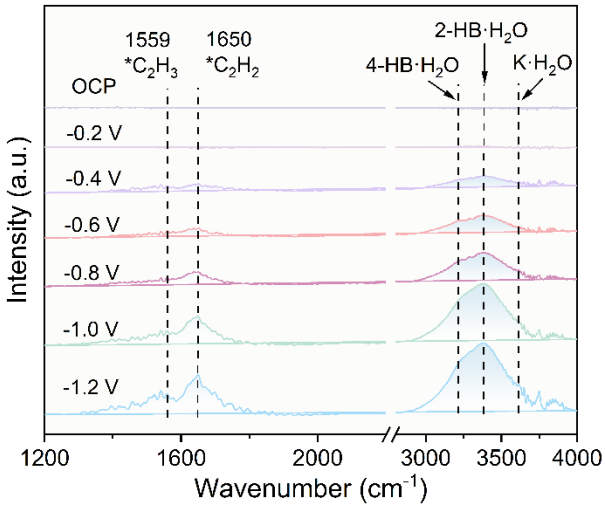

Fig. R32 | In situ electrochemical FT-IR spectra of CoPc/NCNT electrode for acetylene semi-hydrogenation in acetylene-saturated 1 M KOH solution.

Comment 5: The selectivity performance using *t*-BuOH in electrolyte should be provide to the demonstrate the role of $^*H$, while the LSV curves are not enough.

Response to comment 5: We appreciate the reviewer's valuable suggestion.

In addition to the LSV curves, we have now evaluated the catalytic performance in the presence

of *t*-BuOH and quantified the product distribution (Fig. R33). When *t*-BuOH is added to the electrolyte, the LSV limiting current density decreases markedly, and both the Faradaic efficiencies of the gaseous products and the acetylene conversion exhibit a pronounced decline. These results indicate that *t*-BuOH perturbs the formation and/or coverage of proton-derived hydrogen intermediates on the catalyst surface, thereby suppressing the electrocatalytic hydrogenation of acetylene. This behavior supports the crucial role of surface-adsorbed *H in driving the semi-hydrogenation reaction rather than a pathway that is insensitive to the availability of hydrogen intermediates.

The corresponding data and discussion have been added to the revised manuscript (Page 15-16) and Supplementary Information (Supplementary Fig. S39).

Page 15-16: "Upon addition of *t*-BuOH, the polarization current density and C_2H_2 conversion decrease markedly (Supplementary Fig. S39). The combination of a weak pH dependence and a strong sensitivity to *H scavenging indicates that surface-bound *H, rather than a direct proton-coupled electron-transfer step, serves as the key reactive intermediate in the electrocatalytic hydrogenation of C_2H_2 on CoPc/NCNT."

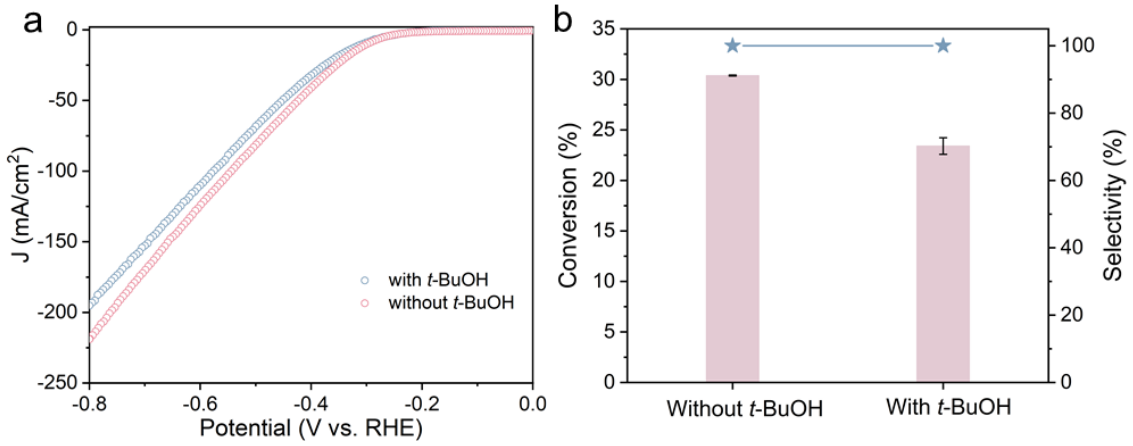

Fig. R33 | (a) LSV curves and (b) C_2H_2 conversion over CoPc/NCNT in 1 M KOH solution with and without 20 mM *t*-BuOH.

Comment 6: The authors design a tandem system to generate high-purity C_2H_4. However, the reviewer wants know if such a design has practical significance. Whether the added big-area reactor is better than other methods for removing low concentrations of C_2H_2. The technical economic analysis may be better to demonstrate the necessity of the design.

Response to comment 6: We thank the reviewer for pointing out this issue.

In our preliminary tests, we first evaluated the catalysis performance of CoPc/NCNT in a 1 cm^2 flow cell at different C_2H_2 concentrations. As shown in the revised Fig. R34, when the C_2H_2 content is reduced to the 10%, the Faradaic efficiency for C_2H_4 drops sharply. We attribute this mainly to the very low solubility of C_2H_2 in alkaline electrolyte and to mass-transport limitations in bringing highly dilute C_2H_2 through the gas-diffusion layer to the catalyst surface. Under such conditions, a larger geometric electrode area at similar local current density is required to maintain both high single-pass conversion and high selectivity. Using a large-area electrolyser for the low-concentration stage is therefore a practical way to compensate for these mass-transport limitations, and is in line with common practice in recent EASH studies (Nat. Catal. **4**, 565-574 (2021); Nat. Catal. **4**, 557-564 (2021)).

To ascertain the economic potential of electrochemical acetylene semihydrogenation by our designed tandem system, we carried out a techno-economic analysis based on the model reporte recently[1-3]. The electricity price used in this study was adopted from recently published literature, while the cell voltage was determined based on experimental data obtained from our system. Furthermore, the stack cost of 275.55 \$ kW^{-1} was recalculated based on the stack cost from DOE Current Central H2A, 460 \$ kW^{-1} according to the literature. The electrolyzer cost per unit area is a function of current density and operating cell voltage[3]. The costs of coal-derived acetylene was confirmed as 767.74 \$ ton^{-1} based on the recently published literature[4]. Accordingly, the costs consist of three components, namely the capital costs, operating costs and materials costs.

The specific sample for the calculation of ESAE for ethylene under optimistic case assumptions:

Taking the 10000 kg daily capacity of C_2H_4 as an example at a current density of 0.5 A cm^{-2} (small electrolyzer) and 0.040 A cm^{-2} (big) with 99% selectivity of C_2H_4 as an example.

The specific assumptions made for the TEA are listed as follows:

1. The electricity price was considered to be 0.03 \$ kWh.

2. The operating voltages were set as 2.1 V and 2.5 V.

3. The electrolyzer cost per area was calculated as follows:

$$\text{Electrolyzer cost per area (small)} = 275.55\ \$\ kW^{-1} \times \frac{0.5\ \text{A}}{\text{cm}^2} \times 2.1\ V \times \frac{10^4\text{cm}^2}{\text{m}^2} \times \frac{\text{kW}}{1000}$$

$$= 2893.28\ \$\ \text{m}^2$$

Electrolyzer cost per area (big)= 275.55 \$ kW^{-1} × $\frac{1\ A}{25\ cm^2}$ × 2.5 V × $\frac{10^4 cm^2}{m^2}$ × $\frac{kW}{1000}$

= 275.55 \$ m^2

4. The anticipated service life of the electrolyzer was 20 years and the working time per year was 350 days. The power of separation equipment was 0.25 kWh/m^3

Thus, the parameters needed in the cost calculation are determined as follows：

The required total current is calculated as:

$Total\ Current$ = $\frac{10000\ kg}{day}$ × $\frac{day}{86400\ s}$ × $\frac{1000\ g}{kg}$ × $\frac{mol}{28\ g}$ × 2 e^- × $\frac{96500\ C}{mol}$ × $\frac{1}{0.99}$ = 805843 A

The required C_2H_2 feedstock inlet with 99% single-pass conversion was calculated as:

C_2H_2 Inlet = 805843 A × $\frac{1}{2e^-}$ × $\frac{1}{96485\ C\ mol^{-1}}$ × $\frac{0.026\ kg}{mol}$ × $\frac{86400\ s}{day}$ × $\frac{1}{0.99}$ = 9475.7 kg day^{-1}

The outlet gas at the cathode side consisted of C_2H_2, C_2H_4, and H_2:

C_2H_4 Outlet Flow Rate = 10000 × $\frac{kg}{day}$ × $\frac{m^3}{1.25\ kg}$ × $\frac{day}{24\ h}$ = 333.33 $m^3\ h^{-1}$

H_2 outlet = 814066 A × (1-0.99) × $\frac{m^3}{0.089\ kg}$ × $\frac{1}{2e^-}$ × $\frac{1}{96485\ C\ mol^{-1}}$ × $\frac{0.002\ kg}{mol}$ × $\frac{86400\ s}{day}$ × $\frac{day}{24\ h}$ = 3.42 m^3 h^{-1}

Total Outlet Flow Rate = (333.33 + 3.42) $m^3\ h^{-1}$= 336.75 $m^3\ h^{-1}$

The needed electrolyzer area was determined as:

Electrolyzer Area (small) = 805843 A × $\frac{1}{0.5\ A\ cm^{-2}}$ × $\frac{m^2}{10^4\ cm^2}$ = 161.17 m^2

Electrolyzer Area (big) = 805843 A × $\frac{1}{0.04\ A\ cm^{-2}}$ × $\frac{m^2}{10^4\ cm^2}$ = 2014.60 m^2

The input power was calculated as follows:

Power = (2.1 V +2.5 V) × 805843 A × $\frac{W}{10^6\ MW}$ =3.79 MW

The total cost of the proposed ESAE process consisted of capital cost, operating cost, and material cost.

Capital cost:

1. Electrolyzer:

   Electrolyzer Cost per ton Ethylene

   = (161.17 m^2 × 2893.28 \$ m^2 + 2014.60 m^2 × 275.55 \$ m^2) × $\frac{1}{20\ year}$ × $\frac{year}{350\ day}$ × $\frac{day}{10\ ton}$ = 14.59 \$ $ton_{C_2H_4}^{-1}$

2. Balance of Plant:

Balance of Plant Cost per ton Ethylene

$= 14.59\ \$\ ton_{C_2H_4}^{-1} \times 0.39/0.67 = 8.49\ \$\ ton_{C_2H_4}^{-1}$

3. Separation Equipment (calculated as the reported reference)[1]:

Separation Equipment Cost per ton Ethylene

$$= 1989043\ \$ \times \left(\frac{336.75\ m^3\ h^{-1}}{1000\ m^3\ h^{-1}}\right)^{0.7} \times \frac{1}{20\ year} \times \frac{year}{350\ day} \times \frac{day}{10\ ton} = 13.26\ \$\ ton_{C_2H_4}^{-1}$$

Operating Cost:

1. Electricity:

$$3.79\ MW \times \frac{1000\ kW}{MW} \times 24\frac{h}{day} \times 0.03\frac{\$}{kWh} \times \frac{1\ day}{10\ ton} = 272.88\ \$\ ton_{C_2H_4}^{-1}$$

2. Separation:

$$336.75\ m^3\ h^{-1} \times 0.25\frac{kWh}{m^3} \times 0.02\frac{\$}{kWh} \times \frac{24\ h}{day} \times \frac{1\ day}{10\ ton} = 6.06\ \$\ ton_{C_2H_4}^{-1}$$

Materials Cost:

1. The cost of coal-derived C_2H_2: 767.74 $\$\ ton_{C_2H_4}^{-1}$

2. Water:

$$805843\ A \times \frac{1}{4e^-} \times \frac{1}{96485\ C\ mol^{-1}} \times \frac{0.18\ kg}{mol} \times \frac{0.2642\ gal}{kg} \times \frac{86400\ s}{day} \times 0.0054\frac{\$}{gal} \times \frac{1\ day}{10\ ton} = 0.46$$

$\$\ ton_{C_2H_4}^{-1}$

The total cost:

Total cost = (14.59 + 8.49 + 13.26 + 272.88 + 6.06 + 767.74 + 0.46) = 1083.48 $\$\ ton_{C_2H_4}^{-1}$

Take the above together, the total production cost for C_2H_4 at a rate of 10,000 kg per day is $1083.48 per ton. Given the current market price of C_2H_4 at $1,350 per ton, this yields a gross profit of approximately $266.52 per ton and a gross margin of about 19.7%. Within this commonly used TEA framework, the analysis suggests that employing a tandem electrolyser to produce C_2H_4 is both technically reasonable and potentially compatible with economically viable operation, while recognising that more detailed process engineering and techno-economic studies would still be required for an industrial implementation.

The corresponding data and discussion have been added to the revised manuscript (Page 20) and Supplementary Information (Page S32, Supplementary Note 2).

Page 20: "A preliminary techno-economic analysis based on recently reported EASH models suggests that, under literature-consistent assumptions, this tandem configuration can operate within

an economically reasonable regime (Supplementary Note 2).”

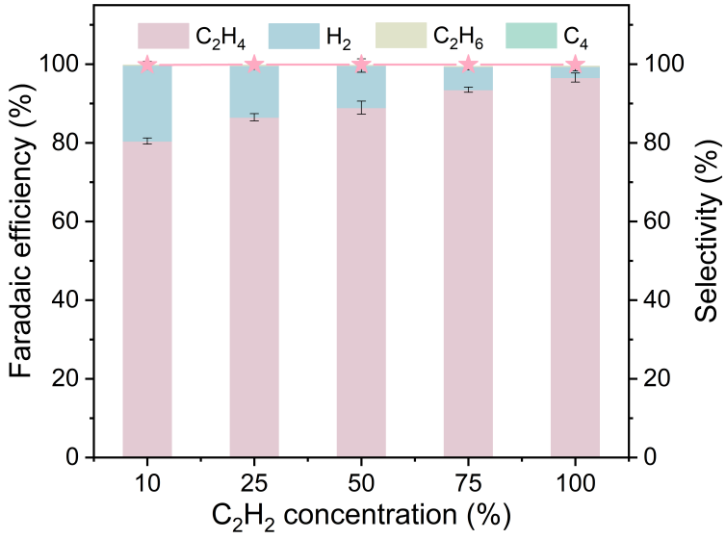

Fig. R34 | The Faradaic efficiency and specific selectivity of ethylene versus acetylene concentration at −100 mA cm^{-2} in 1 cm^2 flow cell.

Reference:

1. Jouny, M., et al. General techno-economic analysis of CO_2 electrolysis systems. Ind Eng. Chem. Res. **57**, 2165-2177 (2018).

2. Lum, Y., et al. Tuning OH binding energy enables selective electrochemical oxidation of ethylene to ethylene glycol. Nat. Catal. **3**, 14-22 (2020).

3. Shin, H., et al. Techno-economic assessment of low-temperature carbon dioxide electrolysis. Nat. Sustain. **4**, 911-919 (2021).

4. Zhao, B. et al. Economically viable electrocatalytic ethylene production with high yield and selectivity. Nat. Sustain. **6**, 827-837 (2023).

Comment 7: Some typographical typos exist in the manuscript and the authors should carefully check it (e.g., affinity—strong, Y-axis title of Figure 5d, the calculation of FE in Performance assessment).

Response to comment 7: We thank the reviewer for carefully checking the manuscript and pointing out these typographical issues. We have thoroughly rechecked the entire text and corrected all typos. In particular, the expression involving “affinity” in the Introduction has been revised for grammatical correctness and clarity (Page 2), the Y-axis title of Figure 5d (Fig. R35) has been corrected, and the description and formula for the Faradaic efficiency calculation in the “Performance assessment”

section have been revised to ensure accuracy and consistency (Page 24). We have also carefully proofread the manuscript to minimize any remaining typographical errors.

Page 24: "$FE\ (\%) = \frac{n \times m \times F}{I \times t} \times 100\% \quad (4)$"

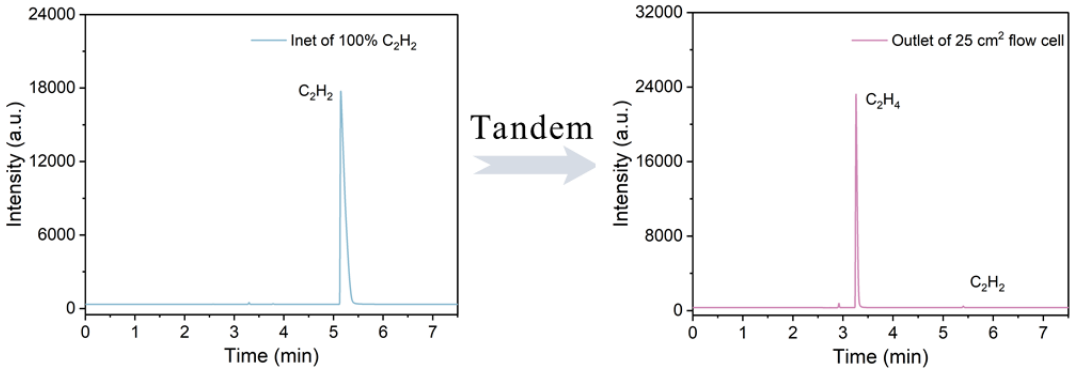

Fig. R35 | Electrosynthesis of high purity ethylene under 100%C_2H_2 by the tandem flow cells.

Response to Reviewer #4:

General Comments:

This manuscript reports the synthesis of carbon nanotube-supported cobalt phtalocyanine (CoPc) complexes through silanoxyl links, and their electrocatalytic activity during the selective semi-hydrogenation reaction of acetylene to ethylene, mainly in pure form but also in ethylene-rich streams (actual commercial process). The characterization of the materials is comprehensive, the electrocatalytic results are well executed and the mechanistic part is sound. The results demonstrate that the axially NH_2-complexed CoPc material is much more selective than the others (O- or SH-) due to the electronics of the coordination sphere, which allows a faster H_2O dissociation and slower undesired C-C coupling. The fact that such a subtle change in the coordination of the supported Co cation enables a significant increase of the selectivity without compromising the catalytic activity is remarkable, moreover in a solid-supported catalyst, and will guide the design of future solid catalysts for this reaction. Therefore, publication in Nat. Commun. is suitable and recommended. However, it must be said that many electrocatalysts for this reaction has been recently published (many of them cited in the text but not compared in Table S3, which is clearly uncomplete), thus some work must be done to really contextualize the new catalyst. Some comments follow:

Response: Thank the reviewer very much for these kind comments and constructive suggestions on our manuscript. Regarding the concerns of the reviewer, we have provided a point-by-point response. To save the reviewer's valuable time, key revisions are displayed on a yellow background in the revised manuscript and Supplementary Information. We are sure that the quality of this work has been greatly improved after these revisions.

Specific Comments:

Comment 1: The key finding here is the action of the N-axial ligand on the metal Pc. This is the point to highlight. I would prepare the N-axial ligand/Cu-Pc material and confirm that the catalytic activity improves in the same way (no need for a deep characterization, the ligation should be similar to the Co complex).

Response to comment 1: We acknowledge the reviewer's helpful comments and suggestions.

Following the suggestion, we have prepared an N-axially coordinated CuPc catalyst (CuPc/NCNT) and compared it with CuPc/OCNT under identical conditions. In Ar-saturated 1 M KOH, the LSV curves show that CuPc/NCNT exhibits a more positive onset potential and higher current density in the HER region than CuPc/OCNT (Fig. R36a), indicating more facile water dissociation and $^*H$ generation at the N-axially coordinated Cu sites. In a C_2H_2 atmosphere, CuPc/NCNT also displays a more positive EASH onset and higher current density (Fig. R36b). The EASH performance was then evaluated between −50 and −500 mA cm^{-2} (Fig. R36c, d). At 100 mA cm^{-2}, CuPc/OCNT delivers Faradaic efficiencies of 52.2% for C_2H_4, 1.58% for C_2H_6, 1.40% for C_4H_6, and 43.9% for H_2. Under the same conditions, CuPc/NCNT reaches a higher C_2H_4 FE of 75.9%, while the FEs of C_2H_6, C_4H_6, and H_2 decrease to 1.03%, 0.80% and 21.9%, respectively. These results show that introducing an N-axial ligand on CuPc also enhances water activation and suppresses undesired hydrogen evolution and C–C coupling, indicating that the axial N-coordination strategy is not limited to CoPc but can be extended to other metal–phthalocyanine systems.

We added the above results and discussions to the revised Manuscript (Page 18) and Supplementary Information (Supplementary Fig. S45 and S46).

Page 18: "Importantly, a similar coordination regulation also improves the performance of Cu phthalocyanine. Guided by the CoPc/NCNT design, we prepared an N-coordinated CuPc/NCNT analogue by immobilising CuPc on amino functionalised CNTs using the same procedure as for CoPc/NCNT. In Ar-saturated 1.0 M KOH, CuPc/NCNT displays a more positive HER onset potential and higher current density than CuPc/OCNT, indicating a similar enhanced water dissociation at the Cu sites (Supplementary Fig. S45). Under EASH conditions, this enhanced water dissociation translates into higher ethylene selectivity and suppressed side reactions. At 100 mA cm^{-2}, the Faradaic efficiency for C_2H_4 increases from 52.2 to 75.9% when moving from CuPc/OCNT to CuPc/NCNT, while the C_4H_6 FE decreases from 1.40 to 0.80% (Supplementary Fig. S46)."

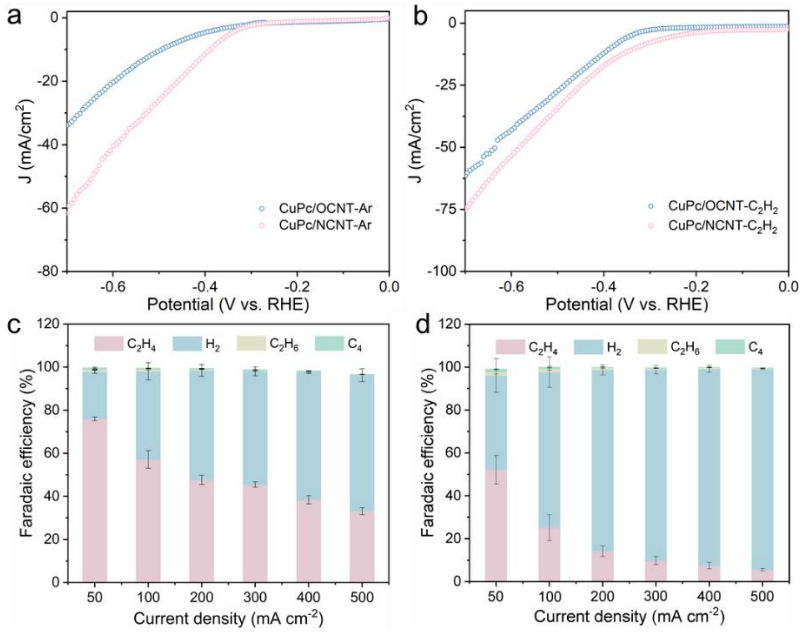

Fig. R36 | LSV curves under (a) Ar and (b) C_2H_2 over CuPc/OCNT and CuPc/NCNT. Faraday efficiency of the obtained products over (c) CuPc/OCNT and (d) CuPc/NCNT.

Comment 2: The catalyst must be characterized after reaction. Is the complex stable? Evolves to an active species?

Response to comment 2: We thank the Reviewer's constructive comment.

To examine the structural stability of CoPc/NCNT after long-term operation, the catalyst recovered from the EASH cycling test was characterised by XPS and AC-STEM (Fig. R37). The Co 2p XPS spectrum of the used CoPc/NCNT (Fig. R37a) shows binding energies and peak shapes that are essentially identical to those of the fresh sample, indicating that the Co centres return to a CoPc-like $Co^{\delta+}$ state after electrolysis and that no irreversible change in oxidation state is detected within the resolution of XPS. AC-STEM imaging of the same sample (Fig. R37b) reveals only isolated bright spots assigned to individual Co atoms, with no observable Co nanoparticles or clusters, demonstrating that the single-atom dispersion of Co on NCNT is preserved after reaction. These results indicate that the CoPc/NCNT complex is structurally stable under the applied EASH conditions and does not evolve into larger Co aggregates within the detection limits of XPS and AC-STEM.

The corresponding data and discussion have been added to the revised manuscript (Page 12) and Supplementary Information (Supplementary Fig. S26).

Page 12: "Post-electrolysis XPS and AC-STEM characterisation (Supplementary Fig. S26) shows nearly unchanged Co 2p features and only isolated Co sites without detectable nanoparticles or clusters, indicating that the CoPc-like single-atom configuration is preserved under EASH operating conditions."

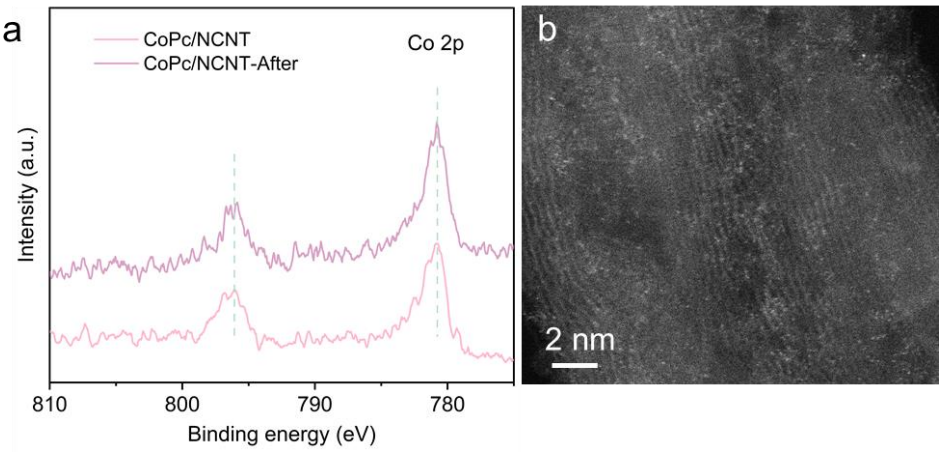

Fig. R37 | (a) Co 2p XPS spectra of CoPc/NCNT catalyst after stability measurements. (b) AC-STEM image of CoPc/NCNT catalyst after stability measurements.

Comment 3: With the better numbers obtained here, could the process substitute the current thermocatalytic process in any way?

Response to comment 3: Conventional thermocatalytic acetylene hydrogenation has been developed over many decades, with mature reactor technologies, well-established process integration in existing ethylene plants, and straightforward scale-up to very large throughputs. These are clear advantages that any alternative route must match. Electrocatalytic EASH offers a different set of benefits: operation at ambient temperature and pressure, direct use of water as the hydrogen source, inherent compatibility with renewable electricity, a simpler process scheme without external H_2 handling, and intrinsically high safety. The CoPc/NCNT system reported here already reaches activity and selectivity metrics that are comparable to, or in some respects exceed, those of state-of-the-art thermocatalysts under relevant feed compositions. However, electrocatalytic EASH is still a young technology, with systematic development only starting in 2021. Although the present results underline its potential as a future alternative to thermocatalytic processes, there is still a substantial gap to industrial implementation. The field is currently at the stage of moving from laboratory cells to prototype or pilot-scale demonstrations. Key challenges include reactor scale-up, reproducible

large-area fabrication of stable gas-diffusion electrodes, and demonstration of long-term operation and overall energy efficiency at the system level with realistic process integration and economics. We therefore regard the present work as evidence that an electrocatalytic alternative is technically plausible and worth further development, while acknowledging that at the current stage it still falls well short of replacing the established thermocatalytic process.

Comment 4: The conversion and selectivity numbers given in the introduction for the industrial semi-hydrogenation reaction of acetylene in ethylene streams are clearly underestimated, since a >99.99% selectivity for acetylene conversion is required (<10 ppm in the final stream). See and cite if appropriate: Nat. Catal., 2024, 7, 452–463. Indeed, the reaction conditions are also exaggerated, the industrial process operates at <100 ºC.

Response to comment 4: We thank the reviewer for this correction.

In the revised Introduction (Page 2), the description of industrial front-end acetylene semi-hydrogenation has been updated to state that acetylene is typically reduced to <10 ppm in the ethylene product and that commercial units generally operate at temperatures below ~100 °C. The original values have been removed, and Nat. Catal. 2024, 7, 452–463 is now cited in the revised manuscript to support these statements.

Page 2: "In both cases, efficient and highly selective conversion of C_2H_2 to C_2H_4 is indispensable to meet the requirement of polymer-grade ethylene, where the residual C_2H_2 content must be below 10 ppm. Nowadays, conventional thermocatalytic hydrogenation can reach over 99% C_2H_2 conversion and 90% C_2H_4 selectivity. However, this process requires an excess of hydrogen (molar ratio of H_2 to C_2H_2 >2), elevated temperatures (<100 °C), as well as high pressures (10-30 atm), which increases energy consumption and favours over-hydrogenation to ethane (C_2H_6)."

Comment 5: The necessity or not of carbon nanotubes to support the complexes must be justified. If a carbon support with dangling hydroxyls could also do the job, this should be commented in the text, since that would give a much more affordable catalyst (perhaps worth of study in a different study). Other hydroxyl-containing supports could also be suitable, please read and cite if appropriate the following examples on semi-hydrogenation reaction of acetylene in ethylene streams under industrial conditions: ACS Catal. 2017, 7, 3721−3729; J. Am. Chem. Soc. 2018, 140, 8827−8832.

Response to comment 5: We thank the reviewer for raising this point and for the helpful literature suggestions.

The cost and availability of hydroxyl-containing carbon supports are indeed attractive. To test their suitability in our system, a hydroxyl-rich carbon support was prepared and evaluated under identical EASH conditions. As shown in Fig. R38a, this OH-functionalised carbon without CoPc gives very low EASH performance, with the FE for C_2H_4 remaining below 30% over the whole range from −50 to −500 mA cm^{-2}. After introducing CoPc, the catalytic performance increases by about threefold under the same conditions, indicating that the molecular CoPc centre is essential for activity in this system (Fig. R38b). In our design, CNTs not only provide surface hydroxyls for axial ligation, but also offer a conductive, tubular framework that facilitates electronic communication and efficient gas–liquid–solid transport, which appears to be critical for high current density EASH in a GDE configuration. Hydroxyl-functionalised carbons are nevertheless an interesting and potentially more economical class of supports, and systematic optimisation of such materials for EASH will be an important direction for our future work. The suggested references (ACS Catal. 2017, 7, 3721–3729; J. Am. Chem. Soc. 2018, 140, 8827–8832) have been added to the revised manuscript and are cited in the discussion of support effects.

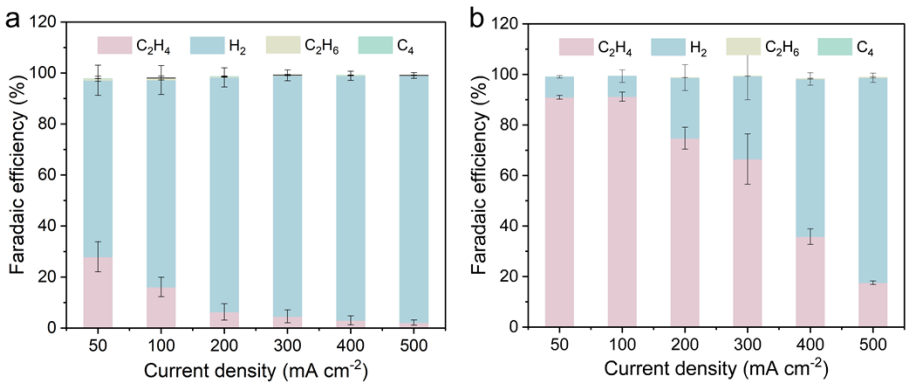

Fig. R38 | Faraday efficiency of the obtained products over (a) OCNT and(b) CoPc/OCNT.

Comment 6: Table S3 must be properly completed, or removed. The comparison between electro and thermocatalysts is perhaps unnecessary, otherwise the Table can be huge (see SI in the above-suggested references).

Response to comment 6: We thank the reviewer for this comment.

In the revised manuscript, Table R9 has been reorganised and its scope narrowed. The previous

mixed comparison between electrocatalysts and thermocatalysts has been removed, and the table now only summarizes representative electrocatalytic EASH systems, including the present CoPc/NCNT catalyst.

Table R9 | Performance summary of recently reported acetylene semi-hydrogenation electrocatalysts.

Entry	Material	Flow composition	SV (mL g_{cat}^{-1} h^{-1})	TOF (min^{-1})	Selectivity (%)	Stability (h)	Ref.
1	CoPc/NCNT	C_2H_2=100	3×10^5	**9.7×10^3**	100	60	This work
2	CoPc/NCNT	$C_2H_2/C_2H_4/Ar$=0.5/20/79.5	1.5×10^5	**4.6**	99.5	110	This work
3	ED-Cu NPs	C_2H_2=100	9×10^5	**5.3×10^2**	100	56	Nat. Sustain. **6**, 827-837 (2023)
4	Cu-F	C_2H_2/Ar=70/30	1.6×10^3	**17.6**	94	43	Nat. Commun. **14**, 8384 (2023)
5	Cu MPs	Saturated by C_2H_2	1.4×10^3	**5.1**	80	100	Nat. Commun. **12**, 7072 (2021)
6	NHC-Cu	C_2H_2/C_2H_4=1/99	9.6×10^5	**1.26**	99	100	Nat. Commun. **12**, 6574 (2021)
7	Cu dendrites	C_2H_2=100	6.6×10^4	/	98	120	Nat. Catal. **4**, 557-564 (2021)
8	LD-Cu	C_2H_2/Ar=5/95	/	/	92	5	Nat. Catal. **4**, 565-574 (2021)
9	Ag NWs	C_2H_2/C_2H_4=1/99	/	/	99	60	CCS Chem. **5**, 200-208 (2023)
10	Cu NDs	$C_2H_2/C_2H_4/Ar$=0.5/20/79.5	1.4×10^5	/	94	130	Nat. Commun. **14**, 2137 (2023)
11	Cu-PCC	C_2H_2/C_2H_4=15/85	/	/	97	12	Nat. Commun. **14**, 2137 (2023)
12	CuO_{1-x} NRs	C_2H_2/C_2H_4=2.2/97.8	/	/	95.1	20	Adv. Mater. **36**, 2408681 (2024)
13	Cu SA/NC	C_2H_2/C_2H_4=1/99	/	/	97	8	Angew. Chem. Int. Ed. e202307848 (2023)
14	CuBcpi-BuOK	C_2H_2/Ar=15/85	9×10^5	/	93	200 (MEA electrolyzer)	Angew. Chem. Int. Ed. **64**, e202509501 (2025)
15	v-Cu NCs	C_2H_2/C_2H_4=1/99	/	/	97.4	50	CCS Chem. **7**, 2844–2853 (2025)

Response to *Reviewers*' Comments

Dear Editors and Reviewers:

We are grateful for the opportunity to submit a revised version of our manuscript for further consideration.

We have carefully studied the reviewer's comments and tried our best to revise the manuscript accordingly. The manuscript has been revised following the comments and suggestions of the reviewers, and point-by-point replies are given below. We sincerely thank the editors and reviewers for their time, effort, and constructive feedback, which have significantly improved the quality and clarity of the manuscript.

Molecular Cobalt Catalysts for Highly Selective Electrocatalytic Acetylene Semi-Hydrogenation

Research Article, No. NCOMMS-25-62672B, Nature Communications

Response to Reviewer #1:

General Comments:

In the revised manuscript, many of the comments have been addressed. However, several key concerns remain:

Response: We appreciate the reviewer's thoughtful summary and constructive suggestions. These opinions help to improve the academic rigor of our article. In response, we have carefully revised the manuscript and Supplementary Information, incorporating new experimental data, figures, references, and discussion to address each of the reviewer's comments point by point. Detailed descriptions of these amendments are provided below. We believe that these revisions have substantially improved the overall quality of this work.

Specific Comments:

Comment 1: Figure captions throughout the manuscript still frequently lack essential details. For example, in Fig. R2, the inclusion of a higher CoPc loading should be explicitly explained in the caption. Similarly, in Fig. R3, it would be helpful to specify that the data correspond to the Co K-edge. This issue occurs repeatedly across the manuscript, and more detailed figure captions would greatly improve clarity and readability.

Response: We appreciate the reviewer's constructive suggestion and agree that several figure captions in the original submission lacked essential experimental/contextual details, which could affect clarity and readability. In the revised manuscript, we have systematically enriched the figure captions throughout to ensure that key information is explicitly stated. Specifically, for Fig. R2, we have added a clear explanation for the higher CoPc loading: CoPc/NCNT-10 is now defined in the

caption as the sample with a CoPc-to-NCNT mass ratio of 1:10 (Fig. R1). For Fig. R3, as suggested, we have clarified in the revised manuscript that the presented XAFS results correspond to the Co K-edge (Page 10). Moreover, we have expanded most figure captions to include crucial experimental parameters and key results. These changes are highlighted throughout the revised manuscript, but, for the sake of brevity, are not listed individually here. We believe these enhancements significantly improve the clarity and consistency of the work.

Page 10: "Notably, the Co K-edge and pre-edge features exhibit a systematic energy shift that correlates with the specific heteroatom in the CNT support. Relative to pristine CoPc (7750.5 eV), the absorption edge of CoPc/OCNT shifts toward higher energy (7751.4 eV), whereas a significant shift toward lower energies is observed for CoPc/NCNT (7745.7 eV) and CoPc/SCNT (7744.0 eV). This energy hierarchy (CoPc/OCNT > CoPc > CoPc/NCNT > CoPc/SCNT) underscores the potent electron-withdrawing nature of axial O relative to N and S, which induces a higher Co oxidation state in CoPc/OCNT and a progressively more reduced state in the N- and S-coordinated analogues. These observations are in excellent agreement with the XPS results."

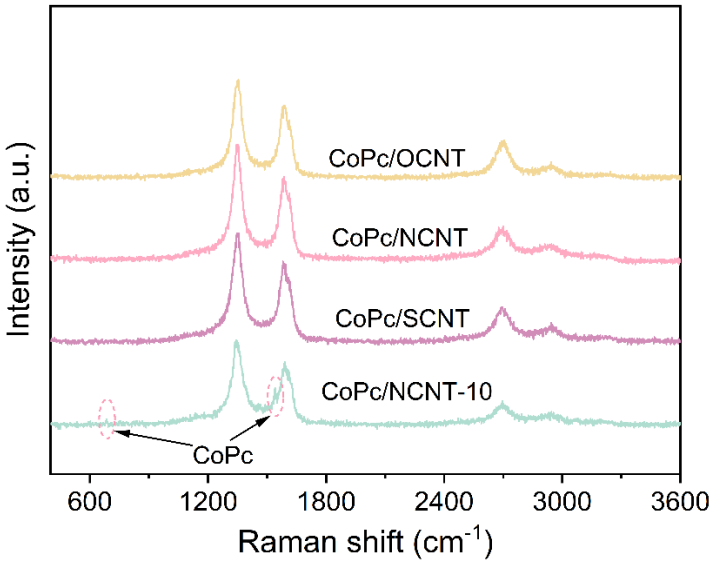

Fig. R1 | Raman spectra of CoPc/OCNT, CoPc/NCNT, CoPc/NCNT-10 (CoPc/NCNT=1:10, m/m), and CoPc/SCNT.

Comment 2: In Fig. R5, the newly added colour scale is still not visible.

Response to comment 2: We apologize for the omission. We have updated Fig. R5 (Fig. R2) in the revised manuscript to include a visible color scale.

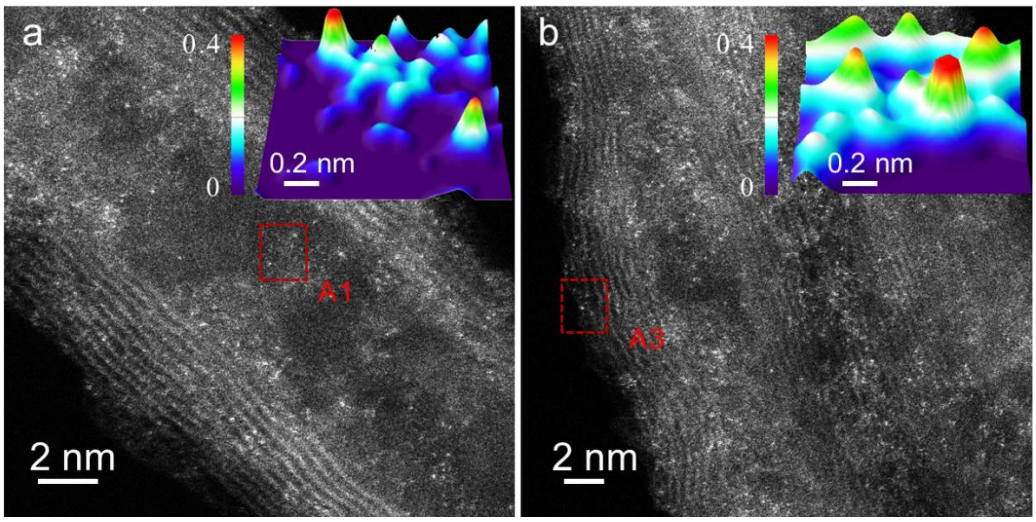

Fig. R2 | AC-STEM images and 3D atom-overlapping Gaussian-function maps for (a) CoPc/OCNT and (b) CoPc/SCNT. The red dashed frames delineate the regions used to generate the 3D atom-overlapping Gaussian-function maps.

Comment 3: For Tables R1 and R2, the authors should clearly state how the error bars were obtained. In addition, the magnitude of the error bars should be consistent with the reported values. In Table R2, some errors are larger than the corresponding values, which suggests that there may be an issue with the data analysis or error estimation.

Response to comment 3: We thank the reviewer for raising this point. The metal loadings were determined by ICP–OES (Agilent 5110) using three independently synthesized batches of CoPc/OCNT, CoPc/NCNT, and CoPc/SCNT. The values presented in Table R1 represent the *mean ± standard deviation (s.d.)* for $n=3$ independent batches, and the error bars correspond to the standard deviation across these batch-to-batch measurements.

For Table R2, the uncertainties represent the 1σ statistical errors estimated from the covariance matrix during the EXAFS refinement process in Artemis. In our previous fit, some parameters were insufficiently constrained (i.e., choice of paths/model and parameter correlations), which inflated the formal uncertainties and, in a few cases, made them even larger than the fitted values. To address this, we refined the EXAFS fitting using optimized coordination models and more appropriate scattering-path selections, retaining the solutions that yielded stable convergence and physically reasonable parameters. The updated fitting results, now provided in Table R2, exhibit uncertainty magnitudes consistent with established literature standards (Adv. Mater. 2023, 35, 2303818; Adv.

Mater. 2022, 34, 2204021; Angew. Chem. Int. Ed. 2022, 61, e202209849; *Nat Commun* 2022, 13, 723; Adv. Funct. Mater. 2022, 32, 2110857).

Table R1 | Cobalt mass content in CoPc/OCNT, CoPc/NCNT, and CoPc/SCNT. Error bars represent the standard deviation derived from three independently synthesized batches of CoPc/OCNT, CoPc/NCNT, and CoPc/SCNT.

Catalysts	Loading (wt. %)	Standard Deviation (%)
CoPc/OCNT	0.55	±0.01
CoPc/NCNT	0.47	±0.055
CoPc/SCNT	0.57	±0.026

Table R2 | Co K-edge EXAFS curve-fitting parameters of CoPc/XCNT and reference sample (Co foil).

Sample	Path	CN	R (Å)	σ^2 ($\times10^{-3}$Å^2)	ΔE_0 (eV)	R factor
Co foil	Co-Co	12	2.49±0.003	6±0.3	0.7±0.03	0.001
CoPc/OCNT	Co-N	4.2	1.91±0.02	2.6±1.2	7.8±1.96	0.010
	Co-O	0.9	1.96±0.03	8.8±7.2		
CoPc/NCNT	Co-N1	4.0	1.92±0.01	2.4±1.0	4.9±1.98	0.010
	Co-N2	1.0	2.18±0.03	9.1±5.7		
CoPc/SCNT	Co-N	4.1	1.90±0.02	3.2±1.3	·1.08±0.66	0.018
	Co-S	0.9	2.19±0.02	5.5±2.8		

Comment 4: I am concerned that iR compensation has not been applied. Without proper iR correction, it is difficult to meaningfully compare the LSV behavior at higher current densities across different catalysts.

Response to comment 4: We agree with the Reviewer that iR compensation is essential for a meaningful comparison of electrocatalytic activity, particularly at high current densities. Accordingly, we have now applied iR correction to all polarization curves. The ohmic resistance (R_S)

was determined via an electrochemical workstation under operating conditions, and the potentials were corrected using the formula, $E_{corr.} = E - iR_S$. The revised figures are now reflected in the revised manuscript.

Comment 5: The Methods section still lacks important experimental details. For example, if a sputtered gold film was required for the FIT measurements, the sputtering procedure should be described. In addition, it is unclear whether the XANES measurements were performed using a laboratory setup or at a synchrotron facility. The use of "RapidXAFS 2M" is mentioned, but this technique/setup is not sufficiently explained and is unfamiliar without further clarification.

Response to comment 5: We appreciate the reviewer's comment regarding missing methodological details. To address this concern, we have updated the Methods section to provide a detailed account of the gold sputtering process for in situ FTIR measurements. Specifically, we have specified the instrumentation, deposition duration, and applied current used to ensure the formation of a high-quality Au film. We have also clarified that the Co K-edge in situ XANES data were acquired using a laboratory (bench-top) XAFS instrument (RapidXAFS 2M, Anhui Absorption Spectroscopy Analysis Instrument Co., Ltd.), rather than at a synchrotron facility. To support this, we have added a comprehensive description of the RapidXAFS 2M configuration (including the crystal analyzer) together with key acquisition parameters and the operando electrochemical protocol. These details have been included in the revised manuscript (Page 23).

Page 23: "In situ FTIR measurements were conducted using a Nicolet IS50 spectrometer equipped with a liquid-nitrogen-cooled MCT-A detector. A gold-coated Ge prism served as the working electrode, prepared via sputter-coating (Quorum SC7620) at 30 mA for 60 s to ensure a uniform conductive surface."

"In situ XANES measurements at the Co K-edge were performed using an ultra-high flux benchtop X-ray absorption fine structure spectrometer (RapidXAFS 2M, Anhui Absorption Spectroscopy Analysis Instrument Co., Ltd.). The instrument was operated at 20 kV and 40 mA and equipped with a Si (533) spherically bent crystal analyzer (radius of curvature: 500 mm), which serves for energy selection of the incident X-ray beam and enables rapid acquisition of XANES spectra under operando conditions."

Response to Reviewer #2:

General Comments:

The authors have made substantial improvements to the work in response to the previous round of review. The revised version is significantly more polished and addresses many of the concerns raised in the initial evaluation. Based on the current quality and scientific merit of the study, I, in principle, recommend that this work be considered for publication in Nature Communications. However, while the overall structure, methodology, and presentation of results are now much stronger, there are still several details that require careful revision and clarification before the manuscript can be accepted for publication. These include, but are not limited to, the following points:

Response: We thank the Reviewer for the thoughtful evaluation and constructive feedback. These insights have been instrumental in enhancing the academic rigor of our work. In response, we have carefully revised the manuscript and Supplementary Information, incorporating new experimental data, figures, references, and discussion to address each of the Reviewer's comments point by point. Detailed descriptions of these amendments are provided below. We believe that these revisions have significantly strengthened the quality and clarity of our study.

Specific Comments:

Comment 1: Physical quantities such as E, G, T, S, etc., should be in italic format.

Response to comment 1: We appreciate the reviewer's attention to detail regarding the formatting of physical quantities. We have thoroughly reviewed the manuscript to ensure that all variables and thermodynamic symbols are consistently typeset in italics, in accordance with standard scientific notation and the journal's style guidelines.

Comment 2: The abbreviation for "generalized gradient approximation" should be checked. It is usually GGA, not GCA.

Response to comment 2: We thank the reviewer for pointing this out. The abbreviation for "generalized gradient approximation" was incorrectly written as "GCA" in the original manuscript.

It has now been corrected to "GGA" throughout the revised manuscript (Page 25).

Page 25: "All electron exchange-correlation functionals were calculated using the generalized gradient approximation (GGA) with the revised Perdew-Burke-Ernzerhof (PBE) method using a cutoff energy of 450 eV."

Comment 3: The chemical reaction equations should be checked for correctness. For example:

$^{*}C_2H_2 + H+ e^{-} \rightarrow C_2H_3$ (10)

$2^{*}C_2H_3 + {}^{*}C_2H_3 \rightarrow {}^{*}C_4H_6$ (14)

Response to comment 3: We thank the Reviewer for the meticulous review and attention to detail. In the revised manuscript, we have corrected the two equations accordingly: Eq. (10) has been revised to "$^{*}C_2H_2 + H^{+} + e^{-} \rightarrow {}^{*}C_2H_3$", and Eq. (14) has been revised to "$2^{*}C_2H_3 \rightarrow {}^{*}C_4H_6$", ensuring consistent surface-adsorbed notation and correct stoichiometry. In addition, we have carefully rechecked all other reaction equations throughout the manuscript to confirm their correctness and consistency.

Comment 4: Transition states, such as *H–OH, are generally not considered stable states and should be clearly indicated.

Response to comment 4: We thank the reviewer for this helpful comment. In the revised manuscript, we have avoided using transition-state-like notations as if they were stationary surface states. Specifically, we rewrote these descriptions in terms of the underlying elementary processes: *H–OH is now described as the water dissociation step, and *H–H is described as hydrogen coupling to form H_2 (Fig. R3). Related statements and labels were adjusted accordingly throughout the manuscript and figure captions to ensure that transition-state configurations are clearly distinguished from stable intermediates.

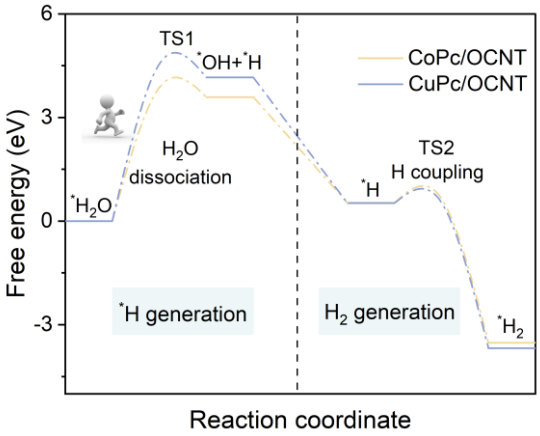

Fig. R3 | Free energy diagram for the *H generation and adsorption, and H_2 generation process of CoPc/OCNT and CuPc/OCNT.

Comment 5: Software tools mentioned in the manuscript, such as VTST, should be properly cited.

Response to comment 5: We appreciate the reviewer's suggestion. In the revised manuscript, we have added the appropriate citations for the software/tools used in our calculations (References 51 and 52), including VTST. We also reviewed the Methods/Computational Details section to ensure that all other software packages mentioned in the manuscript are properly referenced and cited where they first appear.

References:

51. Kresse, G. & Furthmüller, J. Efficient iterative schemes for ab initio total-energy calculations using a plane-wave basis set. *Phys. Rev.* B **54**, 11169 (1996).

52. Henkelman, G. & Jónsson, H. A dimer method for finding saddle points on high dimensional potential surfaces using only first derivatives. *J. Chem. Phys.* **111**, 7010–7022 (1999).

Response to Reviewer #3:

General Comments:

The reviewer appreciates the authors' efforts to revise the manuscript and respond to the comments. However, I regret that the manuscript is still not suitable for publication in this journal. A major concern regarding the novelty of this work is that the CoPc catalytic system has already been reported (Chem. Eng. J. 2022, 431: 134129). A critical issue is that the CoPc catalyst itself does not reach the performance level previously reported in the literature. Consequently, the apparent benefit of introducing NCNT cannot be reliably attributed to a true support effect, and the work fails to demonstrate that NCNT provides a meaningful or generalizable advantage for CoPc-based catalysts. Regarding the tandem system, feeding the exhaust from a small electrolyzer into a larger-area reactor does not convincingly demonstrate practical relevance. Achieving higher conversion in a single appropriately scaled reactor would be more rational and informative. Overall, despite the authors' considerable experimental effort, the manuscript does not demonstrate sufficient novelty or advancement for publication in Nature Communications.

Response: We thank the reviewer for the feedback on our revised manuscript. We appreciate the constructive critique regarding the work novelty, the benchmarking of the CoPc system, the interpretation of the NCNT effect, and the practical relevance of the tandem configuration. We have addressed these concerns through additional analysis and targeted revisions, as detailed in our point-by-point responses below.

Comment 1: The reviewer appreciates the authors' efforts to revise the manuscript and respond to the comments. However, I regret that the manuscript is still not suitable for publication in this journal. A major concern regarding the novelty of this work is that the CoPc catalytic system has already been reported (Chem. Eng. J. 2022, 431: 134129).

Response to comment 1: We appreciate the reviewer's perspective regarding the novelty of our work relative to the CoPc system reported by Liu et al. (Chem. Eng. J. 2022, 431, 134129). We fully acknowledge this pioneering study on CoPc-based EASH, which established metal phthalocyanines as active catalysts and analysed acetylene conversion and selectivity mainly from the viewpoint of

acetylene adsorption and hydrogenation. Our work is conceptually distinct in that it treats the hydrogen source from water electrolysis as an explicit mechanistic and design variable. Specifically, (i) we are, to our knowledge, the first to identify a direct link between water-dissociation–derived hydrogen supply and selective acetylene hydrogenation, which was not addressed in the Chem. Eng. J. work; (ii) using a unified MPc/XCNT platform, we show that promoting water activation provides a general route to suppress C–C coupling; and (iii) we apply axial-coordination engineering to regulate water dissociation and interfacial $^{*}H$ transfer, thereby mitigating severe HER at high current densities and achieving a 24071-fold enhancement in single-site EASH activity compared with the Chem. Eng. J. benchmark.

(1) Water-dissociation–derived hydrogen supply as a controlling step for EASH selectivity.

In our study, we explicitly decompose the alkaline EASH process into two coupled steps: water dissociation at the catalyst–electrolyte interface to generate reactive hydrogen species, and the subsequent adsorption and hydrogenation of acetylene on the active sites. Using the MPc (M = Cu, Co, Ni, Fe)/OCNT platform, we correlate water-dissociation behaviour and subsequent $^{*}H$ utilisation with the full product distribution and show that they are decisive in setting selectivity, including the balance between desired C_2H_4 formation, C–C coupling, and HER. **To our knowledge, this is the first direct confirmation that controlling water dissociation and the ensuing hydrogen supply, rather than acetylene binding alone, is a primary lever for tuning EASH selectivity**.

(2) General suppression of C–C coupling by accelerating water activation

Building on this picture, we examine a series of MPc/OCNT catalysts under identical conditions to test how universal the role of water activation is. We find that the product distribution follows the ability of the metal centre to promote water dissociation and utilise interfacial $^{*}H$: catalysts with faster water activation show a markedly lower tendency toward C–C coupling and C_4 formation. In particular, CoPc/OCNT combines rapid water dissociation with a suitable adsorption environment, leading to strongly suppressed C_4 products, while NiPc/OCNT and FePc/OCNT display similarly low C_4 yields at 100 mA cm^{-2}. These trends indicate that enhancing water activation provides a general route to suppress C–C coupling in EASH, rather than being a catalyst-specific detail, which goes beyond what can be inferred from the MPc focus of the Chem. Eng. J. study.

(3) Axial-coordination regulation of water dissociation and $^{*}H$ transfer to suppress HER at high current densities.

Guided by this mechanistic insight, we develop an axial-coordination strategy in which CoPc is anchored on amino- and thiol-functionalised CNTs (NCNT and SCNT), using the surface groups as well-defined axial ligands that tune the Co coordination environment, water-dissociation kinetics, and partitioning of $^*H$ between HER and acetylene hydrogenation. As a result, CoPc/NCNT delivers a C_2H_4 Faradaic efficiency of 86.7% at –500 mA cm^{-2} under a 100% C_2H_2 feed, with 99.99% C_2H_4 selectivity and complete suppression of detectable C_4 products. The corresponding turnover frequency reaches 7019 min^{-1}, representing a ≈24071-fold enhancement over the 0.29 min^{-1} reported for CoPc at −100 mA cm^{-2} in Chem. Eng. J. 2022, 431, 134129, while using approximately eleven times less CoPc and extending the operational stability from 40 h to 110 h. These data indicate that the axial-coordination regulation of water dissociation and $^*H$ transfer to suppress HER at high current densities, which far exceeds the CEJ study in both performance as well as the understanding of EASH.

Comment 2: A critical issue is that the CoPc catalyst itself does not reach the performance level previously reported in the literature. Consequently, the apparent benefit of introducing NCNT cannot be reliably attributed to a true support effect, and the work fails to demonstrate that NCNT provides a meaningful or generalizable advantage for CoPc-based catalysts.

Response to comment 2: We have to note that this performance gap is attributed to differences in the mass loading of bare CoPc, and when the loading is increased to levels consistent with the previous study, comparable activity of the bare CoPc is achieved. In our main dataset, the CoPc benchmark was prepared so that the amount of CoPc on the gas diffusion electrode matched the CoPc content in the CoPc/XCNT catalysts (≈0.06 mg cm^{-2}). This configuration was chosen to allow a direct comparison of the effect of CNT functionalisation at a fixed CoPc loading. As now shown in the revised manuscript, when the CoPc loading on NCNT is systematically increased, the EASH activity first rises and then approaches a plateau, indicating a clear dependence of activity on loading (Figure S28). When we increased the CoPc loading on the gas diffusion electrode to the same level as in Chem. Eng. J. 2022, 431, 134129, the EASH performance at 50 and 100 mA cm^{-2} was in good agreement with the values reported in that work (Figure R4). The lower absolute activity observed in our main comparison, therefore, arises from the lower CoPc loading used for the support/coordination study, rather than from an intrinsic discrepancy in CoPc performance relative to the literature.

Moreover, we can clearly see that bare CoPc suffers from severe hydrogen evolution at current densities exceeding 100 mA cm^{-2} in both our study and the previous study, but the CoPc/NCNT system maintains exceptional stability and selectivity even at 500 mA cm^{-2}, achieving a C_2H_4 Faradaic efficiency of 86.7% with 99.99% C_2H_4 selectivity and complete suppression of detectable C_4 products. This stark contrast in performance clearly validates the efficacy of our support-based, tunable molecular strategy in regulating the coordination environment of CoPc catalysts to steer reaction pathways even under extreme industrial conditions.

To further validate the efficacy of this strategy and elucidate the underlying mechanism, we systematically evaluated the influence of the NCNT support by maintaining a fixed CoPc loading across the various support platforms. SCNT and NCNT introduce distinct axial coordination environments at the Co centre. On SCNT, the weakened water dissociation and lower H–H coupling barrier favour HER, leading to lower EASH activity and more severe hydrogen evolution. On NCNT, axial N coordination accelerates water dissociation and raises the barrier for H–H recombination, so that a larger fraction of the $^*H$ pool is directed into C_2H_2 hydrogenation rather than HER. Under these conditions, CoPc/NCNT maintains high activity, completely suppresses detectable C_4 products, and strongly mitigates over-hydrogenation. This behaviour reflects a pronounced support effect, indicating that the NCNT environment alters the electronic structure of CoPc and thereby its catalytic behavior.

To demonstrate the universality of this strategy, we extended our investigation to a CuPc-based system. At comparable CuPc loadings and under identical EASH conditions, replacing OCNT with NCNT lowers the water-dissociation barrier, enhances the overall EASH activity, and decreases the C_4H_6 Faradaic efficiency from 1.40% on CuPc/OCNT to 0.80% on CuPc/NCNT at 100 mA cm^{-2}. Taken together with the CoPc results, this behaviour shows that NCNT consistently improves both activity and suppression of C–C coupling across different MPc catalysts. These observations support the conclusion that NCNT provides a meaningful and transferable coordination environment for MPc-based EASH catalysts.

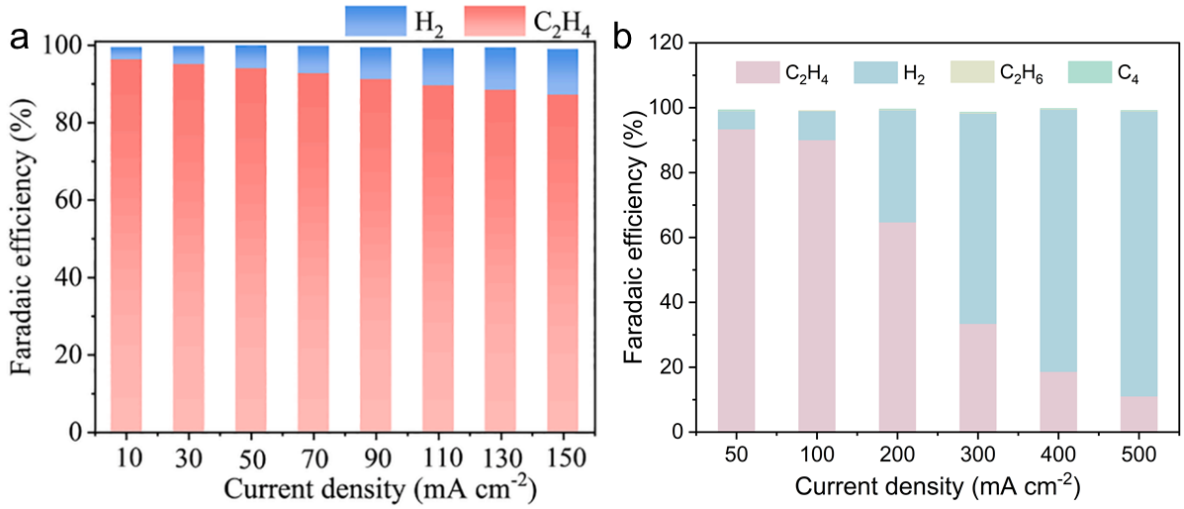

Fig. R4 | (a) Faradaic efficiencies at different current densities over CoPc, adapted from literature. Reprinted with permission from Liu et al. (Chem. Eng. J. 2022, 431: 134129) Copyright 2022 Elsevier. (b) Faraday efficiency at different current densities over CoPc in this work.

Comment 3: Regarding the tandem system, feeding the exhaust from a small electrolyzer into a larger-area reactor does not convincingly demonstrate practical relevance. Achieving higher conversion in a single appropriately scaled reactor would be more rational and informative.

Response to comment 3: We thank the reviewer for this comment.

We agree that performance in a single appropriately scaled reactor is an important benchmark, and we would like to clarify that the staged configuration in this work is not introduced to accommodate a laboratory test using pure acetylene. Rather, it is motivated by a practical process requirement, namely the near-complete removal of acetylene to meet high-purity ethylene specifications. In practice, even when a catalyst remains intrinsically selective, approaching quantitative conversion in a single electrochemical cell becomes increasingly constrained by mass transport once acetylene is depleted to trace levels, because delivery of dilute C_2H_2 through the gas diffusion layer becomes rate-limiting. This transport limitation also explains why, to the best of our knowledge, reported single-cell systems have not exceeded 99% single pass conversion when acetylene approaches low concentration.

To address this concern directly, following the reviewer suggestion, we have operated an enlarged 25 cm^2 flow cell. Under a pure C_2H_2 feed, a single 25 cm^2 cell reaches a maximum single-pass conversion of 96.4% with 99.9% C_2H_4 selectivity. More importantly, under an industrially relevant

crude ethylene stream containing 0.5% C_2H_2 and 20% C_2H_4 (Ar balance), a single 25 cm^2 cell delivers >99% acetylene conversion with >99% ethylene selectivity, demonstrating that high concentration ethylene can be obtained in one reactor under realistic compositions.

For the more stringent regime in which acetylene becomes highly dilute, and transport dominates, we implement a tandem flow cell scheme in which the first stage reduces 100% C_2H_2 to a lower concentration stream and the second stage serves as a polishing step with an enlarged electrode area. Increasing the electrode area lowers the local flux of dilute C_2H_2 per unit area and increases its contact probability with active sites, enabling deeper depletion of residual acetylene while maintaining high selectivity and reducing the burden on downstream separation. We also carried out a detailed techno-economic assessment in response to the reviewer's request, which indicates that this approach is economically viable when the cost of removing trace acetylene by conventional separation is taken into account.

Response to Reviewer #4:

General Comments:

The revision has fulfilled this Reviewer´s requirements. The manuscript seems ready for publication:

Response: We would like to thank the reviewer again for the considerable time and effort dedicated to our work.